Parameter Input Estimation and Temperature Control of RC Thermal Dynamic Systems

by

Vahid Zamani

A thesis submitted in partial fulfillment of the requirements for the degree of

Master of Science

in

Civil (Cross-disciplinary)

Department of Civil and Environmental Engineering

University of Alberta

Abstract

The world's energy consumption and greenhouse gas emissions are on the rise due to increasing energy usage in buildings. To address this problem, it is important to design energy-efficient buildings with advanced control systems. One key aspect of these systems is having reliable thermal dynamic models can provide necessary information for the control systems. Thermal resistor-capacitor (RC) models are one of the commonly used methods for thermal dynamic modeling in control systems. RC models represent the thermal behavior of building components using parameters related to fundamental physical principles. The R's and C's in the model are equivalent thermal resistors and capacitors that represent the effective resistance to heat flow and thermal energy storage capacity of the nodes, respectively. These model parameters are used to relate system inputs (e.g., heating and cooling supply) and temperature states. RC model parameters and inputs (e.g., actual solar heat gain) are difficult to be directly measured but can be estimated with historical data. Accordingly, this thesis aims to develop a practical and dependable method for estimating RC model parameters and input simultaneously with and without partially missing states. By estimating model parameters and creating a trustable thermal dynamic model the developed method will be used to obtain required heating, ventilation, and air conditioning (HVAC) outputs for temperature control purposes.

To estimate unknown parameters and inputs, the method uses unscented Kalman filter (UKF) in combination with nonlinear least square (NLS) estimation method. To evaluate the effectiveness of this method, two case studies are conducted. The first case study involves made-up data, while the second case study uses real-world data from a single detached house. The performance of the method is assessed by comparing estimated parameter and input values to true values in the made-up case, as well as the accuracy of the updated thermal dynamic model (created based on the last

estimated model parameters) in predicting temperature responses in the real-word case. Both estimation and prediction studies indicate that the developed method can accurately estimate the unknown model inputs and parameters.

The method can also be used to estimate the required heating and cooling supply for controlling the temperatures of multiple zones. To evaluate the effectiveness of this approach, two case studies are conducted: one with made-up data and one with real-world data from a single detached house. The performance of the method is assessed by simulating the thermal model with applying the estimated heating and cooling supply to the model and generate the system response for the zone temperature that requires control and verify whether the controlled zone's temperature meets the expected temperature or not. The results of the two case studies indicate that the method can accurately estimate the heating and cooling supply.

Overall, the primary objective of this thesis is to develop a practical and dependable method for estimating RC model parameters and inputs simultaneously, even when some states are partially missing. Furthermore, the developed method will be used to obtain the required HVAC outputs for temperature control purposes. Achieving these goals will not only advance the relevant field but also provide feasible solutions for real-world applications.

Preface

This thesis includes original research conducted by Vahid Zamani and is divided into four Chapters, with Chapters 1 and 4 serving as the introduction and conclusion, and Chapters 2 and 3 presenting the research in the form of journal papers.

Chapter 2 provides an overview of the research focused on developing a method for parameter-input estimation of thermal dynamic systems. The chapter covers the introduction, methodology, model validation, results, and discussion. It concludes with a summary of the main points and will be submitted for publication as ***"Parameter-Input Estimation of RC Thermal Models of Buildings using Unscented Kalman Filter and Nonlinear Least Square Method." Vahid Zamani, Shaghayegh Abtahi, Yuxiang Chen, Yong Li.,*** Vahid Zamani was responsible for conceptualization, developing methodology, analysis implementation, and writing the original draft. Shaghayegh Abtahi was in charge of assisting in writing the draft. Both Drs. Yuxiang Chen and Yong Li were in charge of supervision, conceptualization, and manuscript revisions.

Chapter 3 employs the developed method for estimating the necessary heating and cooling supply for controlling zone temperatures at desired levels. The chapter covers the introduction, methodology, model validation, results, and discussion. It concludes by highlighting the key points and will be submitted for publication as ***"Heating and Cooling Supply Estimation to Control Building Temperature Using RC Thermal Models, Unscented Kalman Filter and Nonlinear Least Square Method." Vahid Zamani, Shaghayegh Abtahi, Yong Li, Yuxiang Chen.,*** Vahid Zamani was responsible for conceptualization, developing methodology, analysis implementation, and writing the original draft. Shaghayegh Abtahi was in charge of assisting in writing the draft. Both Drs. Yuxiang Chen and Yong Li were in charge of supervision, conceptualization, and manuscript revisions.

Dedication

To my wife Mahsa,

And my family

Acknowledgments

I would like to express my deepest gratitude to my supervisor, Dr. Yuxiang Chen, and co-supervisor, Dr. Yong Li, for their exceptional guidance and support throughout my research. Their invaluable insights and expertise made the completion of this thesis possible.

I would also like to extend my appreciation to Dr. Shaghayegh Abtahi, and my friends, *Mohammad*, and *Farzad*, for their feedback and support throughout the writing and revision process. Your encouragement and constructive criticism were instrumental in shaping this thesis.

I am grateful to my wife *Mahsa and* my family for their unwavering love and support throughout my academic journey. Your belief in me and my work has been a source of inspiration and motivation.

Finally, I would like to acknowledge the support of the University of Alberta, Natural Sciences and Engineering Research Council of Canada (NSERC) for their funding of this research. Their support has been invaluable in allowing me to pursue my passion for research in this field.

Vahid Zamani

Table of Contents

List of Tables

List of Figures

Nomenclature

Abbreviations

MAPE	Mean Absolute Percentage Error
NLS	Nonlinear least squares
ODE	Ordinary differential equation
RC	Resistor-Capacitor
SP	Sigma points
UKF	Unscented Kalman filter
UT	Unscented Transformation

Symbols

α	Constant parameter related to distribution of sigma points around mean
β	Factor relative to weight of each sigma points
Δ	Difference between the predicted mean of measurement vector and measurement
Δt	Duration of time step
$\boldsymbol{\theta}$	Model parameters vector
κ	Secondary scaling parameter
$\boldsymbol{v}$	Measurement noise
$\boldsymbol{\chi}$	Sigma points

$\boldsymbol{A}^c$	Continuous-time state matrix
$\boldsymbol{A}^{cx}$	Adjusted state matrix
$\boldsymbol{A}^{dx}$	Discrete-time state matrix
$\boldsymbol{B}^c$	Continuous-time system input matrix
$\boldsymbol{B}^{cx}$	Adjusted input matrix
$\boldsymbol{B}^{dx}$	Discrete-time input matrix
C	Capacitor or capacitance
f^c	Continuous-time nonlinear state function
$\boldsymbol{G}$	Covariance matrix of process noise
h	Nonlinear measurement function
i	Index of sigma points
k	Step in discrete time
K	Kalman gain
n_θ	Number of model parameters
n_s	Number of states
n_u	Number of model inputs
n_x	Number of state-parameter vector components
$\widehat{\boldsymbol{P}}^{ss}$	Covariance of state vector

$\widehat{\boldsymbol{P}}^{sy}$	Cross covariance matrix between measurement and state vector
$\widehat{\boldsymbol{P}}^{yy}$	Predicted covariance of measurement vector
$\widehat{\boldsymbol{P}}^{xx}$	Covariance of state-parameter vector
$\widehat{\boldsymbol{P}}^{xy}$	Cross covariance matrix between measurement and state-parameter vector
$\widehat{\boldsymbol{P}}^{yy}$	Predicted covariance of measurement vector
$\boldsymbol{Q}$	Heat input
R	Resistor or resistance
$\boldsymbol{S}$	Sigma points
$\boldsymbol{s}$	Temperature state vector
$\dot{\boldsymbol{s}}$	First-order time derivative of state vector
$\hat{\boldsymbol{s}}$	Mean of state vector
$\boldsymbol{s_m}$	Output of measurement function
t	time
T	Temperature
$\boldsymbol{u}$	System input
$\boldsymbol{u}^{kn}$	Known inputs vector
$\boldsymbol{u}^{un}$	Unknown inputs vector
$\boldsymbol{W}$	Weighting coefficients
$\boldsymbol{w}$	Process noise

$\boldsymbol{x}$	State-parameter vector
$\widehat{\boldsymbol{x}}$	Mean of state-parameter vector
$\boldsymbol{x}_m$	Output of measurement function
$\boldsymbol{y}$	Measurement vector
$\widehat{\boldsymbol{y}}$	Predicted mean of measurement vector
$\mathbf{Z}$	Covariance matrix of measurement noise

1 Introduction

The global building sector consumes the most energy, surpassing a third of all final energy and 50% of global electricity usage [1]. Without efforts to enhance energy efficiency, it is projected that energy consumption in the building sector will grow by 50% by 2050 [2]. In response to this growing energy demand, there is a recognition of the importance of energy efficiency in buildings. Thus, actions are being taken to promote and implement energy-efficient measures. These actions include enhancing building codes and standards [3], encouraging the use of energy-efficient technologies [4], and investing in the research and development of new technologies.

Among these practices, building energy management with control systems has demonstrated its critical importance in mitigating the negative impact of the rising trend in building energy consumption [5-7]. Control systems require thermal dynamic models, making it crucial to use a reliable model to achieve energy efficiency in buildings [8]. Thermal dynamic modeling involves creating a mathematical representation of a building or system, which helps in predicting buildings' thermal behavior (e.g., temperature response) and building system behavior (e.g., heating, and cooling supply). There are three types of modeling strategies: white box, black box, and gray box modeling [9-12].

White box (physics-based) modeling like using Energy Plus [13] involves describing building dynamics based on construction information, and utilize parameters derived from technical specifications like geometry, material properties, and equipment specifications [14]. Despite its ability to simulate building dynamics well, collecting these necessary information can be time-consuming, and the model may lack the flexibility to accommodate changes or variations over time [15]. On the other hand, Black box modeling involves pure mathematical

machine-learning techniques, such as Artificial Neural Networks to develop a model from collected data without explicitly taking physical aspects into account. Although this modeling approach requires a significant amount of data to build an accurate model, it may outperform white box modeling in terms of accuracy [16, 17]. Gray box modeling such as thermal resistor-capacitor network (RC) is a hybrid of white box and black box modeling. It combines the physical principles of white box modeling with the data-driven approach of black box modeling. Gray box modeling can be a good choice for systems where the physical principles are only partially understood or where the data is limited. The gray box modeling approach is widely used as a standard modeling strategy for thermal dynamic modeling [18-20].

RC models are based on a set of equivalent model parameters, resistors (R's) and capacitors (C's), to relate system inputs (e.g., heating and cooling supply) and temperature states. The R's and C's in the model are equivalent thermal resistors and capacitors that represent the effective resistance to heat flow and thermal energy storage capacity of the nodes, respectively [21].The model parameters can be influenced by both internal and external factors. Internal factors such as people, furniture, and electric consumption, as well as external factors like adjacent obstructions, infiltration, and weather-related influences, can all impact the model. Therefore, RC model parameters are not meant to be directly measured or simply calculated based on building construction details. Rather than directly measuring the model inputs or estimating the model parameters by calibrating the model based on physical details, the optimal model inputs or parameters can be estimated using purposely measured data (usually temperature states). [21, 22].

Parameter estimation can be conducted via offline estimation (i.e., batch), assuming the parameters are constant within the period of a set of collected measurements and using the

measurements to estimate the parameter. This approach can result in significant inaccuracies in predictions due to ongoing data evolution and uncertainties arising from building conditions, weather changes, temperature, and occupant actions [23, 24]. To address this issue, an online manner (e.g., adaptive) estimation approach can be used to continuously update the model whenever new real-time measurements are available [25]. The Unscented Kalman filter (UKF) based estimation method has been shown to be effective and reliable for applying online estimation to thermal dynamic modeling with RC models for parameter estimation which can handles nonlinear systems and provide accurate estimation [21, 25]. UKF can update its estimates recursively as new measurements arrive. This method enables the model to be updated in real-time based on the most current measurements, resulting in more precise predictions making it efficient in updating parameters in real-time applications. However, the computational complexity of UKF increases with the number of states and measurements, making it less efficient for large systems when used alone [26].

In certain real-life scenarios, estimating RC model parameters can be challenging due to the temporary missing of historical data including heating and cooling supply (i.e., RC model inputs) and the zone's temperature (i.e., RC model state). Such missing data can result from sensor malfunctions or unavailability due to limitations in practices (e.g., too difficult to obtain accurate data) and resources (e.g., too expensive to install many sensors). To overcome this issue, the primary goal of this thesis is to develop a practical and dependable method for jointly estimate model parameters and unknown inputs, with and without partially missing states. Furthermore, after estimating RC model parameters and creating reliable thermal dynamic model, the developed method will be used to obtain the required heating and cooling supplies for building's temperature control purposes. Obtaining the accurate heating and

cooling supply for building temperature control purposes is essential for a number of reasons. First, it can optimize energy consumption, leading to cost savings and a smaller carbon footprint [27, 28]. Second, it can aid in keeping buildings at a comfortable temperature, which is essential for health and productivity [29, 30]. Thirdly, it can aid energy providers in anticipating future demand and ensuring a steady supply [31-33]. The accomplishment of these objectives will not only advance the relevant field but also provide solutions applicable to real-world applications.

1.1 Objective and Scope

The primary objective of this thesis is to develop a dependable and feasible approach for simultaneously estimating RC thermal model parameters and input, even in cases where some states are partially missing. The development of a suitable model structure (i.e., number of temperature nodes, inputs, R, C, and their connections) is beyond the scope of this study and, therefore, will not be discussed in this thesis. After obtaining a suitable model structure, the RC model parameters, inputs, and possibly unavailable states are estimated using a UKF-based parameter-input estimation method integrated with NLS. Specifically, the UKF is mainly used for parameter and state estimation, while the NLS is used to estimate unknown inputs.

Accordingly, once the parameters have been estimated and a trustworthy thermal dynamic model is created, then attention is redirected toward employing the developed method by utilizing the created thermal model to determine the necessary heating and cooling supply for controlling zone temperatures to desired levels. This is one of the key applications of the developed method in situations where the temperature needs to be controlled by obtaining the necessary heating and cooling supply. Controlling the temperature in thermal

zones can be challenging when multiple interconnected zones with different temperatures are involved, especially when estimating the heating and cooling supply needed for the future. This makes the developed method particularly useful in real-world applications. These objectives will be achieved by addressing the following:

Part1:

I. Introduce an RC thermal dynamic modeling and explain how it can be used to simulate thermal behavior of buildings.
II. Develop an estimation method and demonstrate how it can be integrated to estimate the previously developed RC model for parameters, and inputs estimation.
III. Apply the developed method to a simple case study using made-up data to evaluate its performance.
IV. Evaluating of the developed method's capability in real-world scenarios by applying the method to a real single-family detached house.

Part 2:

I. Employing the developed method with known RC model (developed previously) parameters which are estimated based on part 1 for obtaining necessary heating and cooling supply for temperature control purposes.
II. Apply the developed method to case studies using made-up and real-world data in different scenarios, to evaluate its capability in estimating heating and cooling supply for controlling zone temperatures.

To summarize, the thesis's focus is on developing an approach that can estimate RC model parameters (e.g., thermal resistance), and model input (e.g., heating and cooling supply) with or without some missing temperature states. Furthermore, the thesis also highlights employing the developed method with known (i.e., estimated) model parameters to estimate necessary heating and cooling supply to control zone temperatures. The capability of the developed method is evaluated using case studies with made-up and real-world data. It is worth noting that the key difference between the two parts of the thesis is that in the first part, the RC model parameters were estimated in the presence of unknown model input and unmeasured temperature states (if any). In contrast, in the second part, there is not any model parameter estimation, and the estimated parameters are used in the defined RC thermal model for heating and cooling supply estimation. Additionally, in the second part, temperature measurements were considered as the desired temperature level, while in the first part, they came from recorded data.

It is worth noting that the efficacy of the method in determining the necessary heating and cooling supply depends on the accuracy of the created thermal dynamic model. If the estimated model parameters for the presented RC model can accurately represent the thermal behavior of the real system, then the developed method can provide an accurate estimation of the necessary heating and cooling supply. However, the accuracy of the results depends on the structure of an RC thermal model. Creating an appropriate model structure, which includes determining the number of temperature nodes, inputs, as well as the relationships between R, C, and their connections falls outside the scope of this study and will not be addressed in this thesis.

1.2 Thesis Organization

The thesis is structured into four chapters, with the research presented in Chapters 2 and 3 in a journal paper format. Chapter 4 concludes the thesis with a summary of key points and proposals for future work and limitations.

The remaining chapters of the thesis are arranged as follows:

Chapter 2 - Develop a method for estimating RC model parameters and input simultaneously with and without partially missing states. The method is evaluated using two case studies, one with made-up data and another with real-world data.

Chapter 3 - Employ the developed method to estimate necessary heating and cooling supply to control temperature. The method is evaluated with case studies with made-up and real-world data with different case studies.

Chapter 4 Conclusion - Summarizes key findings from chapters 2 and 3. Following that, potential future work and limitations are discussed.

2 Parameter-Input Estimation of RC Thermal Models of Buildings using Unscented Kalman Filter and Nonlinear Least Square Method

2.1 Introduction

Buildings currently consume approximately 40% of global energy and contribute to 31% of world CO2 emissions [34]; therefore, reducing buildings' energy consumption is critical to meeting global sustainability targets [5, 35]. Among the efforts to reduce buildings' energy consumption, building energy management with control systems that can optimize building energy consumption are being developed and deployed [6, 7]. These systems are proven to have the potential to save energy by up to 28% [36]. Control systems require reliable thermal dynamic models in order to estimate buildings' thermal parameters (e.g., effective thermal resistance) and behavior (e.g., temperature response) [6].

Different modeling strategies, including "white box", "black box", and "gray box" modeling, have been developed in the literature to predict the thermal behavior of buildings and their systems [9-12]. White-box (physics-based) modeling , such as using Energy Plus [15], requires detailed construction information (e.g., dimensions) and can simulate building physics in detail [14]. Due to the unknowns of building conditions (e.g., material degradation, user behavior, and operation strategies), using this modeling strategy on existing buildings can be problematic [15]. On the other hand, black-box modeling uses pure mathematical machine-learning techniques, such as using Artificial Neural Network [16], to create non-interpretable (hidden) relationships between input and output data without necessitating physics [37]. Black-box modeling requires a large amount of high-quality data [17]. "Gray box" modeling strategy, such as thermal resistor-capacitor (RC) models, is based on a physics-base model structure and uses mathematical optimization techniques to estimate the equivalent physical parameters of the model. The strategy incorporates the benefits of both white-box to eliminate outliers and that of black-box strategies to reduce the necessity of

detailed information. The gray-box modeling approach has been widely used for thermal dynamic modeling [18-20].

RC models are based on a set of equivalent model parameters, resistors (R's) and capacitors (C's), to relate system inputs (e.g., heating and cooling supply) and temperature states. [21]. The model parameters can be influenced by both internal and external factors. Internal factors include people, furniture, and electric consumption, while external factors encompass adjacent obstructions, air infiltration, and weather-related influences. Thus, RC model parameters are not meant to be directly measured or calculated simply based on the construction details of buildings. The unknown parameters and inputs can be estimated through calibration with measured data (usually temperature states). [21, 22, 25].

RC model parameter estimation is typically an inverse optimization problem, which can be solved by various algorithms (e.g., genetic algorithms [38], least squares regression system identification [39], stochastic filtering [23], linear Kalman filter [40], extended Kalman filter [23], and unscented Kalman filter (UKF) [25]). Using extended Kalman filter and UKF with low-sampling-rate historical data, Baldi et al. [41] estimated the unknown states and parameters of a simple RC model. Later on, Li et al. [25] demonstrated the capability of UKF to jointly estimate the unknown states and model parameters in complex RC models representing real-life buildings.

Parameters can be obtained via offline estimation (i.e., batch) assuming the parameters are constant within the period of a set of collected measurements and using the measurements to estimate the parameter. This approach may result in inaccurate estimations and, consequently inaccurate predictions due to time-variant building physical conditions and occupant behaviors [42] [23, 24]. To address this issue, parameter estimation can be

conducted in an online manner (e.g., adaptive), in which the model parameters are updated continuously with new measurements in a computationally efficient manner [25] [43-45]. There are various online parameter estimation methods in the literature, including recursive least square [46], recursive prediction error minimization [47], linear Kalman filter, extended Kalman filter , and UKF. Numerous studies in the literature have employed the Kalman filter methods to demonstrate how RC models and the Kalman filter can work well together for online parameter estimations [25, 48]. In particular, Radecki et al. [48] demonstrated that temperature predictions are accurate when UKF is used to estimate the parameters of a multi-zone thermal RC model. Later on, a framework was proposed by Maasoumy et al. [49] for an online building model that simultaneously estimates the states and unknown parameters and continuously tunes the model parameters. In another study, extended Kalman filter was applied to an RC model of a passive house [23] to create an online thermal model that can accurately predict indoor temperature states.

In terms of paper organization, Section 2.2, presents a method for online parameter-input estimation of building RC models. The method uses UKF integrated with nonlinear least squares (NLS). Section 2.3, demonstrates and evaluates the newly developed method in two examples: one simple made-up RC model (made-up parameters and inputs, and states simulated using the model) and one complex RC model with real-life data (unknown parameters, and measured inputs and states). Through these two examples, the capability of the developed method is evaluated for estimating unknown model parameters and inputs in different scenarios with different numbers of available temperature states. A conclusion section is present after Section 2.4.

2.2 Problem Statement and Methodology

In practice, some inputs of a building thermal system can be unavailable, immeasurable, or difficult to measure for various reasons, as mentioned earlier in the Introduction Therefore, there is a need to estimate both unknown RC model parameters and inputs. One approach to doing so is to use available system temperature state measurements. Furthermore, it is not often that all the system states are measured and/or can be easily measured, and thus some of them may also be unknown. Accordingly, this study develops a feasible method that can be used to estimate model parameters and unknown inputs with possibly missing states, as illustrated in Figure 2.1. The missing states can also be simultaneously estimated by the proposed method. The development of a suitable model structure (i.e., number of temperature nodes, inputs, R, C, and their connections) is beyond the scope of this study and, therefore, will not be discussed in this paper. After obtaining a suitable model structure, the RC model parameters, inputs, and possibly unavailable states are estimated using a UKF-based parameter-input estimation method integrated with NLS [50-52]. Specifically, the UKF is mainly used for parameter and state estimation, while the NLS is used to estimate unknown inputs. This section presents the two essential components of the developed method: (1) thermal dynamic modeling using RC models and (2) a parameter-input estimation method developed based on the integration of the UKF and NLS.

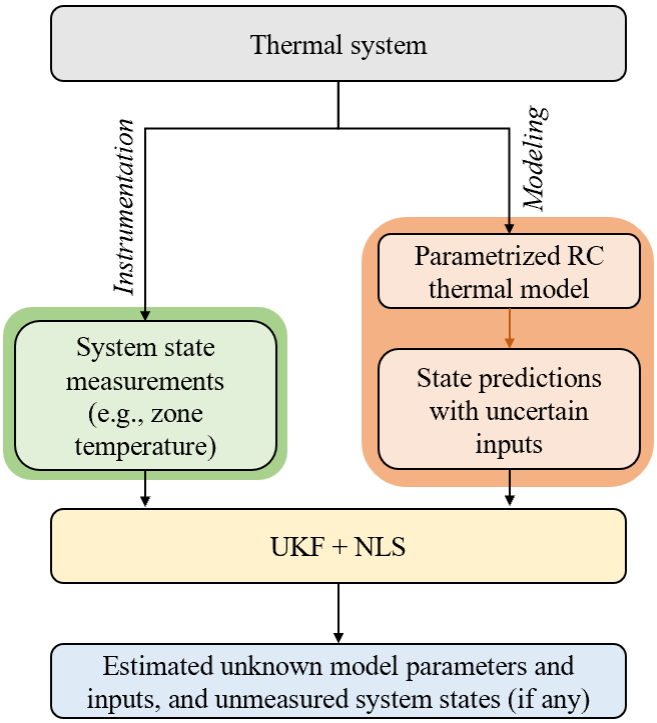

Figure 2.1 General procedure of the proposed parameter-input estimation method

2.2.1 Thermal dynamic modeling using RC models

In using an RC model to model the thermal dynamics of a building thermal zone, the temperature nodes within the zone can be represented by model nodes. Then the model nodes are connected to model parameters (i.e., R's and C's) and inputs (e.g., solar heat gain or mechanical heating/cooling supply). The model nodes are connected to each other through the R's. The parameters, inputs, and model nodes together create a thermal RC network. Running the RC model with inputs (i.e., simulation) will provide temperatures at the model

nodes (i.e., states). The thermal dynamics at each node can be presented by ordinary differential equations (ODEs). The typical equation for a node, say j^{th}, is shown in Eq. (2.1)

$$\frac{dT_j}{dt} = \frac{1}{C_j}\left(\sum_h \frac{T_h - T_j}{R_{h,j}} + \sum_j Q_j\right) \tag{2.1}$$

where, T_j represents the temperature of the j^{th} node, C_j is the thermal capacity associated with the j^{th} node, T_h shows the temperature of the h^{th} node adjacent to the j^{th} node, $R_{h,j}$ denotes the thermal resistance between the j^{th} and h^{th} nodes, and Q_j is the heat input to the j^{th} node, if any. A RC mode can be described by a system of continuous-time linear state ODEs, which can be represented in a matrix form as a shown in Eq. (2.2):

$$\dot{\boldsymbol{s}}(t) = \boldsymbol{A^c s}(t) + \boldsymbol{B^c u}(t) \tag{2.2}$$

where $\boldsymbol{s}$ represents a vector containing the nodal temperatures (i.e., temperature state T_j) of all nodes considered, $\boldsymbol{u}$ denotes for system inputs vector, $\dot{\boldsymbol{s}}$ is the first-order time derivative of the state vector $\boldsymbol{s}$, and $\boldsymbol{A^c}$ and $\boldsymbol{B^c}$ are the state and input matrices, respectively, defined by the model parameters. Note that the superscript *c* denotes a continuous-time model. Examples of Eqs. (2.1) and (2.2) can be found in Appendices A and B.

2.2.2 Parameter-input estimation method

This section describes the method for estimating unknown model parameters, inputs, and unmeasured states, if any, using the UKF integrated with NLS. The model parameters are grouped to form a vector of parameters, denoted by $\boldsymbol{\theta}$. The model parameters are assumed to be time-invariant in this study, but for estimation purposes, it is modeled as a random process [21, 25]. In order to adjust the method for dealing with cases in which information regarding one or more states is also unavailable/unmeasured in addition to the model parameters, the

state-parameter vector $\boldsymbol{x}$ at time *t* is defined by augmenting state vector $\boldsymbol{s}(t)$ (which includes all states of the thermal system) with the model parameter vector $\boldsymbol{\theta}(t)$, at time *t*, as shown in Eq. (2.3) [53]:

$$\boldsymbol{x}(\boldsymbol{t}) = [\boldsymbol{s}(\boldsymbol{t})\ \boldsymbol{\theta}(\boldsymbol{t})] \tag{2.3}$$

After considering additive process noise, which represents the estimation error, Eq. (2.3) can be transformed to a state-transition equation in state-space format shown in Eq. (2.4):

$$\dot{\boldsymbol{x}}(t) = \left[\dot{\boldsymbol{s}}(t)\ \dot{\boldsymbol{\theta}}(t)\right]$$

$$\dot{\boldsymbol{x}}(t) = f^{c}\left(\boldsymbol{x}(t), \boldsymbol{u}^{\boldsymbol{kn}}(t), \boldsymbol{u}^{\boldsymbol{un}}(t)\right) + \boldsymbol{w}^{c}(t) \tag{2.4}$$

$$f^{c}\left(\boldsymbol{x}(t), \boldsymbol{u}^{\boldsymbol{kn}}(t), \boldsymbol{u}^{\boldsymbol{un}}(t)\right) = \boldsymbol{A}^{\boldsymbol{cx}}\boldsymbol{x}(t) + \boldsymbol{B}^{\boldsymbol{cx}}\begin{bmatrix}\boldsymbol{u}^{\boldsymbol{kn}}(t)\\ \boldsymbol{u}^{\boldsymbol{un}}(t)\end{bmatrix}$$

where f^{c} represents the continuous-time nonlinear state function, and $\boldsymbol{u}^{\boldsymbol{kn}}$ and $\boldsymbol{u}^{\boldsymbol{un}}$ are the known and unknown input vectors, respectively. In addition, $\boldsymbol{w}^{\boldsymbol{c}}$ represents the process noise, which is assumed to be Gaussian white noise with zero mean and covariance matrix $\boldsymbol{G}$, and $\boldsymbol{A}^{\boldsymbol{cx}}$ and $\boldsymbol{B}^{\boldsymbol{cx}}$ are state and input matrices adjusted to the state-parameter vector as shown in Eq. (2.5):

$$\boldsymbol{A}^{cx} = \begin{bmatrix}\boldsymbol{A}^{c}{}_{n_s\times n_s} & 0_{n_s\times n_\theta}\\ 0_{n_\theta\times n_s} & 0_{n_\theta\times n_\theta}\end{bmatrix}_{n_x\times n_x} \qquad \boldsymbol{B}^{cx} = \begin{bmatrix}\boldsymbol{B}^{c}{}_{n_s\times n_u}\\ 0_{n_\theta\times n_u}\end{bmatrix}_{n_x\times n_u} \tag{2.5}$$

where n_s, n_θ, n_u, and n_x represent respectively the number of the states, model parameters, model inputs (including known and unknown), and state-parameter vector

components. Eq. (2.4) can be discretized by using the matrix exponential method [53], and become to Eq. (*2.6*):

$$\boldsymbol{x}_{k+1} = f\left(\boldsymbol{x}_k, \boldsymbol{u}_k^{kn}, \boldsymbol{u}_k^{un}\right) + \boldsymbol{w}_k$$
$$\text{where,} f\left(\boldsymbol{x}_k, \boldsymbol{u}_k^{kn}, \boldsymbol{u}_k^{un}\right) = \boldsymbol{A}^{\boldsymbol{dx}}\boldsymbol{x}_k + \boldsymbol{B}^{\boldsymbol{dx}}\begin{bmatrix}\boldsymbol{u}_k^{\boldsymbol{kn}} \\ \boldsymbol{u}_k^{\boldsymbol{un}}\end{bmatrix} \tag{2.6}$$

in which $\boldsymbol{x}_{k+1}$ is the state-parameter parameter vector at time step $(k+1)$, $\boldsymbol{u}_k^{\boldsymbol{kn}}$ and $\boldsymbol{u}_k^{\boldsymbol{un}}$ are the known and unknown input vectors at time step *k*. $\boldsymbol{A}^{dx}$ and $\boldsymbol{B}^{dx}$ in this equation are respectively derived from $\boldsymbol{A}^{cx}$ and $\boldsymbol{B}^{cx}$ to produce the discrete-time state and input matrices. $\boldsymbol{A}^{dx} = e^{\boldsymbol{A}cx\cdot\Delta t}$ and $\boldsymbol{B}^{\boldsymbol{dx}} = \Delta t\boldsymbol{A}^{dx}\boldsymbol{B}^{cx}$, with Δt being the time duration of a time step.

Corresponding measurements of the system states can be linked to predictions from the thermal dynamic model through the measurement equation shown in Eq.*(*2.7):

$$\boldsymbol{y}_{k+1} = h\left(\boldsymbol{x}_{k+1}, \boldsymbol{u}_{k+1}^{kn}, \boldsymbol{u}_{k+1}^{un}\right) + \boldsymbol{v}_{k+1}$$
$$h\left(\boldsymbol{x}_{k+1}, \boldsymbol{u}_{k+1}^{kn}, \boldsymbol{u}_{k+1}^{un}\right) = \boldsymbol{x}_{n,k+1} \tag{2.7}$$

in which $\boldsymbol{y}$ is the measurement vector, h is the nonlinear measurement function whose output is the predicted state vector corresponding to available measurements, v is the measurement noise modeled by Gaussian white noise with zero mean and covariance matrix $\boldsymbol{Z}$, $\boldsymbol{x}_{m,k+1}$ corresponds to the available measurements in the state-parameter vector with *m* representing the index of the measured states, and subscript k denotes the k^{th} step in the discrete-time ($k = 0, 1, \ldots, N-1,$ where N is the total number of data samples). [51]

Using discretely monitored system states (i.e., node temperatures) to estimate unknown thermal dynamic model parameters and inputs necessitates an estimation method dealing with the nonlinear discrete-time state-space model. In this regard, the UKF method is

selected for parameter and state estimation, because it has been proven to be robust and effective for highly nonlinear problems [26, 52]. Furthermore, to efficiently estimate the unknown model inputs, the NLS algorithm is integrated into UKF. The combination of UKF and NLS allows to estimate unknown model inputs and parameters, together with unmeasured states [50-52].

UKF is a Kalman-based technique, employing a prediction-correction two-step strategy based on unscented transformation (UT) [54]. In the prediction step, UT estimates the mean and covariance matrix of the nonlinear state function by evaluating the function using a set of deterministically selected points, known as sigma points (SPs). The unscented transformation requires a selection of $2n_x + 1$ SPs, where n_x is the dimension of the state-parameter vector [55]. Accordingly, SPs are calculated using Eq.(2.8):

$$\boldsymbol{\chi}_{k|k}^{(i)} = \begin{cases} \widehat{\boldsymbol{x}}_{k|k} & if\ i = 0 \\ \widehat{\boldsymbol{x}}_{k|k} + \left[\left(\gamma\sqrt{\widehat{\boldsymbol{P}}_{k|k}^{xx}}\right)_i\right]^T & if\ i = 1, \dots\dots, n_x \\ \widehat{\boldsymbol{x}}_{k|k} - \left[\left(\gamma\sqrt{\widehat{\boldsymbol{P}}_{k|k}^{xx}}\right)_i\right]^T & if\ i = n_x + 1, \dots\dots, 2n_x \end{cases} \tag{2.8}$$

where $\widehat{\boldsymbol{x}}$ and $\widehat{\boldsymbol{P}}^{xx}$ are the mean and covariance of the state-parameter vector, respectively, i denotes the i^{th} row of the corresponding matrix, and k is the k^{th} time step. The value in front of the vertical bar "|" indicates the time step of the prior estimate (prediction step) while the value after the "|" indicates the time step of the posterior estimate (correction step). Furthermore, $\gamma = \sqrt{n_x + \lambda}$ and $\lambda = \alpha^2(n_x + \kappa) - n_x$, in which α is a constant parameter related to the distribution of the SPs around the mean and κ is a secondary scaling parameter. In this paper, α and κ are assigned with 0.01 and 0, respectively [54].

By using the initially determined SPs (i.e., $\boldsymbol{\chi}_{k|k}$) in, a new set of SPs (i.e., $\boldsymbol{\chi}_{k+1|k}$) can be obtained by applying the $\boldsymbol{\chi}_{k|k}$ to the nonlinear state function:

By using the initially determined SPs (i.e., $\boldsymbol{\chi}_{k|k}$) in, a new set of SPs (i.e., $\boldsymbol{\chi}_{k+1|k}$) can be obtained by applying the $\boldsymbol{\chi}_{k|k}$ to the nonlinear state function:

$$\boldsymbol{\chi}_{k+1|k}^{(i)} = f\left(\boldsymbol{\chi}_{k|k}^{(i)}, \boldsymbol{u}_k^{kn}, \boldsymbol{u}_k^{un}\right) \tag{2.9}$$

With these propagated sigma points, prior estimates of the mean vector and the covariance matrix of the nonlinear state function at time step (k+1) can be obtained. However, in cases with unknown inputs in the nonlinear state function, model input estimation becomes a prerequisite for computing a new set of SPs (i.e., $\boldsymbol{\chi}_{k+1|k}$) based on Eq. (*2.10*). Therefore, it is essential to first estimate the unknown input. Using UKF alone to simultaneously estimate states, parameters, and inputs can be computationally demanding [26]. In this study, NLS is integrated into UKF to estimate the unknown model inputs. This integration reduces the number of SPs needed if UKF is used alone, thereby resulting in a more efficient estimation process. This integration not only adds efficiency to the estimation process but also improve the performance of the model [50, 52]. NLS algorithm numerically solves the resulting least-squares problem using gradient-based methods, such as the Levenberg Marquardt method, also known as the damped least-squares method [56]. The Levenberg-Marquardt method interpolates between the Gauss-Newton algorithm and the gradient descent method, which results in increasing the robustness of the approach in locating the global minimum in optimization problems [57].

In order to estimate the unknown model inputs, the developed method works as an optimization tool to minimize the estimation error (i.e., Δ_{k+1}) which is defined as the difference between the predicted mean of the measurement vector (i.e., $\widehat{\boldsymbol{y}}_{k+1|k}$), or in other words, the output of a measurement function h (i.e., SPs $\boldsymbol{\chi}_{m,k+1}^{(i)}$) and measurements ($\boldsymbol{y}_{k+1}$), as shown in Eq. (2.10):

$$\Delta_{k+1} = \boldsymbol{y}_{k+1} - \boldsymbol{\chi}_{m,k+1}^{(i)} \tag{2.10}$$

Therefore, by adjusting the unknown inputs for minimizing estimation error (i.e., Δ_{k+1}), which is the difference between the output of a measurement function and measurements, the estimated model input (i.e., $\boldsymbol{u}_{k+1}^{un(i)}$) is calculated. Accordingly, the final values of the estimated inputs equal:

$$\boldsymbol{u}_{k+1}^{un} = \frac{\sum_{i=0}^{2n_x} \boldsymbol{u}_{k+1}^{un(i)}}{2n_x+1} \tag{2.11}$$

SPs are defined to represent a nonlinear function. Weighting coefficients will be applied to them so they can be used to calculate the mean and covariance of the nonlinear function as shown in Eqs. (2.13) and (2.14). These weighting coefficients can be classified as $W_m^{(i)}$and $W_c^{(i)}$, where m and c correspond to the mean and covariance, respectively. These coefficients can be determined with Eq. (2.12)

:

$$W_m^{(0)} = \frac{\lambda}{n_x + \lambda} \tag{2.12}$$

$$W_c^{(0)} = \frac{\lambda}{n_x + \lambda} + (1 - \alpha^2 + \beta)$$

$$W_m^{(i)} = W_c^{(i)} = \frac{1}{2(n_x + \lambda)}, if\ i = 1, \dots\dots, 2n_x$$

where β is a factor used to emphasize the relative weight of each SPs. In this paper, β equals to 2 [54].

Once the unknown model input is estimated and SPs weighting coefficients are calculated, the prior estimates for the mean vector $\widehat{\boldsymbol{x}}$ and the covariance matrix $\widehat{\boldsymbol{P}}^{\boldsymbol{xx}}$ at time step $(k+1)$ can be determined using Eqs. (2.13) and (2.14).

$$\widehat{\boldsymbol{x}}_{k+1|k} = \sum_{i=0}^{2n_x} W_m^{(i)} \boldsymbol{\chi}_{k+1|k}^{(i)} \tag{2.13}$$

$$\widehat{\boldsymbol{P}}_{k+1|k}^{xx} = \sum_{i=0}^{2n_x} W_c^{(i)} [\boldsymbol{\chi}_{k+1|k}^{(i)} - \widehat{\boldsymbol{x}}_{k+1|k}][\boldsymbol{\chi}_{k+1|k}^{(i)} - \widehat{\boldsymbol{x}}_{k+1|k}]^T + \boldsymbol{G}_k \tag{2.14}$$

Then, the predicted mean and covariance matrices of the measurement vector at time step k +1 can be determined as follows:

$$\widehat{\boldsymbol{y}}_{k+1|k} = \sum_{i=0}^{2n_x} W_m^{(i)} \widehat{\boldsymbol{y}}_{k+1|k}^{(i)} \tag{2.15}$$

$$\widehat{\boldsymbol{P}}_{k+1|k}^{yy} = \sum_{i=0}^{2n_x} W_c^{(i)} [\widehat{\boldsymbol{y}}_{k+1|k}^{(i)} - \widehat{\boldsymbol{y}}_{k+1|k}] [\widehat{\boldsymbol{y}}_{k+1|k}^{(i)} - \widehat{\boldsymbol{y}}_{k+1|k}]^T + \boldsymbol{Z}_{k+1} \tag{2.16}$$

At time step $(k+1)$, the correction step is performed by integrating the measured response y_{k+1} with the posterior mean vector and covariance matrix of vector x_{k+1}, as illustrated in Eqs. (2.17) to (2.20):

$$\widehat{\boldsymbol{x}}_{k+1|k+1} = \widehat{\boldsymbol{x}}_{k+1|k} + \boldsymbol{K}_{k+1}(\boldsymbol{y}_{k+1} - \widehat{\boldsymbol{y}}_{k+1|k}) \tag{2.17}$$

$$\widehat{\boldsymbol{P}}^{xx}_{k+1|k+1} = \widehat{\boldsymbol{P}}^{xx}_{k+1|k} - \boldsymbol{K}_{k+1}\,\widehat{\boldsymbol{P}}^{yy}_{k+1|k}\boldsymbol{K}^{T}_{k+1} \tag{2.18}$$

where:

$$\boldsymbol{K}_{k+1} = \widehat{\boldsymbol{P}}^{xy}_{k+1|k}(\widehat{\boldsymbol{P}}^{yy}_{k+1|k})^{-1} \tag{2.19}$$

$$\widehat{\boldsymbol{P}}^{xy}_{k+1|k} = \sum_{i=0}^{2n_x} W_c^{(i)}[\boldsymbol{\chi}^{(i)}_{k+1} - \widehat{\boldsymbol{x}}_{k+1|k}][\widehat{\boldsymbol{y}}^{(i)}_{k+1|k} - \widehat{\boldsymbol{y}}_{k+1|k}]^{T} \tag{2.20}$$

in which $\widehat{\boldsymbol{P}}^{xy}_{k+1|k}$ is the cross-covariance matrix between the measurement vector and the state-parameter vector, and $\boldsymbol{K}_{k+1}$ is the Kalman gain.

To summarize, Figure 2.2 presents a flowchart for the developed method that can be used for parameter and inputs estimation in cases with unknown model inputs and unmeasured states.

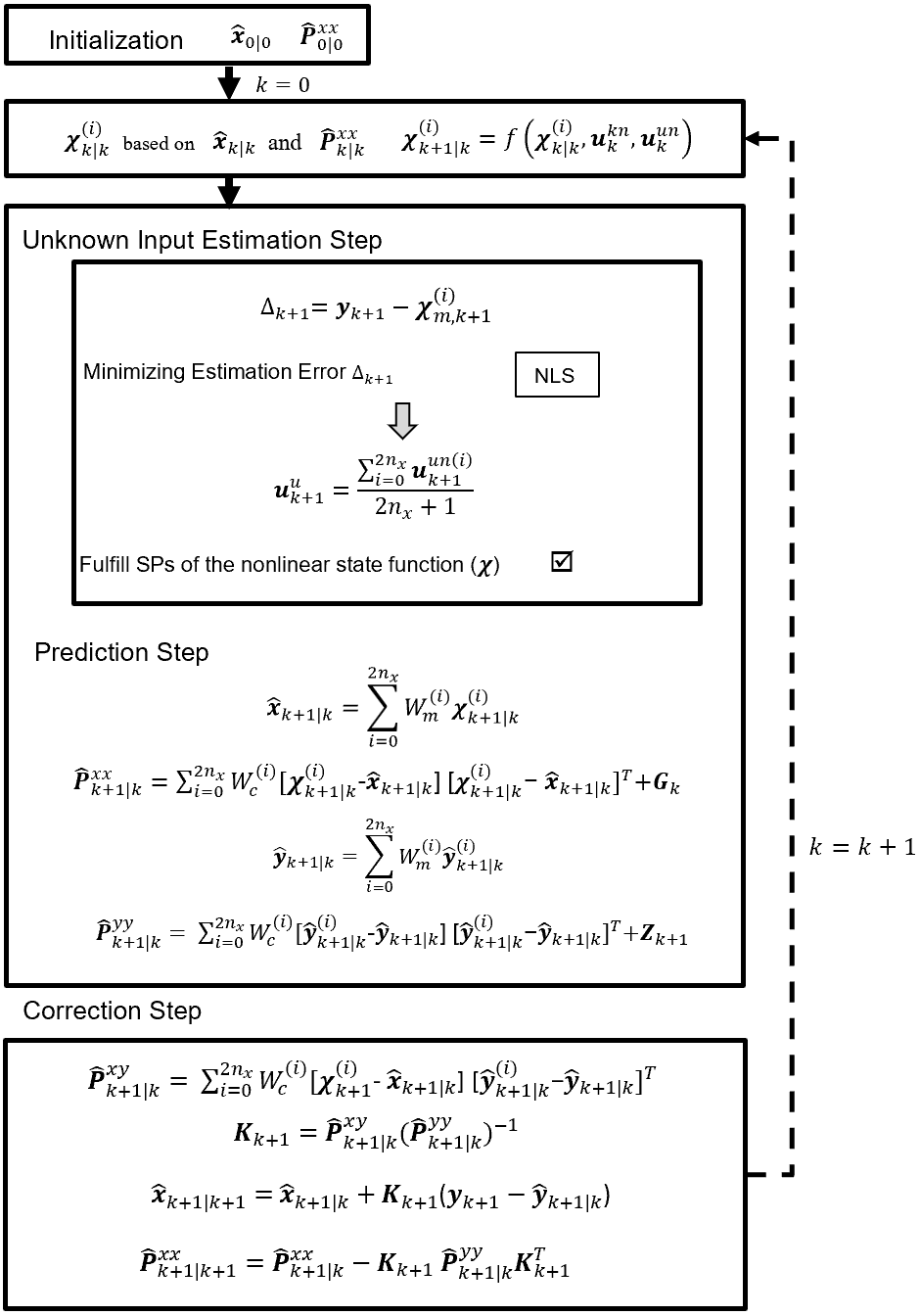

Figure 2.2 Parameter-input estimation method based on UKF integrated with NLS

2.3 Application Examples

Two case studies are presented in this section to illustrate and evaluate the developed method: (1) one simple made-up RC model consisting of two thermal resistors and two thermal capacitances (i.e., 2R2C), for which simulated responses are considered as measurements, and (2) one real-world single-family house with noticeably more complexity (10R6C) and real-world recorded data. The capability of the method is evaluated by comparing the estimated parameters, inputs, and states to the corresponding values in both study cases.

2.3.1 A simple case study

The made-up RC model, labelled as 2R2C, is shown in Figure 2.3. This model consists of four model parameters, two thermal resistors (i.e., R_2 and R_3 in $^{\circ C}/_{kW}$) and two thermal capacitors (i.e., C_2 and C_3 in $^{kWh}/_{^{\circ}C}$), as well as three model inputs: outdoor temperature T_1 in ℃, thermal load Q_1 in kW, and space heating and cooling supply Q_2 in kW.

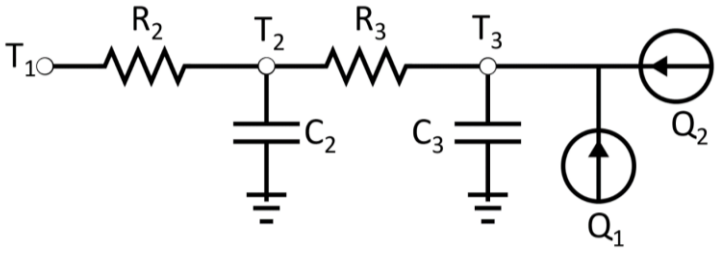

Figure 2.3 2R2C model

The ordinary differential equations of this RC model and three hourly made-up (referred to as "true") model inputs are shown in Appendix A, and the made-up (true) model parameters are shown in Eq. (2.21). To generate responses (i.e., states), the discrete-time linear state equations of the model are derived based on the true model parameters and then

run with made-up inputs. The simulated responses (i.e., temperature states) are considered the true states, and then they are contaminated by adding white Gaussian noise to generate measured states. The noise has a mean of zero and a standard deviation of 0.16 ℃, which is based on the expected accuracy of ±0.5 °C of the thermocouples used in real practice [58]. Hourly data [59] (true inputs, and states) are generated for one month (i.e., 720 hours). The first 540 hours of data are used for estimation and evaluation purposes, while the final 180 hours of data are employed to evaluate the prediction accuracy of the calibrated model, which uses the model parameters estimated at the end of the 540 hours estimation period.

$$\boldsymbol{\theta}_{\text{true}} = \left[R_{2\,\text{true}}\left({}^{\circ\text{C}}/_{\text{kW}}\right) \quad R_{3\,\text{true}}\left({}^{\circ\text{C}}/_{\text{kW}}\right) \quad C_{2\,\text{true}}\left({}^{\text{kWh}}/_{\circ\text{C}}\right) \quad C_{3\,\text{true}}\left({}^{\text{kWh}}/_{\circ\text{C}}\right)\right]^{T} \tag{2.21}$$

$$\boldsymbol{\theta}_{true} = [3.1 \quad 28.5 \quad 2.06 \quad 1.04]^{T} \in \mathbb{R}^{4\times 1}$$

Considering the contaminated responses as measurements, one parameter-input estimation scenario (2R2C-1) and two state-parameter-input estimation scenarios (2R2C-2 and 2R2C-3) are investigated, as summarized in Table 2.1. All model parameters and space heating and cooling supply (Q_2) are unknown in all scenarios. In Scenarios 2 and 3, one of the states (T_2 or T_3) is unknown in addition to the unknown model parameters and input and needs to be estimated.

Table 2.1 Different scenarios defined for the 2R2C model

Scenario	Available states	Unavailable states	Unknown input
2R2C-1	T_2, T_3	None	Q_2
2R2C-2	T_2	T_3	Q_2

2R2C-3	T_3	T_2	Q_2

The state vector of this RC model is defined by $\boldsymbol{s} = [T_2 \quad T_3]^T \in \mathbb{R}^{2\times1}$, model parameters vector is $\boldsymbol{\theta} = [R_2 \quad R_3 \quad C_2 \quad C_3]^T \in \mathbb{R}^{4\times1}$, and the model inputs vector is $\boldsymbol{u} = [\boldsymbol{u^{kn}} \quad \boldsymbol{u^{un}}]^T \in \mathbb{R}^{3\times1}$ which $\boldsymbol{u^{kn}} = [T_1 \quad Q_1]^T$ and $\boldsymbol{u^{un}} = [Q_2]$ .The initial mean estimation of the state-parameter vector, $\hat{\boldsymbol{x}}$, is presented in Eq. (2.22) :

$$\hat{\boldsymbol{x}}_{0|0} = \left[\hat{\boldsymbol{s}}_{0|0} \quad \hat{\boldsymbol{\theta}}_{0|0}\right]^T \in \mathbb{R}^{6\times1}$$
$$\hat{\boldsymbol{s}}_{0|0} = [21 \quad 30]^T \tag{2.22}$$
$$\hat{\boldsymbol{\theta}}_{0|0} = [4.45 \quad 26.35 \quad 2.64 \quad 1.2]^T$$

Since the states and parameters of the RC model are assumed to be uncorrelated, the initial covariance matrix $\hat{\boldsymbol{P}}^{\boldsymbol{xx}}_{\boldsymbol{0|0}}$ is diagonal. The diagonal terms of the initial covariance matrix are determined by $(\hat{\boldsymbol{P}}^{xx}_{0|0})_{\text{states}} = [1.0 \times (\hat{\boldsymbol{s}}_{0|0})]^2$ for the states ($\boldsymbol{s}$). In addition, the diagonal terms of the initial covariance matrix for the model parameters ($\boldsymbol{\theta}$) are defined using $(\hat{\boldsymbol{P}}^{xx}_{0|0})_{\text{parameters}} = [0.05 \times (\hat{\boldsymbol{\theta}}_{0|0})]^2$. The measurement noise covariance matrix is diagonal, time-invariant, and equal to $\boldsymbol{Z} = (0.3°\text{C})^2$. Similarly, the process noise covariance matrix is diagonal, time-invariant, and equal to $\boldsymbol{G} = [1 \times 10^{-5} \times \hat{\boldsymbol{x}}_{0|0}]^2$. The values for initial covariance matrices and process noise covariance matrix are calculated based on references [26, 53].

Figure 2.4 presents the time histories of model parameter estimation for Scenario 2R2C-1, where all the states are measured. In these figures, the dashed black line shows true model parameter values, the red line shows the mean estimate. The shaded grey area shows

the mean +/- two standard deviations obtained from the covariance matrix $\widehat{\boldsymbol{P}}_{k|k}^{xx}$. As shown in Figure 2.4 (a), the thermal resistance parameters R_2 and R_3 are estimated accurately and converged near their true values. Similar estimation results for the thermal capacitances C_2 and C_3 are shown in Figure 2.4 (b). The estimated model parameters' standard deviation is higher at the beginning of the estimation history, indicating a higher level of uncertainty in these values initially. While the estimated model parameters may be sufficiently accurate, they may not reach their true values. This difference is due to the presence of nonlinearity in the system and measurement noise. Nonlinearity can introduce complexities in the input-output relationship, leading to potential numerical errors in the estimation results [60, 61]. It should be emphasized that the model parameter estimation results for Scenarios 2R2C-2 and 2R2C-3 are also converged but are not shown here for brevity. The final estimated model parameters for these scenarios can be found in Appendix A.

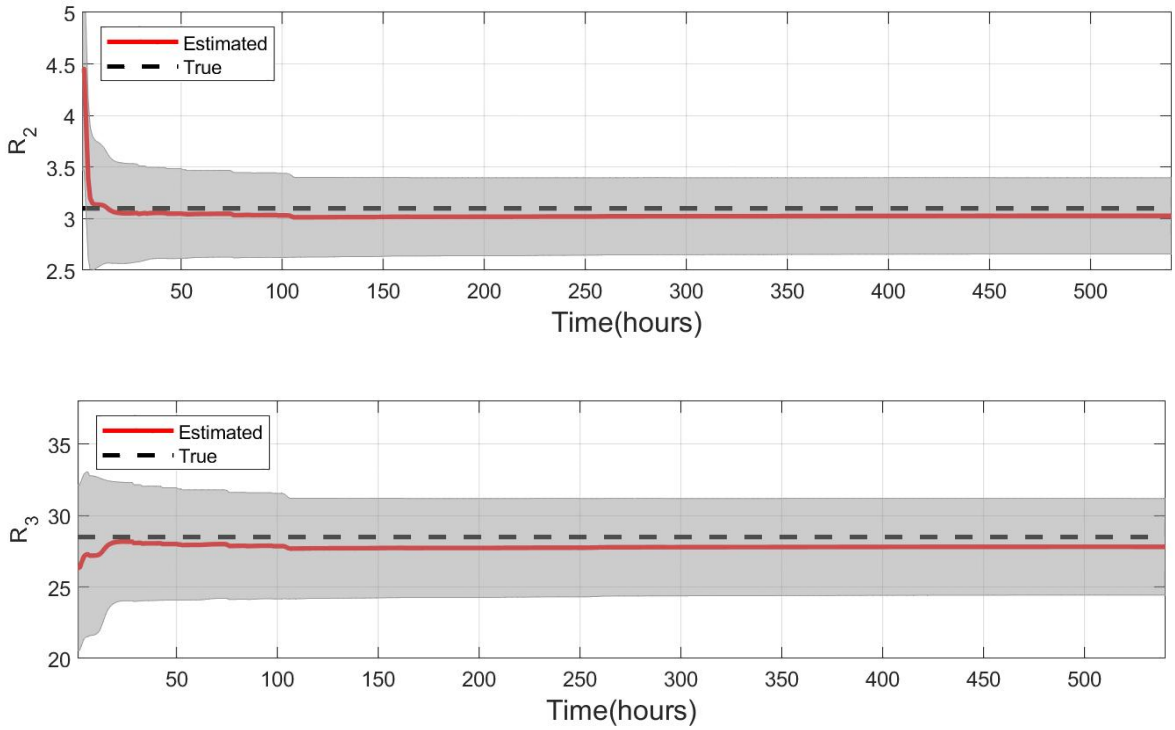

(a)

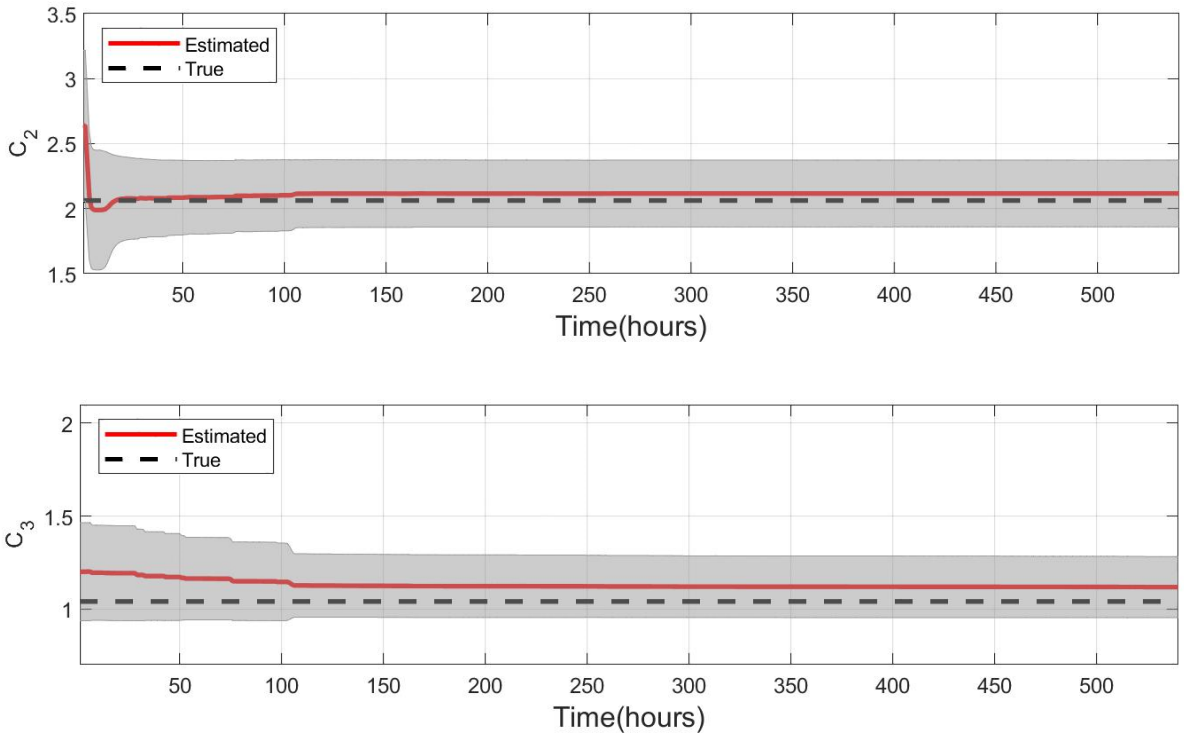

(b)

Figure 2.4 Time histories of model parameter estimations for Scenario 2R2C-1: (a) thermal resistance, and (b) thermal capacitances

Figure 2.5 presents the estimation history of the unknown model input Q_2 compared to its true value in Scenario 2R2C-1. To better illustrate the estimation results, the 540 hours of time histories are divided into three 180-hour segments, of which the first segment is shown in Figure 2.5 and the rest are shown in Appendix A. These results reaffirm that the developed method can accurately estimate the unknown model input. Furthermore, to provide a quantitative comparison, Mean Absolute Percentage Error (MAPE), a measure of precision for constructing fitted time series values when trend estimation is involved [62], is used in this study, as defined by Eq.(2.23):

$$\text{MAPE} = \left(\frac{\sum_{i=1}^{n}\left|\frac{True_i - Calculated_i}{True_i}\right|}{n}\right) \times 100(\%) \tag{2.23}$$

where *True* represents the true value, *Calculated* is the predicted or estimated value, and *n* shows the number of data points. MAPE of model input estimation in Scenario 2R2C-1 is 1.1%, indicating that the developed method can accurately estimate the model input.

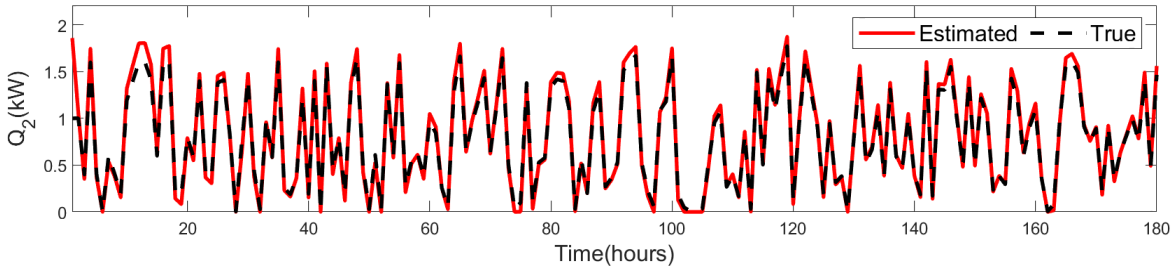

Figure 2.5 Comparison between true and estimated model input for Scenario 2R2C-1

Using the developed method, parameters, input, and states are estimated at each timestep of the estimation period. Figure 2.6 compares the estimated and the true profiles of the two states of the 2R2C model (i.e., T_2 and T_3) in the Scenario 2R2C-1. The MAPE of the estimated state and the true one for both temperatures are 0.4% and 0.82% for T_2 and T_3, respectively, which indicates excellent agreement between the estimated results and the corresponding true states. The accuracy of the estimated T_3 is not as high as that for T_2. This is due to the unknown input, Q_2, in the estimation period being linked to T_3, as shown in Figure 2.3. Figure 2.4 to Figure *2.6* also show that the developed method is able to estimate the parameters, inputs, and states relatively accurate within the first few time steps. This observation indicates the suitability of the method for on-line estimations.

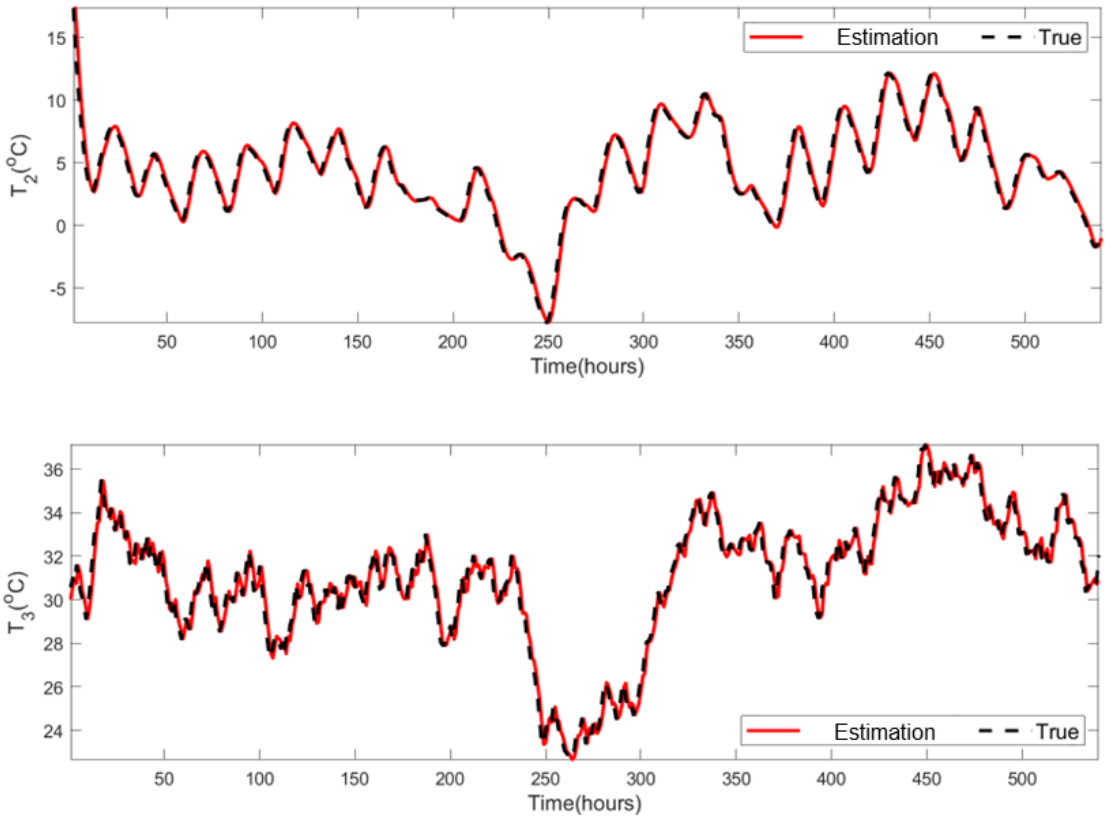

Figure 2.6 Comparison between true and estimated temperature responses for Scenario 2R2C-1

The MAPE value for the estimated model input and states for all scenarios is shown in Table 2.2. The MAPE for the estimated model input in Scenarios 2R2C-2 and 2R2C-3 is slightly higher than that of Scenario 2R2C-1. Additionally, the MAPE of the estimated states for Scenarios 2R2C-2 and 2R2C-3 is also higher but less than 2.5%. These observations reaffirm that more known measurements can result in a more accurate estimation.

Table 2.2 MAPE of estimated input and states for scenarios for 2R2C-2 and 2R2C-3

MAPE	2R2C-1	2R2C-2 (T_2 available)	2R2C-3 (T_3 available)
Q_2	1.1%	2.12%	1.36%
T_2	0.4%	1.83%	2.16%

T_3	0.82%	2.32%	1.26%

Using the parameters obtained at the end of the 540-hour estimation period, the RC models are used to simulate the states in the prediction period (with known inputs). The predicted temperature responses are generated at each time step, hourly from hours 541 to 720. Figure 2.7 compares the predicted temperature responses for Scenario 2R2C-1. It can be observed that both temperature responses T_2 and T_3 are predicted with good accuracy, with the MAPE values being 0.92% and 2.55%, respectively. Again, the accuracy of the predicted response for T_3 is not as high as that for T_2, due to the unknown input, Q_2, in the estimation period linked to T_3, as shown in Figure 2.3. This comparison indicates that the inaccuracy in the parameter estimation will not result in a significant error in states prediction; therefore, the developed method is sufficient for the analysis of building thermal dynamics when all states are measured.

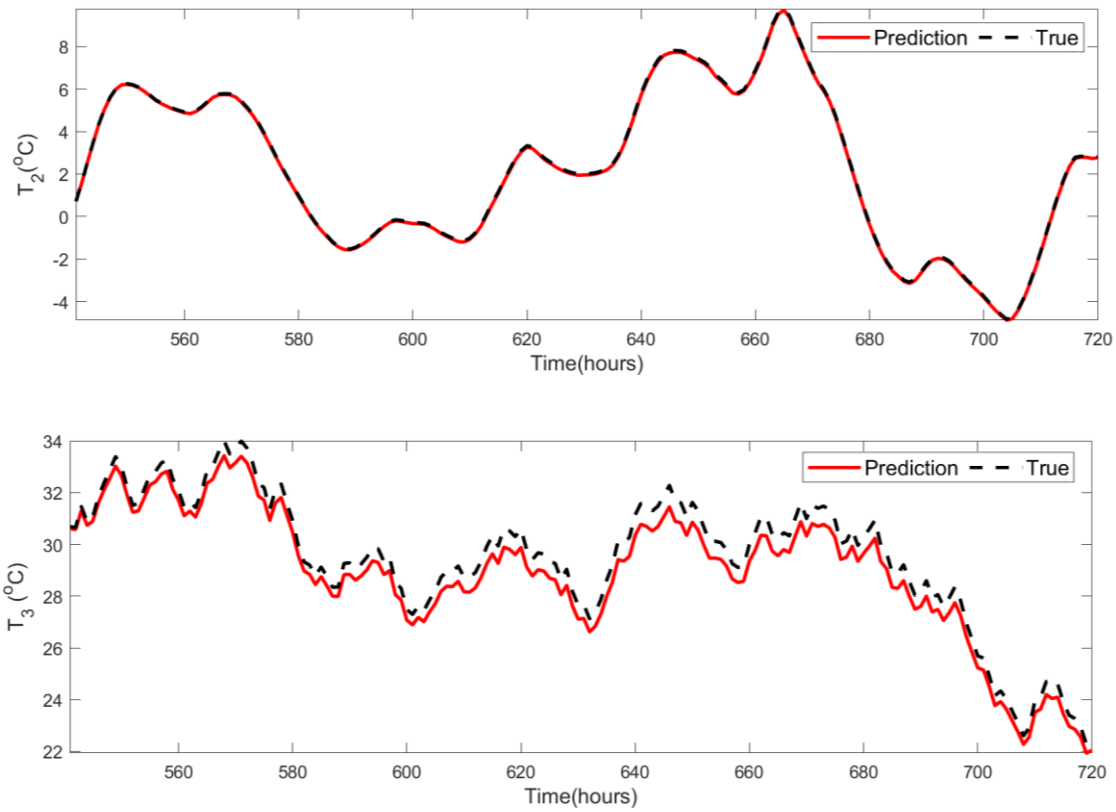

Figure 2.7 Comparison between true and predicted temperature responses for scenario 2R2C-1

Furthermore, the MAPE values calculated for both states in Scenarios 2R2C-2 and 2R2C-3 are found to be less than 5 %, as shown in Table 2.3. These values indicate that the prediction results are acceptable, even when certain state measurements are unavailable. The impact of the quantity of unavailable state measurements will be further investigated in the following real-world case study.

Table 2.3 MAPE of predicted states for scenarios 2R2C-2 and 2R2C-3

MAPE	2R2C-1	2R2C-2	2R2C-3
T_2	0.92%	3.91%	4.41%

T_3	2.55%	4.92%	3.05%

2.3.2 A Case study with real-world data

In this section, the developed method is tested on a real-world low-energy wooden-frame house in Eastman, Quebec, Canada, shown in Figure 2.8 [38]. The study uses 720 hours of measured data. The first 540 hours of data, organized on an hourly basis, are designated as the estimation dataset, and the remainder as the prediction dataset. Various scenarios are defined based on the availability of different state measurements. Accordingly, the effectiveness of the developed method is evaluated by 1) comparing the estimated values of states and input with their measured (true) values in the estimation dataset, and 2) by comparing the predicted responses obtained using the final estimated model parameters with the measured responses in the prediction dataset.

Figure 2.8 A Single-detached house as a case study [38]

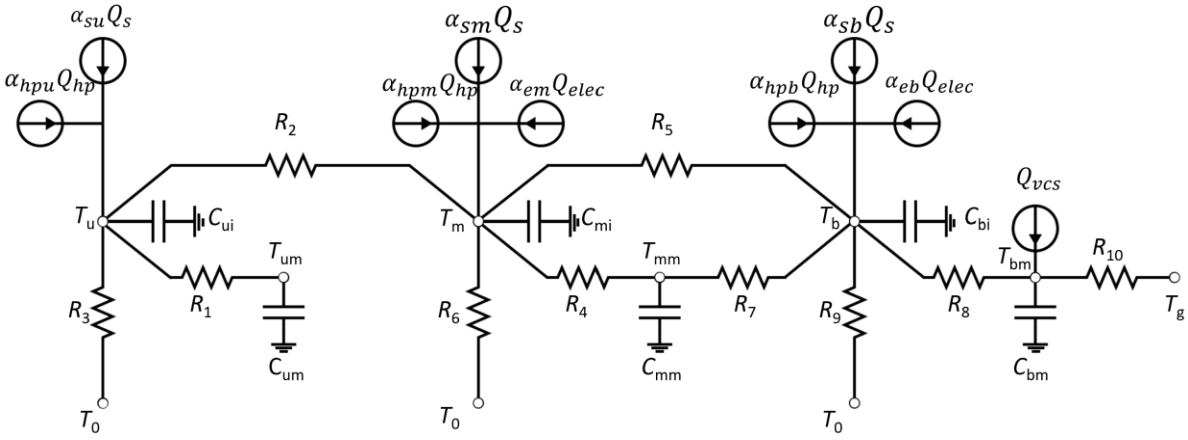

Figure 2.9 RC model Structure for the single detached house

The RC model structure of the detached single-family house shown in Figure 2.9 was developed by Wang et al. [38]. In this RC model, the basement, second floor, and main floor are labeled as *b*, *u*, and *m*, respectively. This RC model is called 10R6C, as it consists of 10

thermal resistances and 6 thermal capacitances, T_m, and T_b in °C represents the zone temperature of the second floor, main floor, and basement, respectively. T_{um}, T_{mm}, and T_{bm} are the internal thermal mass temperature responses, which were not measured. The ODEs of this RC model are shown in Appendix B.

The hourly model inputs for this RC thermal model are shown in Appendix B. The model inputs include 1) global irradiation Q_s in kW per unit area on the south facade, which is used to obtain approximate effective solar heat gains weighted by solar gain factors (α_s), and 2) heating supply from the geothermal heat pump Q_{hp} in kW, which is, considered as the unknown model input. This heating supply is distributed across three levels using the distribution factor α_{hp}. 3) T_g is the ground temperature, which is approximately 13 °C constant. 4) T_0 is the outdoor temperature in °C. 5) Q_{elec} is the gross electricity demand in kW, which is used to calculate internal heat gains weighted according to internal gain factors (α_e). 6) Q_{vcs} in kW is the thermal energy charged to the slab located in the basement.

The state vector of this RC model can be defined by $\boldsymbol{s} = [T_u, T_{um}, T_m, T_{mm}, T_b, T_{bm}]^T \in \mathbb{R}^{6\times1}$, model inputs vector $\boldsymbol{u} = [\boldsymbol{u}^{kn} \quad \boldsymbol{u}^{un}]^T \in \mathbb{R}^{6\times1}$, known input vector $\boldsymbol{u}^{kn} = [T_0, T_g, Q_s, Q_{elec}, Q_{vcs}]^T$, and unknown input vector $\boldsymbol{u}^{un} = [Q_{hp}]$. The state-parameter vector can also be expressed as Eq. (2.24), , where $\boldsymbol{s}$ is the previously described state vector and $\boldsymbol{\theta}$ is the unknown model parameters:

$$\boldsymbol{x} = [\boldsymbol{s} \quad \boldsymbol{\theta}]^T \in \mathbb{R}^{30\times1} \tag{2.24}$$

$$\boldsymbol{\theta} = \left[R^T \quad C^T \quad F_s^T \quad p_e^T \quad \alpha_{hp}^T\right]^T \in \mathbb{R}^{24\times1} \tag{2.25}$$

where $\boldsymbol{R} = [R_1 \quad R_2 \quad R_3 \quad R_4 \quad R_5 \quad R_6 \quad R_7 \quad R_8 \quad R_9 \quad R_{10}]^T \in \mathbb{R}^{10\times1}$, in $^{\circ C}/_{kW}$, and $\boldsymbol{C} = [C_{ui} \quad C_{um} \quad C_{mi} \quad C_{mm} \quad C_{bi} \quad C_{bm}]^T \in \mathbb{R}^{6\times1}$, in $^{kWh}/_{\circ C}$. Additionally, the solar

gain factors are $\boldsymbol{\alpha_s} = [\alpha_{su} \quad \alpha_{sm} \quad \alpha_{sb}]^T \in \mathbb{R}^{3\times1}$, in m^2, and the internal gain factors are $\boldsymbol{\alpha_e} = [\alpha_{em} \quad \alpha_{eb}]^T \in \mathbb{R}^{2\times1}$,. The heating power distribution factor for the second floor, main floor, and basement are $\boldsymbol{\alpha_{hp}} = [\alpha_{hpu} \quad \alpha_{hpm} \quad \alpha_{hpb}]^T \in \mathbb{R}^{3\times1}$, respectively, which should satisfy:

$$\sum_{i=u,m,b} \alpha_{hpi} = 1 \tag{2.26}$$

To evaluate the performance of the developed method, this study considered various scenarios with different available measured temperature responses, as shown in Table 2.4. Scenario 10R6C-1 has all three-room temperature state measurements (T_u, T_m, T_b). Interior thermal mass temperature states (T_{um}, T_{mm}, T_{bm}) are not available in all scenarios.

Table 2.4 Different scenarios for the 10R6C model

Scenarios	Available states	Unavailable states	Unknown Input
10R6C-1	T_u, T_m, T_b	None	Q_{hp}
10R6C-2	T_u, T_m	T_b	Q_{hp}
10R6C-3	T_u, T_b	T_m	Q_{hp}
10R6C-4	T_m, T_b	T_u	Q_{hp}
10R6C-5	T_u	T_m, T_b	Q_{hp}
10R6C-6	T_m	T_u, T_b	Q_{hp}
10R6C-7	T_b	T_u, T_m	Q_{hp}

In the estimation phase, the initial mean estimates for the state-parameter vector can be expressed as follows:

$$\hat{\boldsymbol{x}}_{0|0} = \left[\hat{\boldsymbol{s}}_{0|0} \quad \hat{\boldsymbol{\theta}}_{0|0}\right]^T \tag{2.27}$$

where,

$$\hat{\boldsymbol{s}}_{0|0} = [22 \quad 21.3 \quad 21.1 \quad 22.5 \quad 21.2 \quad 20.5][\text{unit: ℃}]$$

$$\widehat{\boldsymbol{\theta}}_{0|0} = \left[\widehat{\boldsymbol{R}}^T_{0|0} \quad \widehat{\boldsymbol{C}}^T_{0|0} \quad \hat{\alpha}^T_{s\,0|0} \quad \hat{\alpha}^T_{e\,0|0} \quad \widehat{\boldsymbol{\alpha}}^T_{hp\,0|0}\right]^T$$

$$\widehat{\boldsymbol{R}}_{0|0} = [1.36 \quad 1.69 \quad 20.7 \quad 2.4 \quad 4.98 \quad 35.25 \quad 12.75 \quad 2.49 \quad 29.59 \quad 16.13]$$

$$[\text{unit: } {}^{\circ\text{C}}/_{\text{kW}}]$$

$$\widehat{\boldsymbol{C}}_{0|0} = [1.42 \quad 2.67 \quad 2.60 \quad 25.67 \quad 3.74 \quad 9.06]\ [\text{unit: } {}^{\text{kWh}}/_{\circ\text{C}}] \tag{2.28}$$

$$\widehat{\boldsymbol{\alpha}}_{s\,0|0} = [1.83 \quad 2.93 \quad 1.51]^T \quad [\text{unit: m}^2]$$

$$\widehat{\boldsymbol{\alpha}}_{e\,0|0} = [0.50 \quad 0.14]^T \quad [\text{unit: } --]$$

$$\widehat{\boldsymbol{a}}_{hp\,0|0} = [0.25 \quad 0.38 \quad 0.35]^T \quad [\text{unit: } --]$$

As explained in the case study of a simple RC model, the diagonal terms for the states ($\boldsymbol{s}$) of the initial covariance matrix are selected as $(\widehat{\boldsymbol{P}}^{\text{xx}}_{0|0})_{states} = [1.0 \times (\hat{\boldsymbol{s}}_{0|0})]^2$, $(\widehat{\boldsymbol{P}}^{\text{xx}}_{0|0})_{\text{parameters}} = [0.05 \times (\widehat{\boldsymbol{\theta}}_{0|0})]^2$, $\boldsymbol{R} = (0.3°\text{C})^2$ and $\boldsymbol{G} = [1 \times 10^{-5} \times \hat{\boldsymbol{x}}_{0|0}]^2$, respectively.

The results of the estimation of model parameters, including thermal resistances ($\boldsymbol{R}$), thermal capacitances ($\boldsymbol{C}$), solar gain factors ($\boldsymbol{\alpha}_s$), internal gain factors ($\boldsymbol{\alpha}_e$), and heating power distribution factors ($\boldsymbol{\alpha}_{hp}$), for Scenario 10R6C-1, are presented in Appendix B. These results show convergence in some of the thermal resistances and capacitances. No clear convergence trend is observed for the solar gain factors, internal gain factors, and heating power distribution factors. But in general, the variations in the values are small. The variations over the estimated time are due to the constant changes of building conditions, such as closed-open windows or blinds, on-off ventilation systems, and moving furniture.

The performance of the developed method in estimating the model input is demonstrated in Figure 2.10, which compares the estimated model input Q_{hp} to its true value

in Scenario 10R6C-1. To illustrate the estimation results more clearly, the 540 hours of time histories are divided into three 180-hour segments, of which the first segment is shown in Figure 2.10 and the remaining are shown in Appendix B. The MAPE of estimated input is about 10%. Notably, there are specific time periods where Q_{hp} experiences both overestimations and underestimations. A significant contributor to these fluctuations in input estimation can be the global irradiation on the south facade of the house. Elevated levels of irradiation, particularly during the early morning and late afternoon when the sun is not positioned directly in front of the house, tend to result in overestimation. Consequently, these overestimations may introduce errors in the model's parameter estimation during these specific time periods.

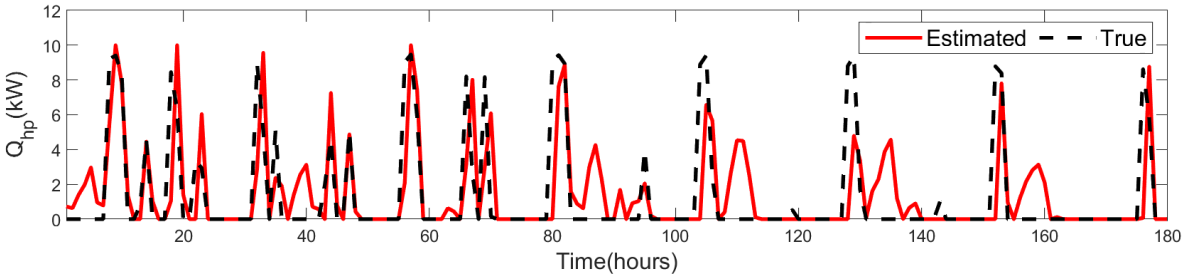

Figure 2.10 Comparison between true and estimated model input for Scenario 10R6C-1

Figure 2.11 compares the estimated and true temperature response histories for Scenario 10R6C-1. The MAPE of the estimated states (T_u, T_m, and T_b) and the corresponding measured (true) values is less than 2% for the three available measurements. indicating a strong agreement between the estimated and the true states. The maximum difference is approximately 1°C. These comparisons demonstrate that the developed method can be effectively applied to real-time temperature prediction for real-world practices.

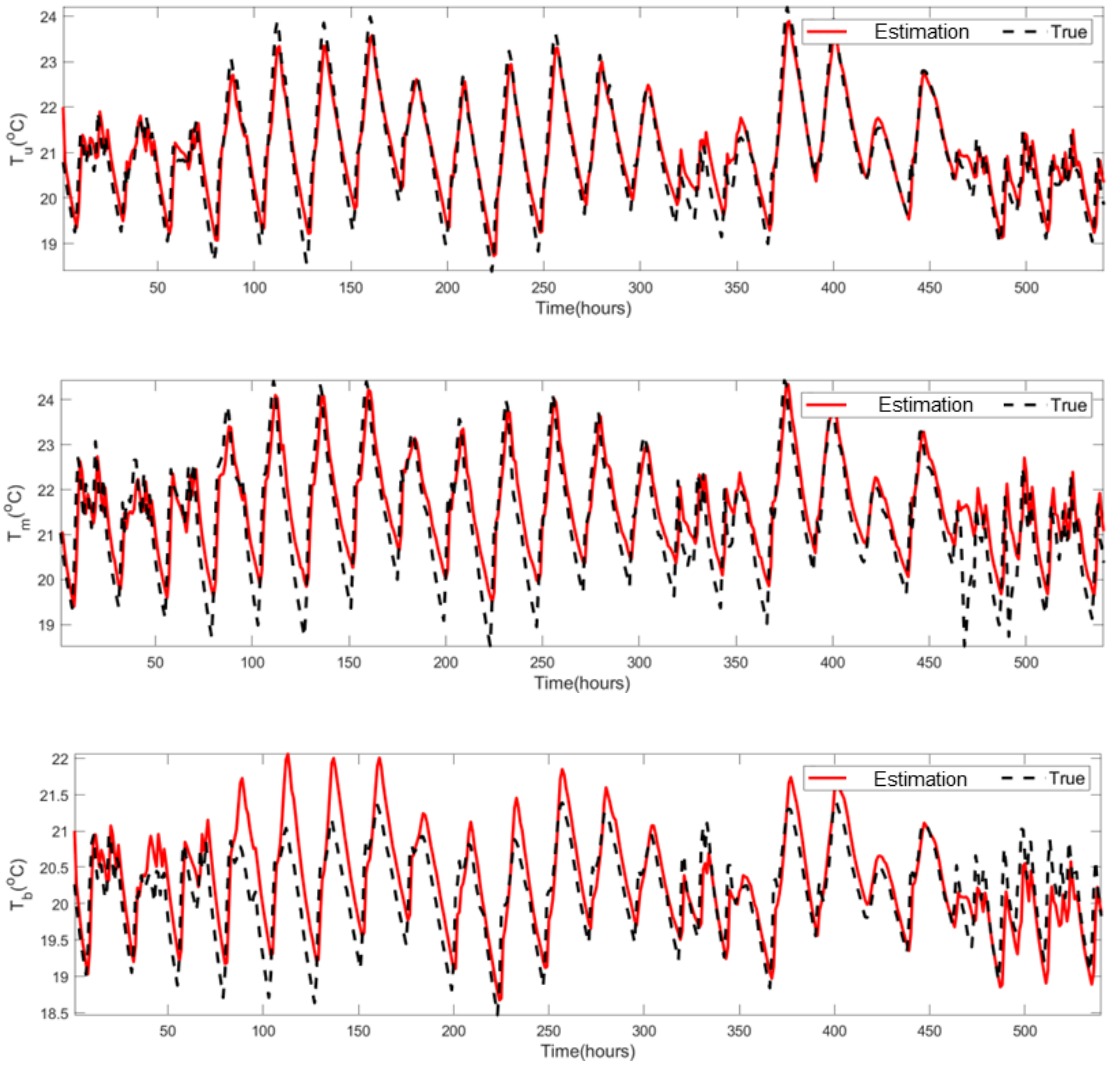

Figure 2.11 Comparison between true and estimated temperature responses for Scenario10R6C-1

Table 2. displays estimation results for the unknown input for all scenarios. Since the maximum MAPE difference between Scenario 10R6C-1 and the other scenarios is only about 4%, it can be concluded that the developed method can estimate the unknown model input with acceptable accuracy even when there are limited available measurements. Additionally, Table 2. displays the MAPEs of state estimation of temperature responses and their true values for the seven scenarios. The difference between Scenario 10R6C-1 with three available measurements and scenarios with only one measurement is approximately 2%, which proves

that when sparse measurements (one or two measurements) are available and included in the estimation process, the state estimation can still be accurate. This observation evaluates the robustness and excellent agreement of both measured and unmeasured responses. Additionally, this verifies that the developed method is suitable for application in buildings where only a limited number of temperature responses can be measured. It is worth noting that the estimation profiles of Scenario 10R6C-3 selected as an example of a scenario with a limited number of temperature responses are shown in Appendix B – Real-world case study information and results for parameter-input estimations, other scenarios are not shown for brevity.

Table 2.5 MAPE of the estimated model input and states for all scenarios of 10R6C

	Scenarios						
MAPE of Estimation	10R6C-1	10R6C-2	10R6C-3	10R6C-4	10R6C-5	10R6C-6	10R6C-7
Q_{hp}	10.38%	12.13%	11.74%	12.36%	14.32%	13.42%	14.03%
T_u	0.82%	1.54%	1.62%	2.12%	3.26%	2.75%	2.95%
T_m	1.13%	1.32%	1.73%	1.45%	3.54%	2.68%	2.74%
T_b	1.58%	1.91%	1.23%	2.01%	3.38%	2.94%	2.65%

To show the performance of the calibrated RC model for temperature state prediction, Figure 2.12 compares the measured temperature responses from the prediction dataset to those predicted responses using the parameters obtained at the end of the 540-hour estimation period, the RC models are used to simulate the states in the prediction period. Predicted temperature responses are computed at each hourly time step within the time span from hour

541 to 720. The MAPE in the predicted state and measured temperature responses is around 2.5% for each available measurement, indicating that the measured and predicted temperatures are in excellent agreement. This also indicates that the error in estimating the input is acceptable because it doesn't cause a significant error in the parameter estimation and state prediction. Table 2. presents the MAPEs of the measured temperatures and predicted states based on the final estimated model parameters derived from the estimation dataset for all scenarios. All MAPE values are less than 5.2%. The accurate predictions of future states reflected by Figure 2.12 and Table 2. indicate that the model parameters were effectively estimated even with a limited number of missing state measurements.

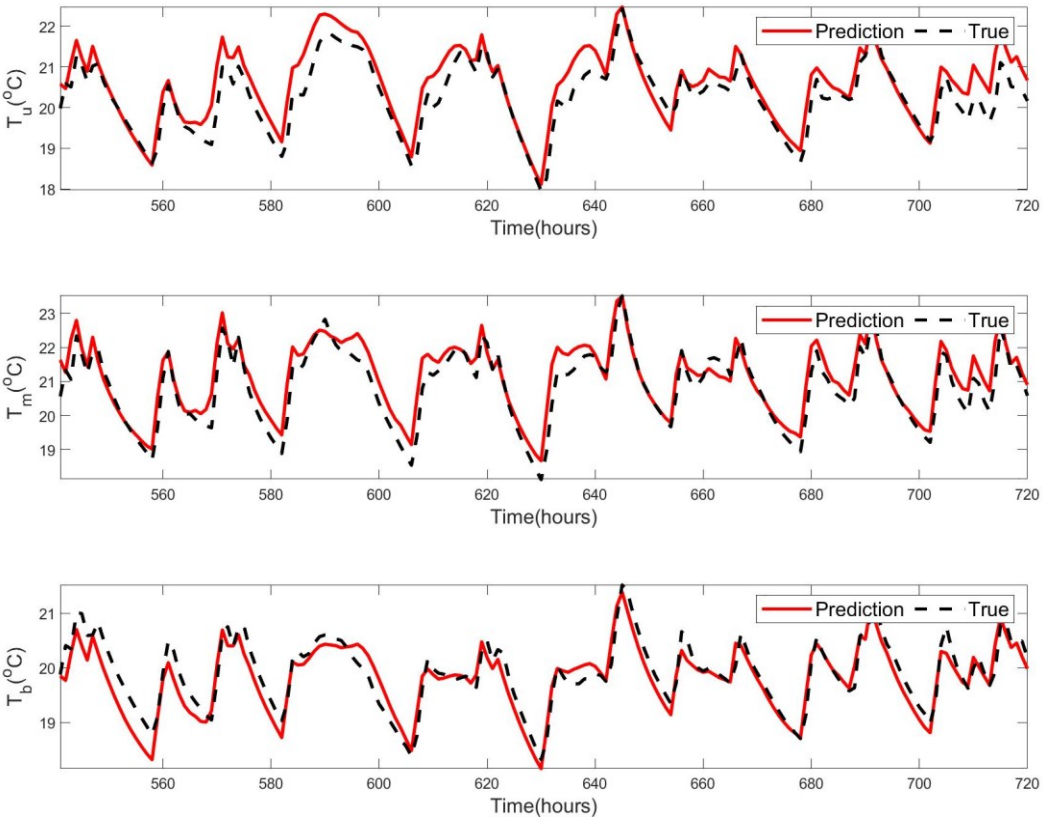

Figure 2.12 Comparison between true and predicted temperature responses for Scenario 10R6C-1

Table 2.6 MAPE of the predicted responses for the 10R6C model in different scenarios

	Scenarios						
MAPE of Prediction	10R6C-1	10R6C-2	10R6C-3	10R6C-4	10R6C-5	10R6C-6	10R6C-7
T_u	2.74%	4.14%	4.11%	4.46%	4.69%	4.87%	4.79%
T_m	2.18%	3.92%	4.21%	4.12%	4.76%	4.36%	5.2%
T_b	2.53%	4.18%	3.82%	4.25%	5.12%	5.03%	4.55%

RC model parameters plays crucial roles, as they can be used to interpret a building's thermal properties [38] and be used in RC thermal models to predict future states. Table 2. summarizes the estimated model parameters at the final time step for all seven scenarios. It can be seen that even with certain missing state measurements, the final estimated parameter values for each scenario are relatively consistent.

Table 2.7 Final estimated parameters in different scenarios for the 10R6C model

	Scenarios							Max error compared to 10R6C-1 %
Parameters	10R6C-1	10R6C-2	10R6C-3	10R6C-4	10R6C-5	10R6C-6	10R6C-7	
R_1	1.32	1.27	1.30	1.38	1.39	1.38	1.36	5%
R_2	1.59	1.57	1.76	1.63	1.72	1.65	1.68	11%
R_3	19.06	18.52	17.72	14.48	14.74	12.87	18.13	32%
R_4	2.78	2.71	2.67	2.79	2.53	2.66	2.42	13%
R_5	5.26	5.06	5.44	5.51	4.98	5.02	5.06	5%
R_6	26.35	18.96	30.41	29.07	30.31	27.51	31.51	28%
R_7	12.49	12.69	12.34	12.49	12.76	12.77	12.9	3%
R_8	2.42	2.48	2.39	2.42	2.48	2.49	2.47	3%
R_9	20.62	23.18	20.55	20.73	26.92	25.62	26.31	31%

R_{10}	13.72	14.37	13.44	13.70	15.20	14.78	14.81	11%
C_{ui}	1.39	1.40	1.39	1.35	1.35	1.36	1.42	3%
C_{um}	2.37	2.46	2.21	2.47	2.44	2.57	2.67	13%
C_{mi}	2.16	1.95	2.52	2.35	2.46	2.21	2.60	20%
C_{mm}	25.96	25.32	25.99	24.87	26.56	25.86	26.47	4%
C_{bi}	3.74	3.66	3.67	3.83	3.71	3.66	3.52	6%
C_{bm}	9.62	9.36	9.92	9.68	9.11	9.03	9.08	6%
α_{su}	1.97	1.78	2.06	2.01	1.80	1.80	1.75	11%
α_{sm}	3.05	2.83	3.05	3.26	2.81	2.83	2.69	12%
α_{sb}	1.22	1.43	1.13	1.14	1.46	1.46	1.38	20%
α_{em}	0.37	0.39	0.43	0.4	0.45	0.42	0.45	22%
α_{eb}	0.13	0.13	0.14	0.14	0.14	0.14	0.13	8%
α_{hpb}	0.35	0.32	0.34	0.35	0.34	0.33	0.36	9%
α_{hpm}	0.40	0.40	0.37	0.39	0.38	0.40	0.36	10%
α_{hpu}	0.23	0.25	0.26	0.24	0.26	0.25	0.25	13%

2.4 Conclusion

Previous research focused on developing methods for model parameter estimation with all model inputs available. This study developed an effective method for estimating RC model parameters and inputs with possible unmeasured temperature states. In this regard, the thermal resistor-capacitor network (RC) is used for thermal dynamic modeling and the unscented Kalman filter (UKF) is integrated with the nonlinear least squares (NLS) method to estimate unknown model parameters and inputs. In order to show the applicability of the developed method, two case studies were conducted: one with made-up data and the other with real-world data. Scenarios with different numbers of available temperature measurements are created to evaluate the capability and performance of the developed method in different circumstances.

The estimated model input and states are compared with their true values. The estimated model inputs in all scenarios of the case study with made-up data have a MAPE (Mean Absolute Percentage Error) less than 2.5%, while less than 14.5% in the scenarios of the case

study with real-world data. Furthermore, comparing model predictions with the true measurements in all scenarios of both case studies shows a maximum MAPE of approximately 5%. These low MAPE values prove that the developed method can effectively estimate unknown model parameters, input, and possible missing states.

3 Heating and Cooling Supply Estimation to Control Temperature Using RC Thermal Model, Unscented Kalman Filter, and Nonlinear Least Square Method

3.1 Introduction

Buildings are responsible for consuming approximately 40% of the world's energy [34]. Hence, it is essential to decrease the energy usage of buildings in order to align with worldwide sustainability objectives [35]. Efforts to decrease buildings' energy consumption involve development and deployment of building energy management systems equipped with control systems that can effectively optimize the energy usage in buildings[6]. Studies suggest that the utilization of these control systems can lead to a notable reduction of up to 30% in building energy consumption [36, 63]. Control systems necessitate thermal dynamic models and estimation methods to estimate heating and cooling supply required for temperature control purposes.

Control systems are widely considered a promising algorithm for achieving energy efficiency in smart buildings [64]. These control systems rely on dynamic and simplified building energy models that describe the thermal behavior of buildings [65]. Various modeling strategies, such as “white box,” “black box,” and “gray box” modeling, have been developed in the literature. [10, 11].

White-box modeling, also known as physics-based modeling, involves describing building dynamics based on construction information and utilizes parameters derived from comprehensive technical documentation, such as geometry, material properties, and equipment specifications [14, 66]. Although white-box modeling can provide accurate simulations of building dynamics, the model's inflexibility may limit its ability to account for

changes and variations over time. As a result, applying white-box models in control systems can be challenging [67, 68]. Conversely, black-box modeling employs pure mathematical machine-learning techniques, such as Artificial Neural Networks, to establish relationships between input and output data without relying on explicit physics-based knowledge [37, 69]. This modeling approach can offer higher precision than white-box modeling but demands a substantial amount of data to build an accurate model [67, 70]. However, employing black-box modeling in control systems can be difficult due to its data-intensive nature, potential lack of interpretability [71].

Gray box modeling, such as thermal resistor-capacitor network (RC), is rooted in a physics-based structure and utilizes mathematical optimization techniques to estimate the model's equivalent physical parameters [18]. This approach combines the advantages of both white-box modeling to eliminate outliers and black-box modeling to reduce the need for detailed information [18]. By striking a well-balanced compromise between interpretability and accuracy, gray box models prove highly suitable for integration into control systems [42]. [42]. RC models are based on a set of equivalent model parameters, resistors (R's) and capacitors (C's), to relate system inputs (e.g., heating and cooling supply) and temperature states. The gray-box modeling approach has been widely used for thermal dynamic modeling. [18, 24, 42]. To develop a reliable control system besides having a reliable thermal dynamic model, a dependable estimation technique is required that can be integrated with RC models to accurately estimate behavior of building systems, particularly for estimating heating and cooling supply (i.e., RC model input).

The successful implementation of control systems relies on the precise controlling of future building’s temperature states with estimation of building systems behavior (i.e., heating

and cooling supply). This is because these estimations directly impact the building's performance and energy efficiency [42]. For instance, in heating, ventilation, and air conditioning systems, inaccurate estimation of supply can cause excessive heating or cooling supply, resulting in increased energy consumption, and operating costs. Such inaccuracies in estimation of building systems behavior (i.e., heating and cooling supply) can significantly affect overall building performance [72]. Therefore, reliable estimation methods should be integrated as part of control systems in addition to thermal models. One such method is Unscented Kalman filter (UKF) which is widely used in estimation problems [21, 25]. As a result, this paper aims to develop an approach for buildings control applications that utilizes the UKF-based estimation technique in combination with RC models to estimate the heating and cooling supply, for controlling the temperature of thermal zones.

In terms of paper organization, Section 3.2, presents a method for combining thermal dynamic models with an estimation method for control systems. This involves a description of the RC models used for thermal dynamic modeling, as well as the UKF integrated by the Nonlinear Least-Square (NLS) as an estimation method. Section 3.3, two application examples will be provided to demonstrate the use of the developed method: The first example will use a made-up simple RC model (made-up parameters and inputs, and states simulated using the model), while the second example will use a complex RC model with real-life data. These examples will test the capability of the developed method in estimating heating and cooling supply for temperature control purposes.

3.2 Problem Statement and Methodology

Controlling temperature in thermal zones can present significant challenges, particularly when estimating and planning the heating and cooling supply. This challenge becomes even

more pronounced when dealing with multiple interconnected zones, each with varying temperatures, as it requires estimating the temperature of uncontrolled zones within the network. To ensure a precise estimation of the required supply for a specific zone, it is crucial to consider the temperatures of other interconnected zones. To achieve this, a method as shown in Figure 3.1 can be developed that can estimate the necessary mechanical supply (i.e., RC model input), based on the expected temperature set points. The developed method utilizes a defined RC thermal dynamic model to represent a thermal system, such as one or multiple thermal zones. To estimate the required mechanical supply of a thermal system represented by an RC thermal model, several additional variables need to be considered. These include the uncontrolled zone temperature which is measured for the current step and estimated for the rest, as well as the temperature set point, which needs to be defined based on the desired temperature level. Additionally, other boundary conditions, such as outdoor temperature and solar irradiation, must be considered. These boundary conditions are measured for the current time and predicted for the rest of the controlling dataset. Accordingly, the method involves the use of RC models and UKF and NLS estimation methods to estimate the necessary mechanical supply for controlling the temperature of different zones.

In this section, thermal dynamic modeling employing RC models will be discussed, followed by the estimation method based on the integration of the UKF and NLS. The UKF is used to estimate the temperatures of the uncontrolled zones, while the NLS is employed to estimate the required heating and cooling supply. It is worth noting that this method operates recursively, allowing it to update itself with new measurements and estimate the heating and cooling supply based on recent data. This adaptive capability enables the tool to adjust to new information, such as outdoor temperature or solar irradiance, and calculate the necessary

adjustments to maintain the desired temperature in the designated zones. As such, this tool can continuously monitor and update its estimates to ensure optimal performance and energy efficiency.

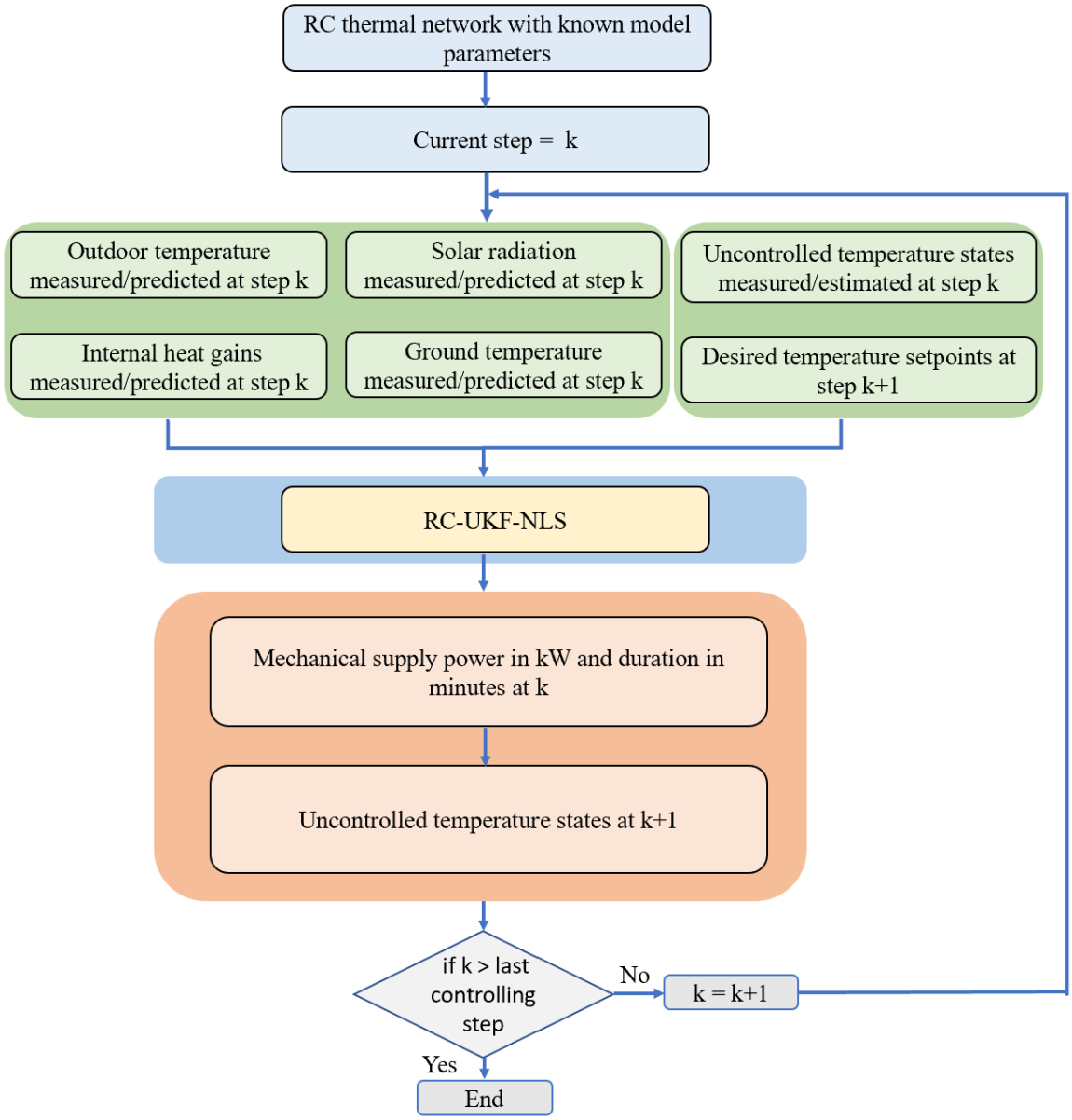

Figure 3.1 General Procedure of mechanical supply estimation to control temperature

3.2.1 Thermal dynamic modeling using RC Models

In modeling the thermal dynamics of a building, the RC model is utilized to represent temperature nodes within the building's thermal zones. Each temperature node is connected to model parameters (represented by R's and C's) and inputs (such as solar heat gain or mechanical heating/cooling supply). These interconnected model nodes form an RC thermal model, where the connections between nodes are represented by R's. The parameters, inputs, and model nodes together create a thermal RC model. Running the RC model with inputs (i.e., simulation) will provide temperatures at the model nodes (i.e., states). The thermal dynamics at each node can be presented by ordinary differential equations (ODEs). The typical equation for a node, say j^{th}, is shown in Eq. (3.1):

$$\frac{dT_j}{dt} = \frac{1}{C_j}\left(\sum_h \frac{T_h - T_j}{R_{h,j}} + \sum_j Q_j\right) \tag{3.1}$$

where Q_j denotes the j^{th} heat input into the j^{th} node (e.g., heating and cooling supply); T_j shows the temperature of the j^{th} node; T_h represents the temperature of the h^{th}node adjacent to the j^{th}node; C_j is the thermal capacity attached to the j^{th} node; and the thermal resistance between the j^{th} and h^{th} node is denoted by $R_{h,j}$. The continuous time linear state equation shown in Eq. (3.2) can be used to calculate the thermal dynamics of a building in matrix form based on these ODEs:

$$\dot{\boldsymbol{s}}(t) = \boldsymbol{A^c s}(t) + \boldsymbol{B^c u}(t) \tag{3.2}$$

where $\boldsymbol{A^c}$ and $\boldsymbol{B^c}$ are the state and input matrices respectively and are defined by the model parameters vector ($\boldsymbol{\theta}$), $\boldsymbol{s}$ denotes the nodal temperatures or states, $\dot{\boldsymbol{s}}$ is the time derivative of the state vector $\boldsymbol{s}$, and model inputs are represented by $\boldsymbol{u}$ including both known and the ones that need to be estimated, and c stands for a model with a continuous time model.

3.2.2 Model input (e.g., heating and cooling supply) estimation method

This section describes the method for estimating unknown model inputs, and uncontrolled temperature states, using the UKF integrated with NLS. Eq. (3.2) can be written as a continues nonlinear state equation in the presence of additive process noise shown in Eq. (3.3):

$$\dot{\boldsymbol{s}}(t) = f^c\left(\boldsymbol{s}(t), \boldsymbol{\theta}, \boldsymbol{u^{kn}}(t), \boldsymbol{u^{un}}(t)\right) + \boldsymbol{w}^c(t)$$
$$\text{Where } f^c\left(\boldsymbol{s}(t), \boldsymbol{\theta}, \boldsymbol{u^{kn}}(t), \boldsymbol{u^{un}}(t)\right) = \boldsymbol{A^c s}(t) + \boldsymbol{B^c}\begin{bmatrix}\boldsymbol{u^{kn}}(t)\\ \boldsymbol{u^{un}}(t)\end{bmatrix} \tag{3.3}$$

where f^c represents the continuous time nonlinear state function, $\boldsymbol{s}, \boldsymbol{\theta}, \boldsymbol{u^{kn}}$ and $\boldsymbol{u^{un}}$ are model states, parameters, and known and unknown (i.e., need to be estimated) model inputs vectors respectively. Moreover, $\boldsymbol{w}^c$ expresses process noise and assumed Gaussian white noise with zero mean and covariance matrix $\boldsymbol{G}$. Then, Eq. (3.3) can be transformed to discrete time (e.g., using the matrix exponential method [53]) as below:

$$\boldsymbol{s}_{k+1} = f\left(\boldsymbol{s}_k, \boldsymbol{\theta}, \boldsymbol{u}_k^{kn}, \boldsymbol{u}_k^{un}\right) + \boldsymbol{w}_k$$
$$f\left(\boldsymbol{s}_k, \boldsymbol{\theta}, \boldsymbol{u}_k^{kn}, \boldsymbol{u}_k^{un}\right) = \boldsymbol{A^d x}_k + \boldsymbol{B^d}\begin{bmatrix}\boldsymbol{u_k^{kn}}\\ \boldsymbol{u_k^{un}}\end{bmatrix} \tag{3.4}$$

where $\boldsymbol{s}_{k+1}$ (i.e., nodal temperatures) are the states at the time step $(k+1)$; $\boldsymbol{A}^d$ and $\boldsymbol{B}^d$ are derived from $\boldsymbol{A}^c$ and $\boldsymbol{B}^c$ to produce the discrete-time state and input matrices, respectively. which $\boldsymbol{A}^d = e^{\boldsymbol{Ac}.\Delta t}$ and $\boldsymbol{B}^d = \Delta t.\ \boldsymbol{A}^d.\ \boldsymbol{B}^c$, e stands for the matrix exponential and Δt is the time step.

In the estimation method, measurements of thermal dynamic model responses (i.e., defined set points or controlled zone's temperature) can be linked to the model prediction through the measurement equation, shown in Eq. (3.5):

$$\begin{aligned} \boldsymbol{y}_{k+1} = \ & h\left(\boldsymbol{s}_{k+1}, \boldsymbol{\theta}, \boldsymbol{u}_{k+1}^{kn}, \boldsymbol{u}_{k+1}^{un}\right) + \boldsymbol{v}_{k+1} \\ & h\left(\boldsymbol{s}_{k+1}, \boldsymbol{\theta}, \boldsymbol{u}_{k+1}^{kn}, \boldsymbol{u}_{k+1}^{un}\right) = \boldsymbol{s}_{m,k+1} \end{aligned} \tag{3.5}$$

in which h^c is continues time nonlinear response function**,** $\boldsymbol{y}$ is the measured or controlled temperature and $\boldsymbol{v^c}$ is the measurement noise, modeled by Gaussian white noise with zero mean and covariance matrix $\boldsymbol{Z}$, $\boldsymbol{s}_{m,k+1}$ corresponds to those temperature nodes that are controlled in the state vector where subscript *m* represents the index of controlled temperature in the state vector, and subscript k denotes the k^{th} step in the discrete time ($k = 0, 1, \dots, N - 1$, where N is the total number of data samples). It is worth noting that those temperature states that do not need to be controlled are not included in the $\boldsymbol{s}_{m,k+1}$ vector. To estimate the heating and cooling supply in order to control the system states (i.e., zone's temperatures), an estimation method requires that be compatible with a discrete nonlinear model. In this study, the UKF integrated with NLS methods is utilized to address this problem. This approach has been chosen because it has been demonstrated to be robust in a variety of nonlinear estimation problems [26, 50-52].

UKF is a Kalman-based technique that combines a measurement-based correction strategy with a prediction strategy based on unscented transformation (UT). In the prediction step, UKF utilizes UT to estimate the mean and covariance matrix of a nonlinear function by evaluating a nonlinear function of a set of deterministically selected points, known as sigma

points (SPs). The UT requires the selection of $2n_s + 1$ SPs (where n_s is the dimension of the state vector). Accordingly, SPs are calculated utilizing Eq. (3.6):

$$\boldsymbol{S}_{k|k}^{(i)} = \begin{cases} \hat{\boldsymbol{s}}_{k|k} & if\ i = 0 \\ \hat{\boldsymbol{s}}_{k|k} + \left[\left(\gamma\sqrt{\hat{P}_{k|k}^{ss}}\right)_i\right]^T & if\ i = 1, \dots\dots, n_s \\ \hat{\boldsymbol{s}}_{k|k} - \left[\left(\gamma\sqrt{\hat{P}_{k|k}^{ss}}\right)_i\right]^T & if\ i = n_s + 1, \dots\dots, 2n_s \end{cases} \tag{3.6}$$

where the state vector's mean and covariance are denoted by $\hat{s}$ and $\hat{P}^{ss}$, respectively. i represents the i^{th} row of the matrix inside the parentheses, k represents the time step which the value in front of the vertical bar "|" indicates the time step of the prior estimate (prediction step) while the value after the "|" indicates the time step of the posterior estimate (correction step). Furthermore, $\gamma = \sqrt{n_s + \lambda}$, $\lambda = \alpha^2(n_s + \kappa) - n_s$, α is a constant relating to the spread of the sigma points around the mean, and κ is a secondary scaling parameter. In this paper, α and κ are assigned with 0.01 and 0, respectively [54].

By using the initially determined SPs (i.e.,$\boldsymbol{S}_{k|k}$) in the k^{th} step to evaluate in the prediction step, a new set of SPs ($\boldsymbol{S}_{k+1|k}$) can be developed with a nonlinear state function:

$$\boldsymbol{S}_{k+1|k}^{(i)} = f\left(\boldsymbol{S}_{k|k}^{(i)}, \boldsymbol{\theta}, \boldsymbol{u}_k^{kn}, \boldsymbol{u}_k^{un}\right) \tag{3.7}$$

With these propagated sigma points, prior estimates of the mean vector and the covariance matrix of the nonlinear state function at time step (k+1) can be obtained. However, as the state function includes model inputs that need to be estimated, estimation of these inputs becomes a prerequisite for calculating a new set of SPs (i.e., $\boldsymbol{S}_{k+1|k}$). Consequently, it is necessary to initially estimate the model inputs. In this study, UKF is integrated with NLS to estimate the model inputs based on defined temperature set points. The integration of UKF

and NLS is utilized to improve the accuracy and efficiency of estimating unknown inputs of the model. This combination is particularly useful in situations where the model input is unavailable or uncertain. Additionally, while UKF is a powerful tool for state and model input estimation, it can be computationally demanding when used alone, leading to long computation times [26]. The incorporation of NLS optimization techniques can reduce computational costs and improve the efficiency of the estimation process by reducing the number of SPs needed if UKF is used alone. The reduced computational burden allows for faster processing times, making it a valuable tool in real-time applications [50, 51]. Overall, the integration of UKF and NLS provides an effective approach for improving the accuracy and computational efficiency of input and state estimation in various scenarios. NLS algorithm numerically solves the resulting least-squares problem by using gradient-based methods, such as the Levenberg-Marquardt method. The Levenberg-Marquardt method is a well-known optimization algorithm, also known as the damped least-squares method [56], which interpolates between the Gauss-Newton algorithm and the gradient descent method. This improves the robustness of the approach and increases the chances of locating the global minimum in optimization problems [57].

In order to estimate heating and cooling supplies (i.e., model inputs), NLS works as an optimization tool to minimize the estimation error. In particular, the estimation error (i.e., Δ_{k+1}) is defined as the difference between the output of a measurement function h (i.e. SPs $\boldsymbol{S}_{m,k+1}^{(i)}$) and defined temperature setpoints ($\boldsymbol{y}_{k+1}$), as shown in Eq. (3.8):

$$\Delta_{k+1} = \boldsymbol{y}_{k+1} - \boldsymbol{S}_{m,k+1}^{(i)} \tag{3.8}$$

Therefore, adjusting the unknown inputs for minimizing estimation error (i.e., Δ_{k+1}), which is the difference between the output of a measurement function and measurements, the estimated model input (i.e., $\boldsymbol{u}_{k+1}^{un(i)}$) is calculated. Accordingly, the final value of the estimated input equals:

$$\boldsymbol{u}_{k+1}^{un} = \frac{\sum_{i=0}^{2n_s} \boldsymbol{u}_{k+1}^{un(i)}}{2n_s + 1} \tag{3.9}$$

SPs are intended to represent a nonlinear function, which necessitates weighting coefficients to calculate the mean and covariance of the nonlinear function as shown in Eqs. (3.9) and (3.10). They categorized as $W_m^{(i)}$ and $W_c^{(i)}$, where *m* and *c* correspond, respectively, to the mean and covariance. These coefficients can be determined with Eq. (3.10):

$$\begin{gathered} W_m^{(0)} = \frac{\lambda}{n_s + \lambda} \\ W_c^{(0)} = \frac{\lambda}{n_s + \lambda} + (1 - \alpha^2 + \beta) \\ W_m^{(i)} = W_c^{(i)} = \frac{1}{2(n_s + \lambda)}, if\ i = 1, \dots, 2n_s \end{gathered} \tag{3.10}$$

where β is a factor used to emphasize the relative weight of each SPs. In this paper, β equals to 2 [54].

Once the model inputs are estimated and SPs weighting coefficients are determined, the prior estimates for the mean vector $\hat{\boldsymbol{s}}$ and covariance matrix $\widehat{\boldsymbol{P}}^{\boldsymbol{ss}}$at the time $(k+1)$, can be calculated as follows:

$$\hat{\boldsymbol{s}}_{k+1|k} = \sum_{i=0}^{2n_s} W_m^{(i)} \boldsymbol{S}_{k+1|k}^{(i)} \tag{3.7}$$

$$\widehat{\boldsymbol{P}}_{k+1|k}^{ss} = \sum_{i=0}^{2n_s} W_c^{(i)} [\boldsymbol{S}_{k+1|k}^{(i)} - \hat{\boldsymbol{s}}_{k+1|k}][\boldsymbol{S}_{k+1|k}^{(i)} - \hat{\boldsymbol{s}}_{k+1|k}]^T + \boldsymbol{G}_k \tag{3.8}$$

Then predicted mean and covariance matrices of the measurement vector at time step $k+1$ can be calculated as shown in Eqs. (3.9) and (3.10), in which covariance matrix of the measurement noise vector is $\boldsymbol{Z}_{k+1}$.

$$\hat{\boldsymbol{y}}_{k+1|k} = \sum_{i=0}^{2n_s} W_m^{(i)} \hat{\boldsymbol{y}}_{k+1|k}^{(i)} \tag{3.9}$$

$$\widehat{\boldsymbol{P}}_{k+1|k}^{yy} = \sum_{i=0}^{2n_s} W_c^{(i)} [\hat{\boldsymbol{y}}_{k+1|k}^{(i)} - \hat{\boldsymbol{y}}_{k+1|k}][\hat{\boldsymbol{y}}_{k+1|k}^{(i)} - \hat{\boldsymbol{y}}_{k+1|k}]^T + \boldsymbol{Z}_{k+1} \tag{3.10}$$

As shown in Eqs. (3.11) to (3.14) the correction step is carried out at time step $(k+1)$ by integrating defined set points (i.e., $\boldsymbol{y}_{k+1}$) with the posterior mean vector and covariance matrix of $\boldsymbol{s}_{k+1}$:

$$\hat{\boldsymbol{s}}_{k+1|k+1} = \hat{\boldsymbol{s}}_{k+1|k} + \boldsymbol{K}_{k+1}(\boldsymbol{y}_{k+1} - \hat{\boldsymbol{y}}_{k+1|k}) \tag{3.11}$$

$$\widehat{\boldsymbol{P}}_{k+1|k+1}^{ss} = \widehat{\boldsymbol{P}}_{k+1|k}^{ss} - \boldsymbol{K}_{k+1} \widehat{\boldsymbol{P}}_{k+1|k}^{ss} \boldsymbol{K}_{k+1}^T \tag{3.12}$$

where:

$$\boldsymbol{K}_{k+1} = \widehat{\boldsymbol{P}}_{k+1|k}^{sy} (\widehat{\boldsymbol{P}}_{k+1|k}^{ss})^{-1} \tag{3.13}$$

$$\widehat{\boldsymbol{P}}_{k+1|k}^{sy} \widehat{\boldsymbol{P}}_{k+1|k}^{sy} = \sum_{i=0}^{2n_s} W_c^{(i)} [\boldsymbol{S}_{k+1}^{(i)} - \hat{\boldsymbol{s}}_{k+1|k}][\hat{\boldsymbol{y}}_{k+1|k}^{(i)} - \hat{\boldsymbol{y}}_{k+1|k}]^T \tag{3.14}$$

$\boldsymbol{K}_{k+1}$ is the Kalman gain, and $\widehat{\boldsymbol{P}}^{sy}_{k+1|k}$ is the cross-covariance matrix between the measurement vector and the state vector.

In summary, Figure 3.2 shows a flowchart for the developed method that can be used for model input (i.e., heating and cooling supply) and uncontrolled zone's temperatures estimation that can be employed for controlling zone's temperature.

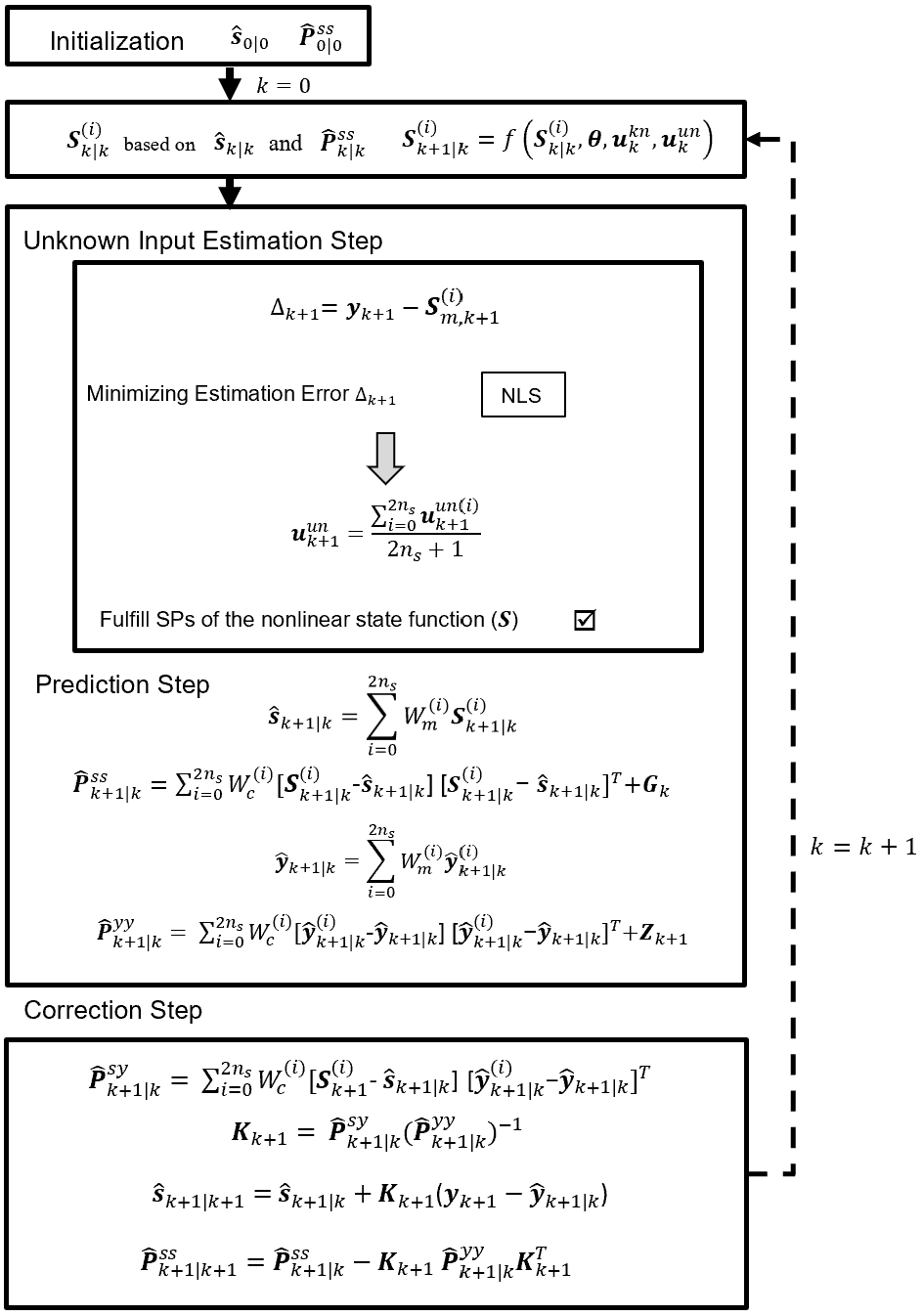

Figure 3.2 Model input estimation method based on UKF integrated with NLS

3.3 Application Examples

Two case studies are presented in this section to illustrate and evaluate the developed method. The first case study uses a simple made-up RC model with two thermal resistances and two thermal capacitances (known as a 2R2C model). The second case study involves a real-world single-family house, which is notably more complex (10R6C). The capability of the developed method in estimating heating and cooling supply (i.e., model inputs) is evaluated by applying the estimated supply and simulating defined RC models to generate the zone temperature and determining whether it is controlled at the desired level or not.

3.3.1 A case study with an artificial RC model

Figure 3.3 shows the made-up RC model, labelled as 2R2C. This model comprises four parameters, including two thermal resistances (i.e., R_2, R_3 in $^{\circ C}/_{kW}$) and two thermal capacitances (i.e., C_2 and C_3 in $^{kWh}/_{^{\circ}C}$). Additionally, it has four model inputs: outdoor temperature T_1 in °C, thermal load Q_1 in kW and heating and cooling supply to nodes 2 and 3 are Q_2 and Q_3 in kW respectively. In this study, outdoor temperature T_1 in °C and thermal load $Q_1$are considered made-up, but in real cases, the outdoor temperature can be determined based on forecasted weather data, while thermal load can be estimated using solar irradiance forecast data and an assumed operating schedule, including occupancy, lighting, and equipment schedules [17, 73].

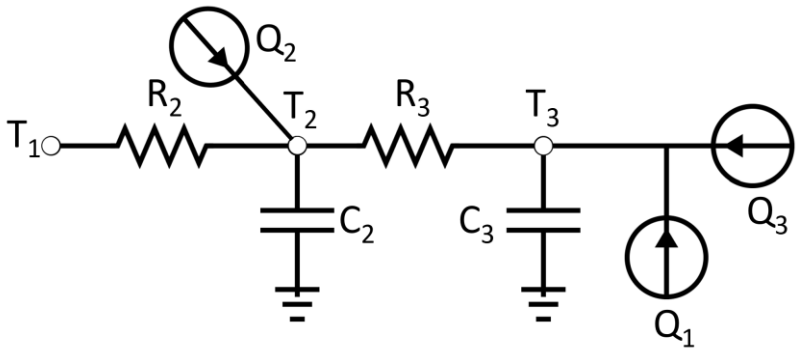

Figure 3.3 2R2C Model

The ordinary differential equations for the made-up RC model, as well as the two assumed known 10-minute made-up model inputs (Q_1 and T_1), are provided in Appendix . The case study with made-up data considers three scenarios. In the first scenario, Q_2 is assumed to be zero, and the aim is to estimate the heating and cooling supply (Q_3), which is required to maintain the temperature of the zone T_3 at 26 ℃ for 6 hours, starting from hour 2 to hour 8. This six-hour period is called the "controlling dataset," and the two hours before it (hours 0 to 2) represents prior control conditions, which taken every 10 minutes (i.e., time step). In the second scenario (2R2C-Ct2), the objective and assumptions are the same as the first scenario, but with a restriction on the amount of heating and cooling supply (Q_3), This means that the equipment providing heating cannot exceed a specific amount. In the last scenario (2R2C-Ct3), both nodes T_3 and T_2 are controlled at 26°C and 3°C, respectively. In this scenario, in contrast with the first two scenarios, heating and cooling supply, Q_2 relating to node T_2 is not zero and is estimated alongside Q_3. These scenarios are summarized in Table 3.1.

Table 3.1 2R2C scenarios

Scenario	Controlled State	Estimated model input
2R2C-Ct1	T_3 at 26 ℃	Q_3

2R2C-Ct2	T_3 at 26 ℃	Q_3 with limitation
2R2C-Ct3	T_3 at 26 ℃ and T_2 at 3 ℃	Q_2 and Q_3 without limitation

Estimated model parameters and initial states of the RC model are presented in Eq. (3.15). These values are gotten from the previous chapter.

$$\boldsymbol{\theta} = \left[R_2(^{\circ}\mathrm{C}/_{kW}) \quad R_3(^{\circ}\mathrm{C}/_{kW}) \quad C_2\,(^{kWh}/_{^{\circ}\mathrm{C}}) \quad C_3(^{kWh}/_{^{\circ}\mathrm{C}})\right]^T \in \mathbb{R}^{4\times 1}$$

$$\boldsymbol{\theta} = [3.02 \quad 27.81 \quad 2.11 \quad 1.11]^T$$

$$\hat{\boldsymbol{s}}_{0|0} = [\mathrm{T}_2 \quad \mathrm{T}_3]^T \tag{3.15}$$

$$\hat{\boldsymbol{s}}_{0|0} = [-0.5 \quad 31]^T$$

The initial covariance matrix $\hat{P}^{ss}_{0|0}$ is assumed to be diagonal, which it's diagonal terms of the are determined by the expression $\hat{P}^{ss}_{0|0} = [1.0 \times (\hat{s}_{0|0})]^2$. Additionally, it is assumed that the measurement noise covariance matrix is diagonal, time-invariant, and equal to $\boldsymbol{Z} = (0.3^{\circ}\mathrm{C})^2$, and the process noise covariance matrix is also diagonal, time-invariant, and equal to $\boldsymbol{G} = [1 \times 10^{-5} \times \hat{s}_{0|0}]^2$. The values of the initial covariance matrix and the process noise covariance matrix are derived from [26, 53].

In Scenario 2R2C-Ct1, in addition to the Q_3, the model state T_2 is also estimated to show behavior of T_2 when T_3 is controlled. Figure 3.4 depicts estimated heating and cooling supply (Q_3) and uncontrolled state (T_2) for the controlling dataset. Accordingly, Figure 3.4. (a) displays the estimated heating and cooling supply Q_3 with an initial value of – 5.2 kW (negative means cooling supply) and then varies between 0 to 1 kW to maintain T_3 at 26 °C.

In addition, Figure 3.4 (b) illustrates the estimated state T_2 which varies between 0 °C and 8 °C when T_3 is controlled.

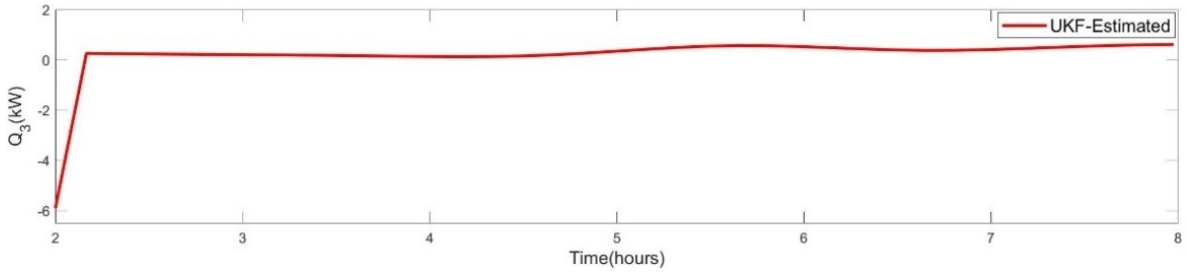

(a)

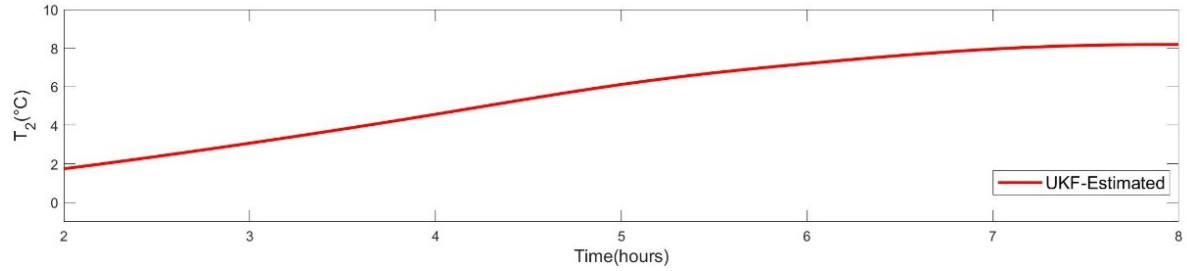

(b)

Figure 3.4 (a) Estimated heating and cooling supply, (b) Estimated state T_2 when T_3 controlled at $26°C$

To validate the estimated heating and cooling supply, the estimated Q_3 must be taken into account and the previously described 2R2C model simulated in order to generate the system response for T_3 and determine whether it is controlled at 26°C or not. Accordingly, Figure 3.5 depicts the simulation result for T_3 in the controlling dataset. The graphs show that T_3 falls sharply from 31°C to 26°C in the first 10 minutes and remains at 26°C for the rest of the controlling period, which starts from hours 2 to 8, it is worth noting that hours 0 to 2 indicate zone temperature T_3 behavior prior controlling. This demonstrates that the presented method can accurately estimate the required heating and cooling supply to control T_3.

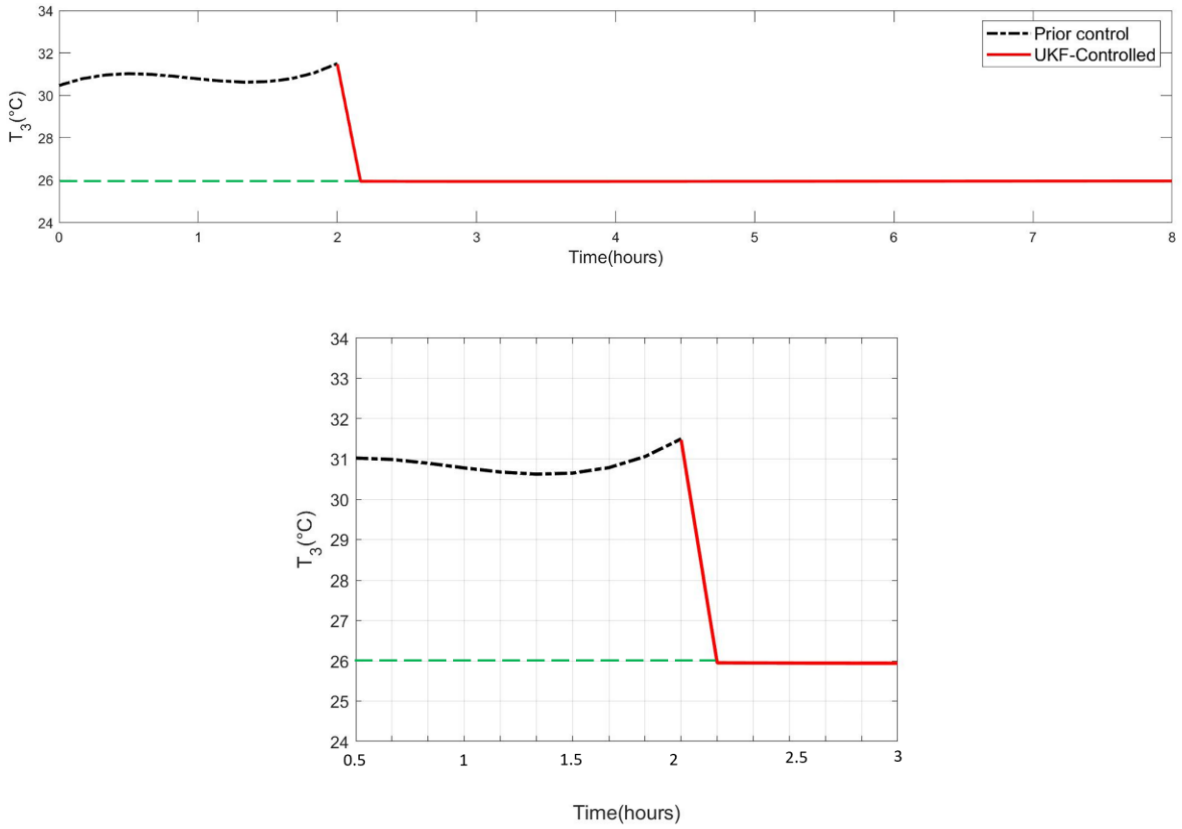

Figure 3.5 T_3 in the controlling dataset

For Scenario 2R2C-Ct2 there is a limitation on the maximum value of the model input, or in other words, equipment with a limited heating and cooling supply capacity. Specifically, the maximum capacity is set at 1kW. Figure 3.6 presents the results of this scenario, showing the estimated Q_3 in this scenario. To maintain T_3 at 26°C and manage the demand for heating and cooling supply, it is essential to sustain the estimated supply at its maximum capacity for an extended period. This is necessary because the required amount of heating and cooling exceeds the capacity of the equipment providing these services.

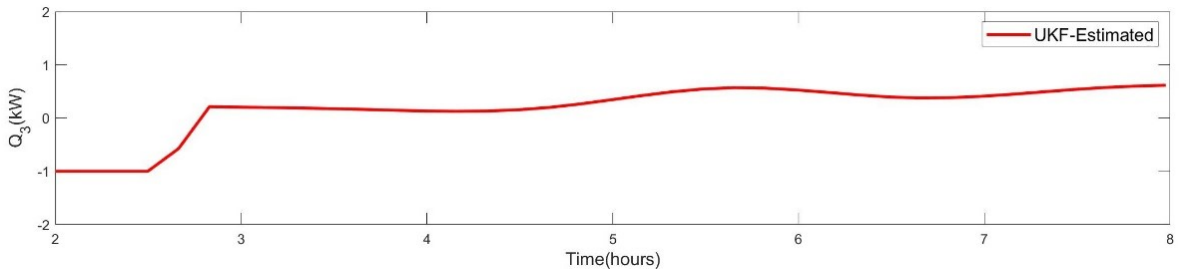

Figure 3.6 Limited heating cooling supply to 1kW

Figure 3.7 compares the simulated T_3 response in two instances, one where Q_3 is not limited and the other where Q_3 is constrained to a maximum of 1kW. The first red line corresponds to the scenario in which Q_3 is not limited, while the blue line represents the scenario where Q_3 is limited to 1kW. It can be observed that when the estimated Q_3 is limited, T_3 takes longer to reach 26°C due to the insufficient heating and cooling supply. This highlights the significance of accounting for equipment capacity limitations while estimating the heating and cooling supply and managing building energy. Although the developed method can still estimate the optimal heating and cooling supply required to maintain a constant temperature within the zone, even with limited equipment capacity, it may take more time to achieve the desired temperature.

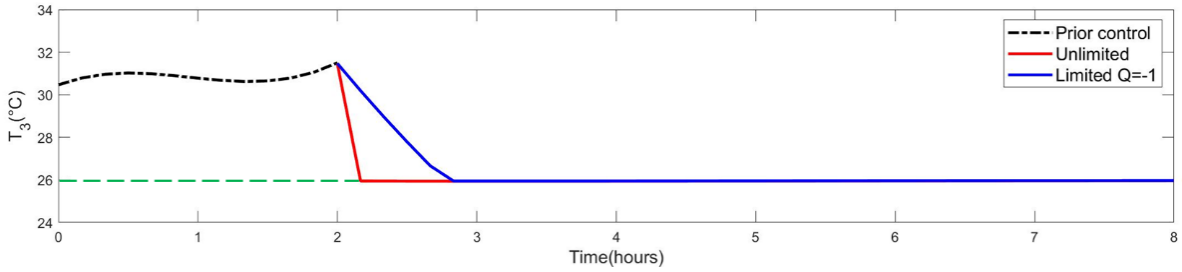

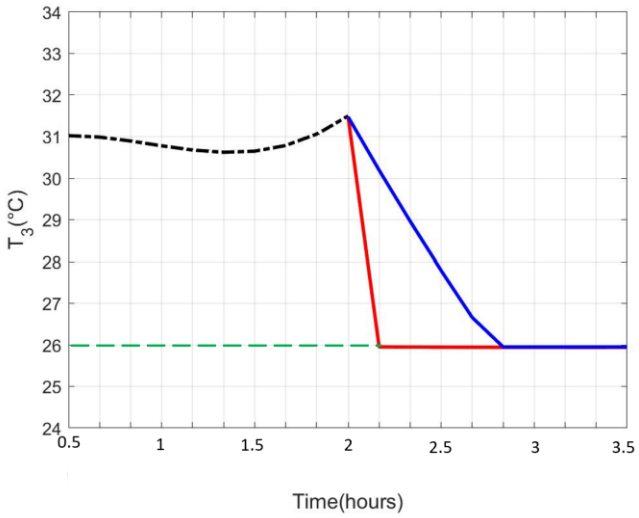

Figure 3.7 comparison of T_3 for two Scenarios 2R2C-Ct1 and 2R2C-Ct2

In some situations, it may be necessary to control the temperature of multiple zones simultaneously. In such cases, it is important to estimate the required heating and cooling supply for each zone. For this purpose, Scenario 2R2C-Ct3 is defined, which the objective of this scenario is to control T_3 and T_2 at 26°C and 3°C respectively, while determining the corresponding heating and cooling supplies needed to sustain these zones at their expected temperatures.

The estimated heating and cooling supply (Q_2) required to control node T_2 at 3°C is illustrated in Figure 3. (a). The estimated Q_2 initially amounts to 7.8 kW and varies between 0 and -2 kW (negative, meaning cooling) to maintain T_3 at 26°C. Figure 3. (b) depicts sharp increase in T_2 from about 0°C to 3°C within the first 10 minutes, after which it remains constant for the control period. Additionally, Figure 3. (a) depicts the estimated heating and cooling supply required to control T_3 at 26°C. The initial Q_3 is -5.5 kW and varies between 0 and 1 kW to maintain T_3 at 26°C. Figure 3. (b) displays the simulation results for T_3 in the

control dataset. It is observed that T_3 drops quickly from 31°C to 26°C within the first 10 minutes and stays at 26°C for the remainder of the control period.

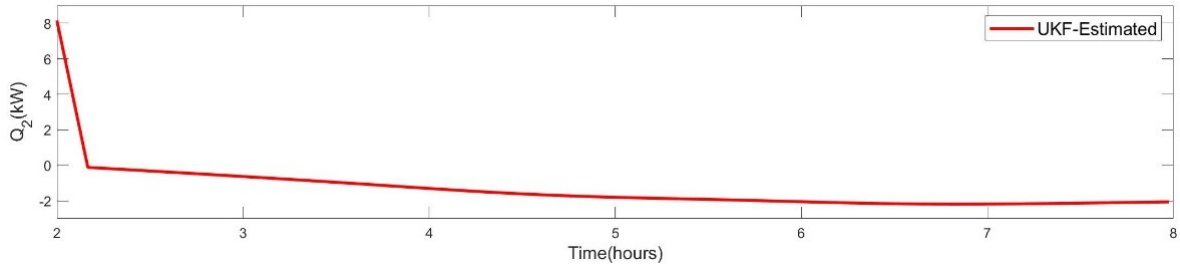

(a)

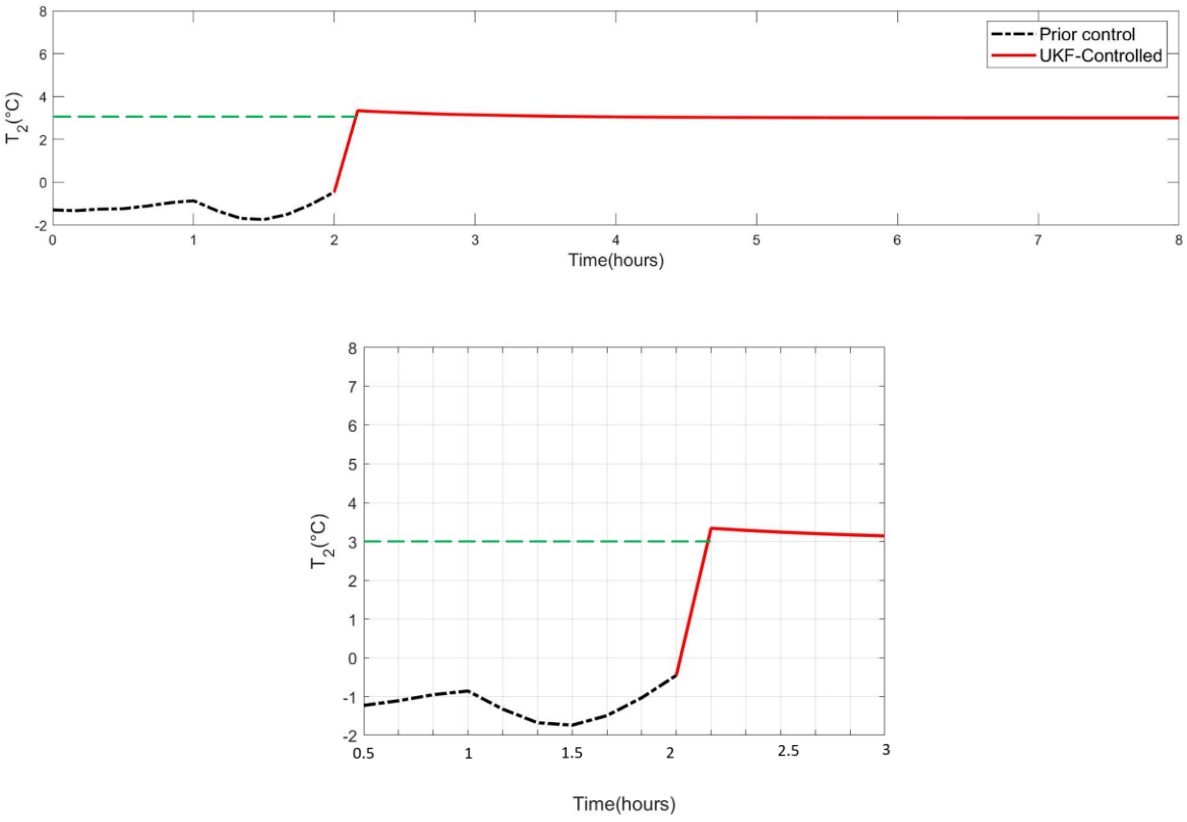

(b)

Figure 3.8 (a) Estimated heating and cooling supply Q_2, (b) T_2 in controlling dataset

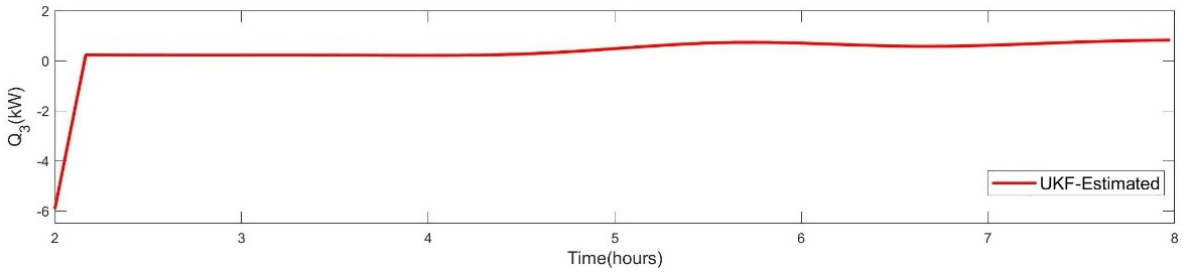

(a)

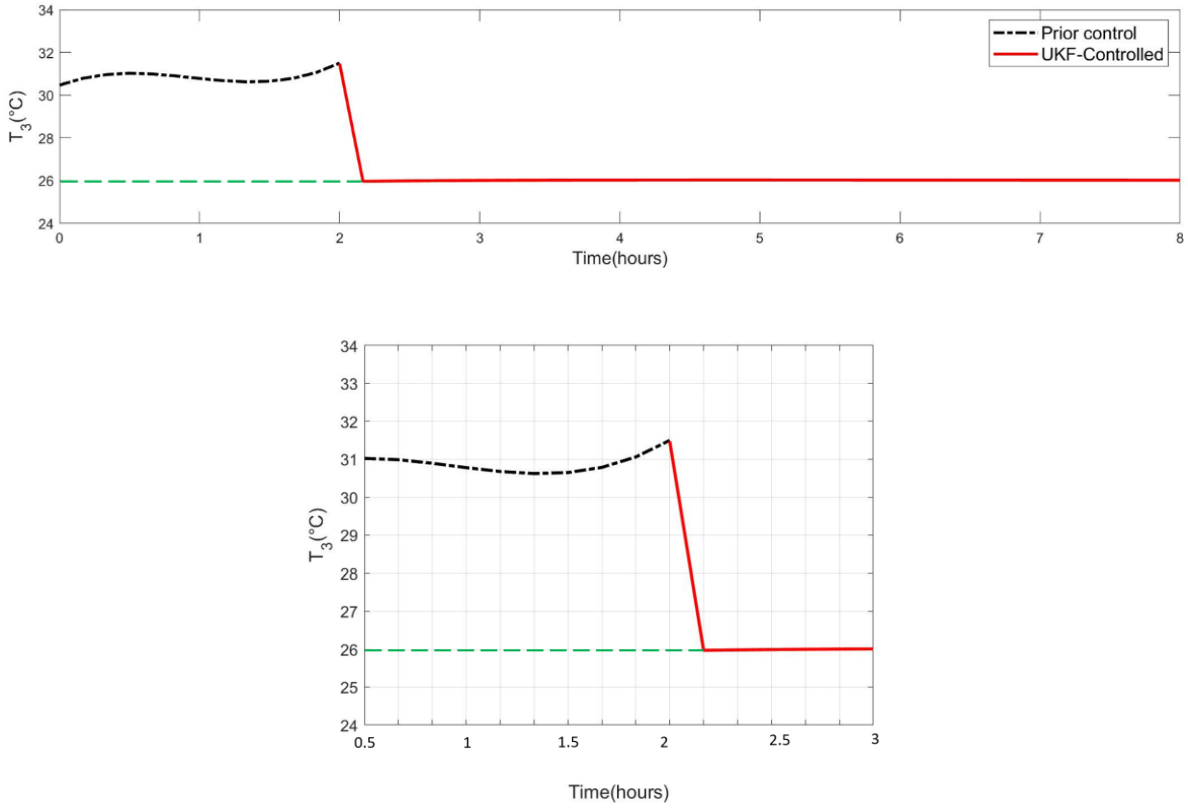

(b)

Figure 3.9 (a) Estimated heating and cooling supply Q_3, (b) T_3 in controlling dataset

3.3.2 Case study with real-world data

In this section, the developed method is tested on a real-world low-energy wooden-frame house in Eastman, Quebec, Canada, shown in Figure 3.8. The RC thermal model structure for this house shown Figure 3.9, and was developed by Wang et al. [38]. This RC model is used for heating and cooling supply estimation for controlling the temperature of different zones of this house for a period of 6 hours at 10-minute intervals (control dataset). Two scenarios are defined based on controlling different zones temperatures. Accordingly, the capability of the developed method is evaluated by applying the estimated supplies and simulating the RC model to generate the zone temperature and determining whether they are controlled at the desired level or not.

Figure 3.8 A single detached house as a case study [38]

This RC model is called a 10R6C, as it consists of 10 thermal resistances and 6 thermal capacitances corresponding to 6 temperature nodes, indicated by T_u, T_m, and T_b in °C for the temperature responses of the second floor, main floor, and basement, respectively. Note that T_{um}, T_{mm}, and T_{bm} are the auxiliary internal temperature responses. The ODEs of this RC model are shown in Appendix .

The 10-minute model inputs for this RC thermal model in the controlling dataset (6 hours including hours 2 to 8) are shown in Appendix . These inputs include 1) global irradiation Q_s in kW per unit area on the south façade, which is used to obtain approximate effective solar heat gains and is weighted by solar gain factors (α_s). 2) T_g ground temperature, which is approximately at 13 C° constants as shown by measurements. 3) T_0 outdoor temperature in C°. 4) Q_{elec} gross electricity demand in kW and used to calculate internal heat gains and are weighted according to internal gain factors (α_e). 4) Q_{hp} in kW is the heating supply from the geothermal heat pump, which needs to be estimated in order to control the main floor temperature. 5) Q_{hp} is distributed using the alpha distribution factor (α_{hp}) across three levels. It's worth noting that for this case study, the known inputs are based on recorded data. However, it's possible to predict these inputs as well. For example, the outdoor temperature can be predicted based on forecast weather data, and the gross electricity can be predicted based on the operating schedule of lighting and electrical equipment [17, 73].

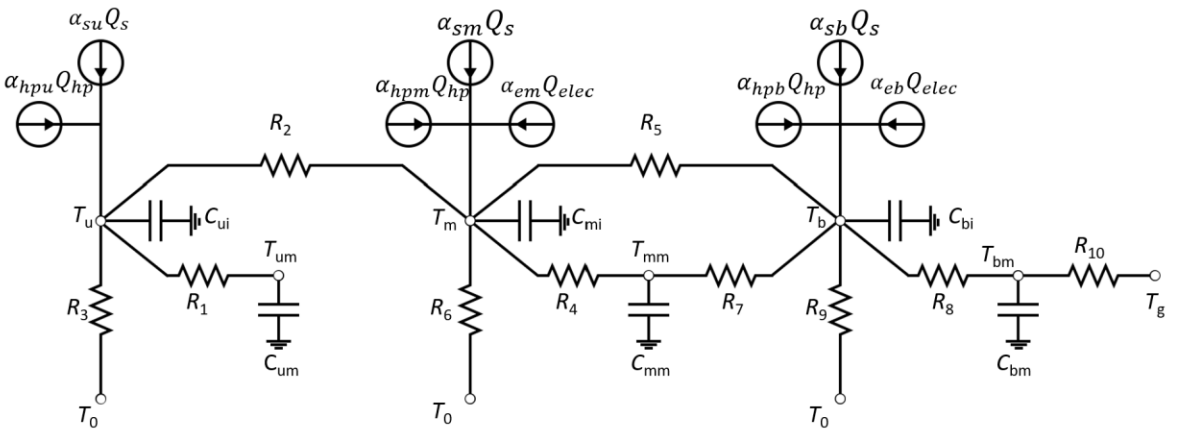

Figure 3.9 Single-detached house RC model

The state vector of this RC model can be defined by $\boldsymbol{s} = [T_u, T_{um}, T_m, T_{mm}, T_b\ , T_{bm}]^T \in \mathbb{R}^{6\times1}$, additionally, the model parameters of this single detached house can be described as thermal resistances, $\boldsymbol{R} = [R_1 \quad R_2 \quad R_3 \quad R_4 \quad R_5 \quad R_6 \quad R_7 \quad R_8 \quad R_9 \quad R_{10}]^T \in \mathbb{R}^{10\times1}$ in $^{\circ}\mathrm{C}/_{kW}$; thermal capacitances, $\boldsymbol{C} = [C_{ui} \quad C_{um} \quad C_{mi} \quad C_{mm} \quad C_{bi} \quad C_{bm}]^T \in \mathbb{R}^{6\times1}$ in $^{\mathrm{kWh}}/_{^{\circ}\mathrm{C}}$; solar gain factor, $\boldsymbol{\alpha_s} = [\alpha_{su} \quad \alpha_{sm} \quad \alpha_{sb}]^T \in \mathbb{R}^{3\times1}$, in m^2; internal gain factor $\boldsymbol{\alpha_e} = [\alpha_{em} \quad \alpha_{eb}]^T \in \mathbb{R}^{2\times1}$, unitless and heating power distribution factor for the second, main floor, and basement respectively as $\boldsymbol{\alpha_{hp}} = [\alpha_{hpu} \quad \alpha_{hpm} \quad \alpha_{hpb}]^T \in \mathbb{R}^{3\times1}$. To evaluate the performance of the developed method, this study considered two scenarios. The first scenario involves controlling the temperature of the main floor (T_m) at 22°C and estimating the required heating and cooling supply (Q_{hp}) to maintain the desired temperature. In the second scenario, the objective is to control the temperature of both the main and second floors. In this scenario, Q_{hp} is eliminated, and two separate heating sources (Q_m and Q_u) are added to the main and second floors,

respectively, as shown in Figure 3.10. No heating to T_b, these two heating sources are estimated to control the temperatures of both floors. Table 3.2 shows these scenarios.

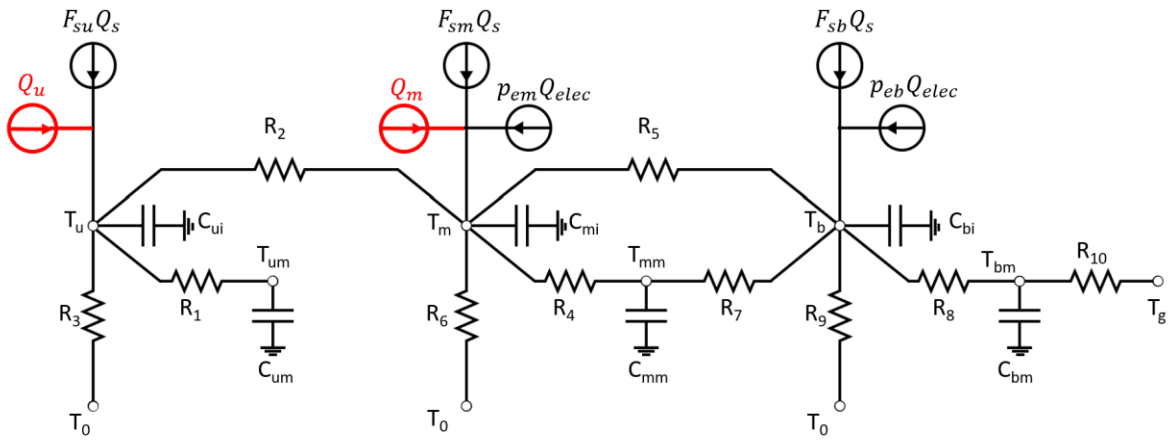

Figure 3.10 Thermal model for controlling two zones' temperature

Table 3.2 10R6C scenarios

Scenario	Controlled State	Estimated model input
10R6C-Ct1	T_m at 22 ℃	Q_{hp}
10R6C-Ct2	T_m at 23 ℃ and T_u at 21 ℃	Q_m and Q_u

The estimated model parameters and initial states of the RC model is presented in Eq. (3.16) and are gotten from the previous chapter.

$$\hat{\boldsymbol{s}}_{0|0} = [20.30 \quad 20.45 \quad 20.96 \quad 21.2 \quad 19.8 \quad 18.8]^T \ [unit: ℃]$$

$$\boldsymbol{\theta} = \begin{bmatrix} R^T & C^T & F_s^T & p_e^T & \alpha_{hp}^T \end{bmatrix}^T \tag{3.16}$$

$$\boldsymbol{R} = [1.32 \quad 1.59 \quad 19.06 \quad 2.78 \quad 5.26 \quad 26.35 \quad 12.49 \quad 2.42 \quad 20.62 \quad 13.72]$$

$$[unit: {}^{℃}/_{kW}]$$

$$\boldsymbol{C} = [1.39 \quad 2.37 \quad 2.16 \quad 25.96 \quad 3.74 \quad 9.62]\ [unit: {}^{\mathrm{kWh}}/_{\circ\mathrm{C}}]$$

$$\boldsymbol{F_s} = [1.97 \quad 3.05 \quad 1.22]^T [unit: m^2]$$

$$\boldsymbol{p_e} = [0.37 \quad 0.13]^T [unit: --]$$

$$\boldsymbol{a_{hp}} = [0.35 \quad 0.40 \quad 0.23]^T [unit: --]$$

As explained in the case study of a simple RC model, the initial covariance matrix $\hat{P}_{0|0}^{ss}$ is diagonal, with diagonal terms selected as $\widehat{\boldsymbol{P}}_{0|0}^{ss} = [1.0 \times (\hat{\boldsymbol{s}}_{0|0})]^2$. The measurement noise covariance matrix is assumed to be diagonal and time-invariant, equal to $\boldsymbol{Z} = (0.3°\mathrm{C})^2$. The process noise covariance matrix is also assumed to be time-invariant and diagonal entries having values equal to $\boldsymbol{G} = [1 \times 10^{-5} \times \hat{\boldsymbol{s}}_{0|0}]^2$ as described in [26, 53].

In Scenario 10R6C-Ct1, the developed method employed to estimate the heating cooling supply Q_{hp} to maintain the main floor temperature T_m at 22°C. Furthermore, T_u and T_b representing second floor and basement temperature will also be estimated during the expected controlling dataset. It is important to note that the maximum capacity of the heat pump installed in this house is 10.55 kW, so the estimated Q_{hp} cannot exceed this value.

Figure 3.11 (a) shows the estimated Q_{hp} and uncontrolled state (T_u and T_b) for the controlling dataset. The estimated Q_{hp} starts with an initial value of 5 kW and then mostly varies between 0 to 4 kW to maintain T_m at 22°C. Figure 3.11 (b) displays the estimated temperature for the second floor and basemen which are around 21°C and 20.5°C, respectively, when temperature of the main floor is controlled.

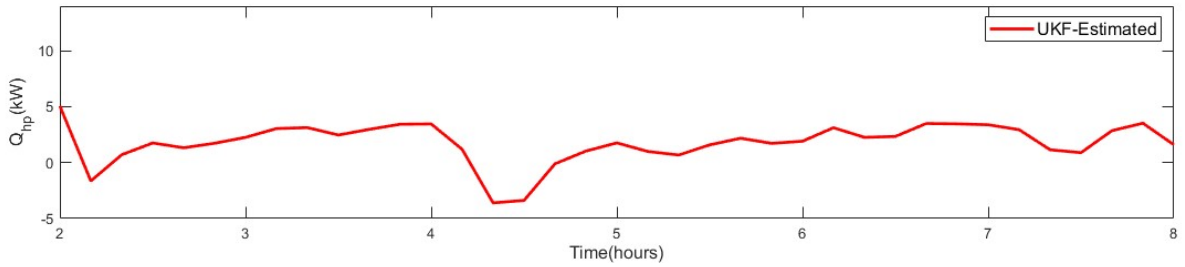

(a)

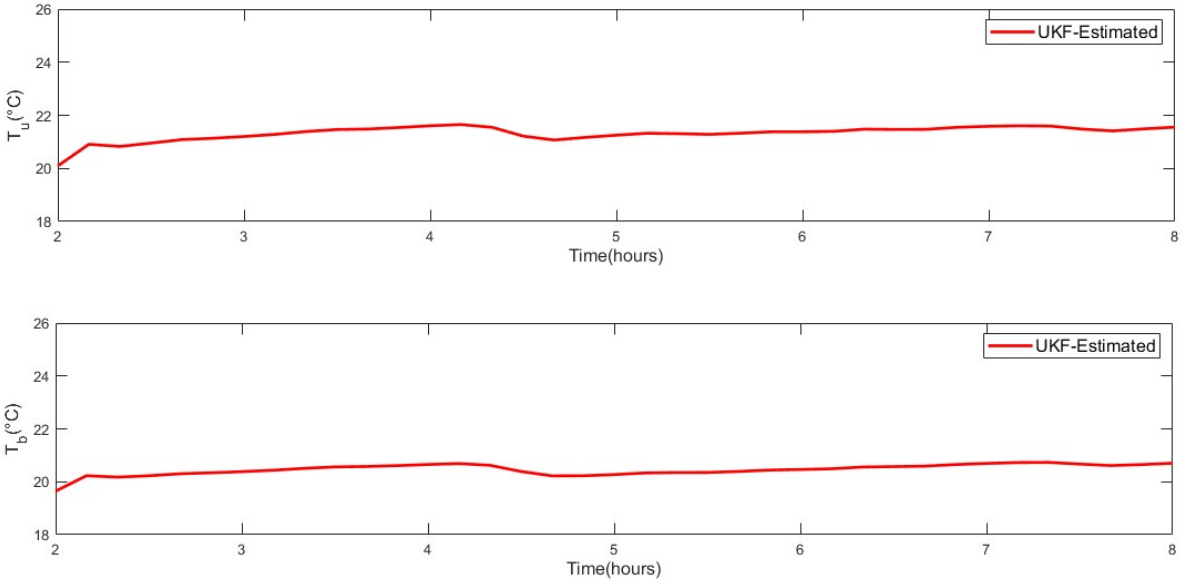

(b)

Figure 3.11 (a) Estimated heating and cooling supply. (b) Second floor and basement estimated temperature when T_m controlled

To validate the estimated heating and cooling supply, the estimated Q_{hp} is taken into account and the previously described 10R6C model is simulated to check if the temperature T_m is controlled at 22°C or not. Figure 3.12 shows the simulation result for T_m in the controlling dataset. It can be observed that T_m increases rapidly from around 21°C to 22°C in the first 10 minutes and remains at 22°C for the remainder of the controlling period which starts from hours 2 to 8, it is worth noting that hours 0 to 2 indicates zone temperature T_m

behavior prior controlling. This indicates that the presented method can accurately estimate the required heating and cooling supply to control the temperature of the main floor T_m.

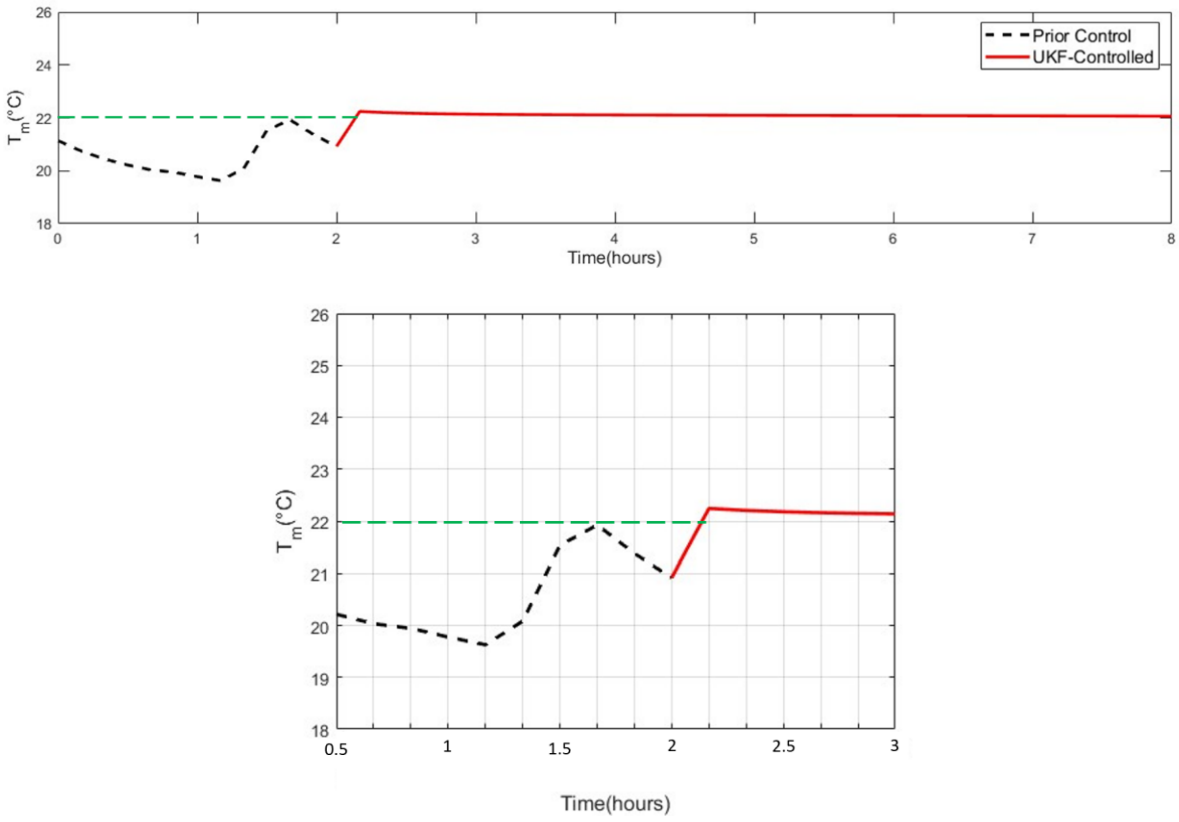

Figure 3.12 Tm results for the controlled data set

Scenario 10R6C-Ct2 focuses on controlling the temperature of multiple zones, specifically the main floor (T_m) and second floor (T_u), with estimation of corresponding heating and cooling supplies. To accomplish this, Q_m and Q_u have been added to the corresponding floor's node (i.e., main and second floors). ODEs relating to this scenario are shown in Appendix . The goal of this scenario is to maintain the temperature of the main floor at 23°C and the second floor at 22°C.

Figure 3.13 (a) illustrates the estimated heating and cooling supply Q_u which is used to control the temperature of second floor T_u at 22°C. Initially, the estimated Q_u is 3.1 kW,

but it varies between 0 and 0.5 kW to maintain T_u at the desired temperature. Figure 3.13 (b) shows generated responses for T_u when estimated Q_u is applied. It can be observed that T_u quickly increases from about 20.5 to the expected temperature (22°C) within the first 10 minutes and remains constant throughout the control dataset.

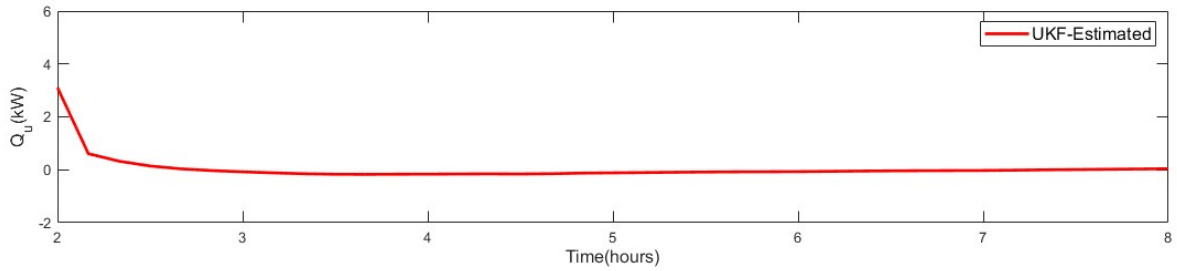

(a)

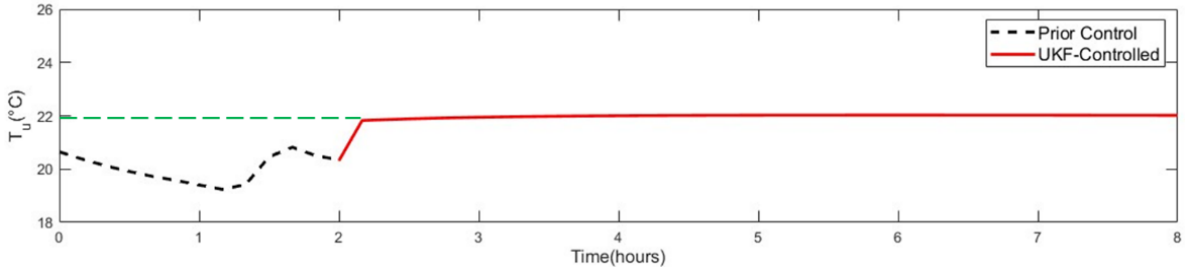

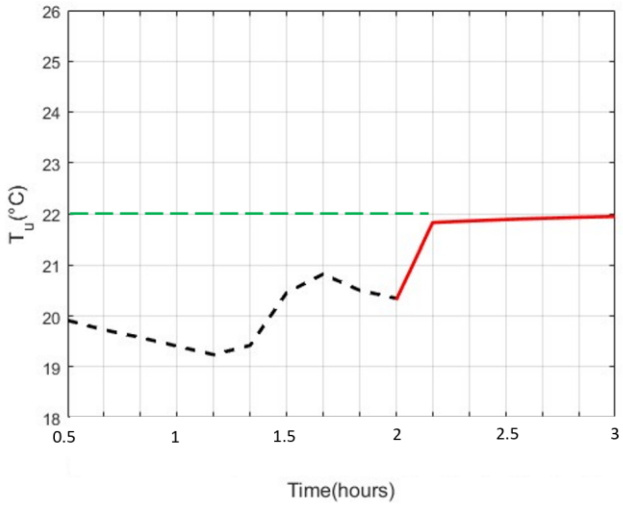

(b)

Figure 3.13 (a) Estimated heating and cooling supply Q_u, (b) T_u results in controlling dataset

Figure 3.14. (a) shows the estimated heating and cooling supply represented as Q_m, used to control the temperature of the main floor (T_m) at a constant value of 23°C. The initial value of estimated Q_m is 4 kW and it mostly varies between 0 and 3 kW to maintain T_m at the desired temperature. Figure 3.14 (b) illustrates the generate temperature response of the main floor in the control dataset when estimated Q_m is applied to the RC model. It is observed that T_m increases rapidly from about 21°C to 23°C in the first 10 minutes and stays at 23°C for the entire control period.

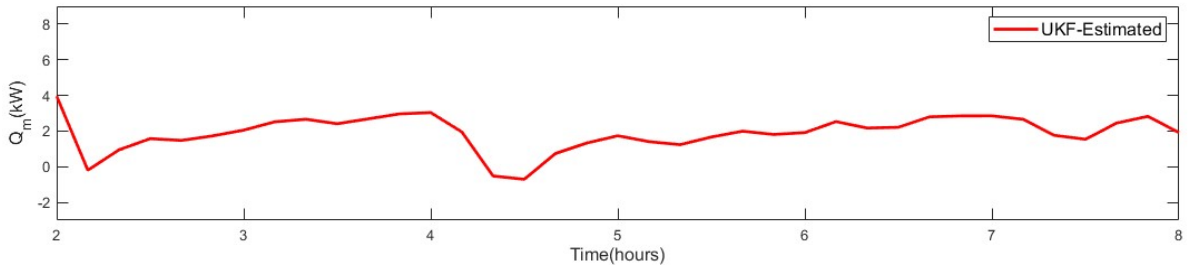

(a)

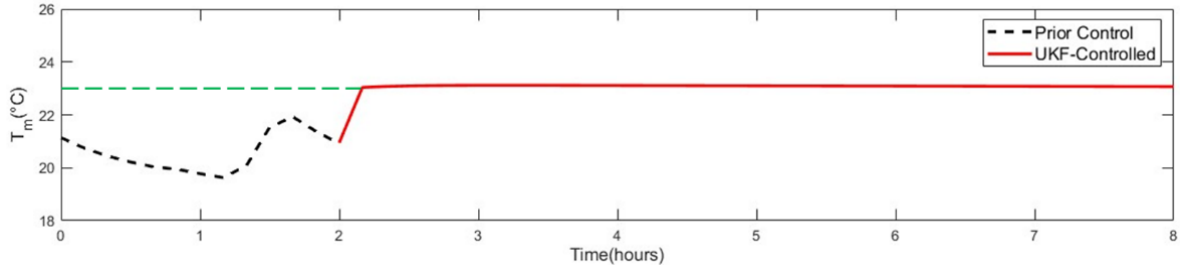

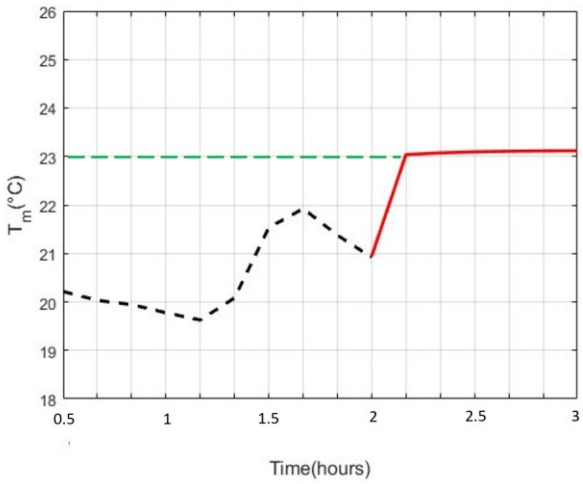

(b)

Figure 3.14 (a) Estimated heating and cooling supply Q_m, (b) T_m results in a controlling dataset

3.4 Conclusion

This study develops a method for estimating heating and cooling supplies (i.e., RC thermal model inputs) for temperature control purposes. In this regard, the method employs thermal resistor-capacitor network (RC) for thermal dynamic modeling and the Unscented Kalman filter (UKF), integrated with the Nonlinear Least Square (NLS) method, to estimate the heating and cooling supply. To evaluate the capability of the developed method, two application examples are presented: one using made-up data and the other using real-world data. Different scenarios, including limiting the maximum amount of the heating and cooling supply and controlling temperatures in multiple zones, are created to evaluate the capability and performance of the developed method in different circumstances.

In the case study with made-up data, the estimated heating and cooling supply sharply drops the zone's temperature from about 30°C to 26°C in the first 10 minutes and maintains

that temperature for the remainder of the controlling dataset. Similarly, in the case of real-world data, the developed method accurately estimates the heating and cooling supply to control one and two zones. The considered zone temperatures reach the expected temperature set points of 22°C and 23°C in the first 10 minutes and remain constant throughout the controlling dataset. These accurate estimation of heating and cooling supply and controlling zone's temperature on their expected level prove that the developed method is an effective technique for estimating heating and cooling supply of RC thermal models and can be used in control strategies.

4 Conclusion

4.1 Summary

To summarize, the focus of this thesis is to develop and evaluate a method for simultaneously estimating thermal resistor and capacitor (RC) model parameters and inputs, even when some states are partially missing. The method uses RC models for thermal dynamic modeling and incorporates Unscented Kalman Filter (UKF) and Nonlinear Least Square (NLS) estimation method. The developed method is evaluated using both made-up and real-world data from a single-family detached house. Once the parameters have been estimated and a trustworthy thermal dynamic model is created, then attention is redirected towards employing the developed method without parameter estimation to determine the necessary heating and cooling supply for controlling zone temperatures to desired levels. The capability of this method is also evaluated using case studies with made-up and real-world data as well.

4.2 Contribution

This research introduces a method for estimating RC model parameters and inputs, even in cases where some states are partially missing. Furthermore, the developed method is utilized to control zone temperatures by estimating the required heating and cooling supply. In this context, the major contributions of this thesis include:

Part 1:

I. Development of RC model parameters and input estimation method: The developed method is a new approach for estimating RC model parameters and inputs with and without partially missing states. This method utilizes RC thermal

model and UKF and NLS estimation method to estimate the unknown parameters and inputs.

II. Evaluation of the developed method using different case studies: The capability of the developed method is demonstrated by applying it to case studies both with made-up and real-world data in different scenarios. The case studies show that the developed method performs well in estimating the RC model parameters, and inputs, even when the temperature states are partially missing.

Part 2:

I. Employing the developed method without parameter estimation for controlling zone temperature purposes: The developed method is used for estimating the necessary heating and cooling supply for controlling zone temperatures to desired levels.

II. The developed method's capability in terms of estimating necessary heating and cooling supply is evaluated through case studies that employ made-up and real-world data in diverse scenarios. These case studies demonstrate the method's capability in estimating the required heating and cooling supply to regulate zone temperatures accurately.

4.3 Future works and limitations

Several future works can be considered to expand the scope and applicability of the developed method. Firstly, the developed method can be validated using data from other complex buildings with varying building types, sizes, and thermal characteristics to assess its generalizability. Secondly, investigating the potential for integrating the developed method with existing building automation systems can enable real-time control and optimization of heating and cooling supply, thus enhancing building energy efficiency, and reducing operating costs. Additionally, designing user-friendly toolboxes that allow for easy implementation of the developed method can enhance its accessibility and usability. These toolboxes can include graphical user interfaces, documentation, and open-source codes to facilitate the adoption of the developed method by building energy practitioners and researchers.

While the developed method is deemed reliable, there are still some challenges that need to be addressed. One of these challenges is the assumption that the RC model accurately represents the thermal behavior of the building, which may not always hold true. This means that the accuracy of the estimated parameters and control strategies is reliant on the quality of the RC model. Additionally, uncertainties in input and state measurements may also impact the performance of the proposed method, and it is necessary to investigate the extent of this impact.

References

1. González-Torres, M., et al., *A review on buildings energy information: Trends, end-uses, fuels and drivers.* Energy Reports, 2022. **8**: p. 626-637.
2. Policy, I.E.A.D.o.S.E., *Transition to sustainable buildings: strategies and opportunities to 2050*. 2013: Organization for Economic.
3. Begyor, S., et al., *MEASURES TO IMPROVE THE ENERGY EFFICIENCY OF MODERN AND RECONSTRUCTED BUILDINGS.* Journal of new century innovations, 2022. **18**(1): p. 157-161.
4. Mushafiq, M., et al., *Energy Efficiency and Economic Policy: Comprehensive Theoretical, Empirical, and Policy Review.* Energies, 2023. **16**(5): p. 2381.
5. Mostafavi, F., M. Tahsildoost, and Z. Zomorodian, *Energy efficiency and carbon emission in high-rise buildings: A review (2005-2020).* Building and Environment, 2021. **206**: p. 108329.
6. Shaikh, P.H., et al., *A review on optimized control systems for building energy and comfort management of smart sustainable buildings.* Renewable and Sustainable Energy Reviews, 2014. **34**: p. 409-429.
7. Braun, J.E., *Reducing energy costs and peak electrical demand through optimal control of building thermal storage.* ASHRAE transactions, 1990. **96**(2): p. 876-888.
8. Hilliard, T., M. Kavgic, and L. Swan, *Model predictive control for commercial buildings: trends and opportunities.* Advances in Building Energy Research, 2016. **10**(2): p. 172-190.
9. Wang, Z. and Y. Chen, *Data-driven modeling of building thermal dynamics: Methodology and state of the art.* Energy and Buildings, 2019. **203**: p. 109405.
10. Li, X. and J. Wen, *Review of building energy modeling for control and operation.* Renewable and Sustainable Energy Reviews, 2014. **37**: p. 517-537.
11. Ali, U., et al., *Review of urban building energy modeling (UBEM) approaches, methods and tools using qualitative and quantitative analysis.* Energy and buildings, 2021. **246**: p. 111073.
12. Ahmad, T., et al., *A comprehensive overview on the data driven and large scale based approaches for forecasting of building energy demand: A review.* Energy and Buildings, 2018. **165**: p. 301-320.
13. *Energy Plus. Energy.* https://energyplus.net.
14. Harish, V. and A. Kumar, *A review on modeling and simulation of building energy systems.* Renewable and sustainable energy reviews, 2016. **56**: p. 1272-1292.
15. Martínez, S., et al., *A performance comparison of multi-objective optimization-based approaches for calibrating white-box building energy models.* Energy and Buildings, 2020. **216**: p. 109942.
16. Mohandes, S.R., X. Zhang, and A. Mahdiyar, *A comprehensive review on the application of artificial neural networks in building energy analysis.* Neurocomputing, 2019. **340**: p. 55-75.
17. Zhou, Q., et al., *A grey-box model of next-day building thermal load prediction for energy-efficient control.* International Journal of Energy Research, 2008. **32**(15): p. 1418-1431.
18. Li, Y., et al., *Grey-box modeling and application for building energy simulations-A critical review.* Renewable and Sustainable Energy Reviews, 2021. **146**: p. 111174.
19. Ogunsola, O.T. and L. Song, *Application of a simplified thermal network model for real-time thermal load estimation.* Energy and buildings, 2015. **96**: p. 309-318.
20. Bueno, B., et al., *A resistance-capacitance network model for the analysis of the interactions between the energy performance of buildings and the urban climate.* Building and Environment, 2012. **54**: p. 116-125.

21. Chen, Y., et al., *Parameter estimation of resistor-capacitor models for building thermal dynamics using the unscented Kalman filter.* Journal of Building Engineering, 2021. **34**: p. 101639.
22. Johnson, M.L. and L.M. Faunt, *[1] Parameter estimation by least-squares methods*, in *Methods in enzymology*. 1992, Elsevier. p. 1-37.
23. Fux, S.F., et al., *EKF based self-adaptive thermal model for a passive house.* Energy and Buildings, 2014. **68**: p. 811-817.
24. Wang, S. and X. Xu, *Simplified building model for transient thermal performance estimation using GA-based parameter identification.* International journal of thermal sciences, 2006. **45**(4): p. 419-432.
25. Li, Y., et al., *Real-time thermal dynamic analysis of a house using RC models and joint state-parameter estimation.* Building and Environment, 2021. **188**: p. 107184.
26. Astroza, R., H. Ebrahimian, and J.P. Conte, *Performance comparison of Kalman− based filters for nonlinear structural finite element model updating.* Journal of Sound and Vibration, 2019. **438**: p. 520-542.
27. Xuemei, L., et al. *Building cooling load forecasting using fuzzy support vector machine and fuzzy C-mean clustering*. in *2010 international conference on computer and communication technologies in agriculture engineering*. 2010. IEEE.
28. Xuemei, L., et al. *Building cooling load forecasting model based on LS-SVM*. in *2009 Asia-Pacific Conference on Information Processing*. 2009. IEEE.
29. Biyik, E. and A. Kahraman, *A predictive control strategy for optimal management of peak load, thermal comfort, energy storage and renewables in multi-zone buildings.* Journal of building engineering, 2019. **25**: p. 100826.
30. Tien Bui, D., et al., *Predicting heating and cooling loads in energy-efficient buildings using two hybrid intelligent models.* Applied Sciences, 2019. **9**(17): p. 3543.
31. Ferlito, S., et al. *Predictive models for building's energy consumption: An Artificial Neural Network (ANN) approach*. in *2015 xviii aisem annual conference*. 2015. IEEE.
32. Massana, J., et al., *Short-term load forecasting for non-residential buildings contrasting artificial occupancy attributes.* Energy and Buildings, 2016. **130**: p. 519-531.
33. Paudel, S., et al., *Pseudo dynamic transitional modeling of building heating energy demand using artificial neural network.* Energy and Buildings, 2014. **70**: p. 81-93.
34. Bosseboeuf, D., et al., *Energy efficiency trends and policies in the household and tertiary sectors.* An Analysis Based on the ODYSSEE and MURE Databases, 2015.
35. Prada, M., et al., *New solutions to reduce greenhouse gas emissions through energy efficiency of buildings of special importance–Hospitals.* Science of the Total Environment, 2020. **718**: p. 137446.
36. Roth, K.W., et al., *Energy consumption characteristics of commercial building HVAC systems.* 2002., 2002.
37. Coakley, D., P. Raftery, and M. Keane, *A review of methods to match building energy simulation models to measured data.* Renewable and sustainable energy reviews, 2014. **37**: p. 123-141.
38. Wang, Z., Y. Chen, and Y. Li, *Development of RC model for thermal dynamic analysis of buildings through model structure simplification.* Energy and Buildings, 2019. **195**: p. 51-67.
39. Rouchier, S., M. Rabouille, and P. Oberlé, *Calibration of simplified building energy models for parameter estimation and forecasting: Stochastic versus deterministic modelling.* Building and Environment, 2018. **134**: p. 181-190.

40. Li, X. and J. Wen, *System identification and data fusion for on-line adaptive energy forecasting in virtual and real commercial buildings.* Energy and Buildings, 2016. **129**: p. 227-237.
41. Baldi, S., et al., *Dual estimation: Constructing building energy models from data sampled at low rate.* Applied Energy, 2016. **169**: p. 81-92.
42. Drgoňa, J., et al., *All you need to know about model predictive control for buildings.* Annual Reviews in Control, 2020. **50**: p. 190-232.
43. Olivier, A. and A.W. Smyth, *On the performance of online parameter estimation algorithms in systems with various identifiability properties.* Frontiers in Built Environment, 2017. **3**: p. 14.
44. Cao, X., X. Dai, and J. Liu, *Building energy-consumption status worldwide and the state-of-the-art technologies for zero-energy buildings during the past decade.* Energy and buildings, 2016. **128**: p. 198-213.
45. Wen, J. and T.F. Smith. *Development and validation of online models with parameter estimation for a building zone with VAV system*. in *ASME International Mechanical Engineering Congress and Exposition*. 2004.
46. Coley, D.A. and J. Penman, *Second order system identification in the thermal response of real buildings. Paper II: Recursive formulation for on-line building energy management and control.* Building and Environment, 1992. **27**(3): p. 269-277.
47. Zavala, V.M., et al., *On-line economic optimization of energy systems using weather forecast information.* Journal of Process Control, 2009. **19**(10): p. 1725-1736.
48. Radecki, P. and B. Hencey. *Online building thermal parameter estimation via unscented kalman filtering*. in *2012 American Control Conference (ACC)*. 2012. IEEE.
49. Maasoumy, M., et al., *Handling model uncertainty in model predictive control for energy efficient buildings.* Energy and Buildings, 2014. **77**: p. 377-392.
50. Al-Hussein, A. and A. Haldar, *Unscented Kalman filter with unknown input and weighted global iteration for health assessment of large structural systems.* Structural Control and Health Monitoring, 2016. **23**(1): p. 156-175.
51. Al-Hussein, A. and A. Haldar, *Novel unscented Kalman filter for health assessment of structural systems with unknown input.* Journal of Engineering Mechanics, 2015. **141**(7): p. 04015012.
52. Lei, Y., et al., *A novel unscented Kalman filter for recursive state-input-system identification of nonlinear systems.* Mechanical Systems and Signal Processing, 2019. **127**: p. 120-135.
53. Simon, D., *Optimal state estimation: Kalman, H infinity, and nonlinear approaches*. 2006: John Wiley & Sons.
54. Wan, E.A. and R. Van Der Merwe. *The unscented Kalman filter for nonlinear estimation*. in *Proceedings of the IEEE 2000 Adaptive Systems for Signal Processing, Communications, and Control Symposium (Cat. No. 00EX373)*. 2000. Ieee.
55. Julier, S.J. and J.K. Uhlmann. *New extension of the Kalman filter to nonlinear systems*. in *Signal processing, sensor fusion, and target recognition VI*. 1997. Spie.
56. Lourakis, M.I., *A brief description of the Levenberg-Marquardt algorithm implemented by levmar.* Foundation of Research and Technology, 2005. **4**(1): p. 1-6.
57. Nocedal, J. and S.J. Wright, *Numerical optimization*. 1999: Springer.
58. Chen, Y., A. Athienitis, and K. Galal, *Modeling, design and thermal performance of a BIPV/T system thermally coupled with a ventilated concrete slab in a low energy solar house: Part 1, BIPV/T system and house energy concept.* Solar energy, 2010. **84**(11): p. 1892-1907.
59. *ASHRAE, Energy Standard for Buildings (American Society of Heating, Refrigerating, and Air Conditioning Engineers, Inc., 2019).* 2019.

60. Bailey, T., et al. *Consistency of the EKF-SLAM algorithm*. in *2006 IEEE/RSJ International Conference on Intelligent Robots and Systems*. 2006. IEEE.
61. Kandepu, R., B. Foss, and L. Imsland, *Applying the unscented Kalman filter for nonlinear state estimation.* Journal of process control, 2008. **18**(7-8): p. 753-768.
62. Ogunsola, O.T., L. Song, and G. Wang, *Development and validation of a time-series model for real-time thermal load estimation.* Energy and buildings, 2014. **76**: p. 440-449.
63. Brown, R., *US building-sector energy efficiency potential.* 2008.
64. Martinčević, A., A. Starčić, and M. Vašak. *Parameter estimation for low-order models of complex buildings*. in *Ieee pes innovative smart grid technologies, europe*. 2014. IEEE.
65. Yang, S., et al., *A state-space thermal model incorporating humidity and thermal comfort for model predictive control in buildings.* Energy and Buildings, 2018. **170**: p. 25-39.
66. Jorissen, F., et al., *Implementation and verification of the IDEAS building energy simulation library.* Journal of Building Performance Simulation, 2018. **11**(6): p. 669-688.
67. Arendt, K., et al. *Comparative analysis of white-, gray-and black-box models for thermal simulation of indoor environment: Teaching building case study*. in *Proceedings of the 2018 Building Performance Modeling Conference and SimBuild co-organized by ASHRAE and IBPSA-USA, Chicago, IL, USA*. 2018.
68. Gao, H., C. Koch, and Y. Wu, *Building information modelling based building energy modelling: A review.* Applied energy, 2019. **238**: p. 320-343.
69. Cole, W.J., et al., *Reduced-order residential home modeling for model predictive control.* Energy and Buildings, 2014. **74**: p. 69-77.
70. Loyola-Gonzalez, O., *Black-box vs. white-box: Understanding their advantages and weaknesses from a practical point of view.* IEEE Access, 2019. **7**: p. 154096-154113.
71. Cígler, J., et al. *Beyond theory: the challenge of implementing model predictive control in buildings*. in *Proceedings of 11th Rehva world congress, Clima*. 2013.
72. Afram, A. and F. Janabi-Sharifi, *Theory and applications of HVAC control systems–A review of model predictive control (MPC).* Building and Environment, 2014. **72**: p. 343-355.
73. Jin, X., et al., *Integrated optimal scheduling and predictive control for energy management of an urban complex considering building thermal dynamics.* International Journal of Electrical Power & Energy Systems, 2020. **123**: p. 106273.

Appendix A – A simple RC model case study information and results for parameter-input estimations

For the case study with made-up data, i.e., the 2R2C model, the ordinary differential equation can be shown below:

$$C_2 \frac{dT_2}{dt} = \frac{T_1 - T_2}{R_2} + \frac{T_3 - T_2}{R_3} \tag{A.1}$$

$$C_3 \frac{dT_3}{dt} = \frac{T_2 - T_3}{R_3} + Q_1 + Q_2 \tag{A.2}$$

Accordingly, the state-space equation of the 2R2C model, when Q_2 is assumed to be unknown, can be written as:

$$\dot{\boldsymbol{s}}(t) = \boldsymbol{A}^c \boldsymbol{s}(t) + \boldsymbol{B}^c \boldsymbol{u}(t)$$

$$\frac{d}{dt}\begin{bmatrix} T_2 \\ T_3 \end{bmatrix} = \begin{bmatrix} \frac{-1}{R_2 C_2} - \frac{1}{R_3 C_2} & \frac{1}{R_3 C_2} \\ \frac{1}{R_3 C_3} & -\frac{1}{R_3 C_3} \end{bmatrix} \begin{bmatrix} T_2 \\ T_3 \end{bmatrix} + \begin{bmatrix} \frac{1}{R_2 C_2} & 0 & 0 \\ 0 & \frac{1}{C_3} & \frac{1}{C_3} \end{bmatrix} \begin{bmatrix} T_1 \\ Q_1 \\ Q_2 \end{bmatrix} \tag{A.3}$$

$$\begin{aligned} \dot{\boldsymbol{x}}(t) &= \left[\dot{\boldsymbol{s}}(t)\ \dot{\boldsymbol{\theta}}(t)\right] \\ \boldsymbol{x}_{k+1} &= f\left(\boldsymbol{x}_k, \boldsymbol{u}_k^{kn}, \boldsymbol{u}_k^{un}\right) + \boldsymbol{w}_k \\ f\left(\boldsymbol{x}_k, \boldsymbol{u}_k^{kn}, \boldsymbol{u}_k^{un}\right) &= \boldsymbol{A}^{\boldsymbol{dx}} \boldsymbol{x}_k + \boldsymbol{B}^{\boldsymbol{dx}} \begin{bmatrix} \boldsymbol{u}_k^{\boldsymbol{kn}} \\ \boldsymbol{u}_k^{\boldsymbol{un}} \end{bmatrix} \end{aligned} \tag{A.4}$$

$$\boldsymbol{A}^{dx} = \begin{bmatrix} A^{d}{}_{2\times2} & 0_{2\times4} \\ 0_{4\times2} & diag(1)_{4\times4} \end{bmatrix}_{6\times6} \qquad \boldsymbol{B}^{dx} = \begin{bmatrix} \boldsymbol{B}^{d}{}_{2\times3} \\ 0_{4\times3} \end{bmatrix}_{6\times3} \tag{A.5}$$

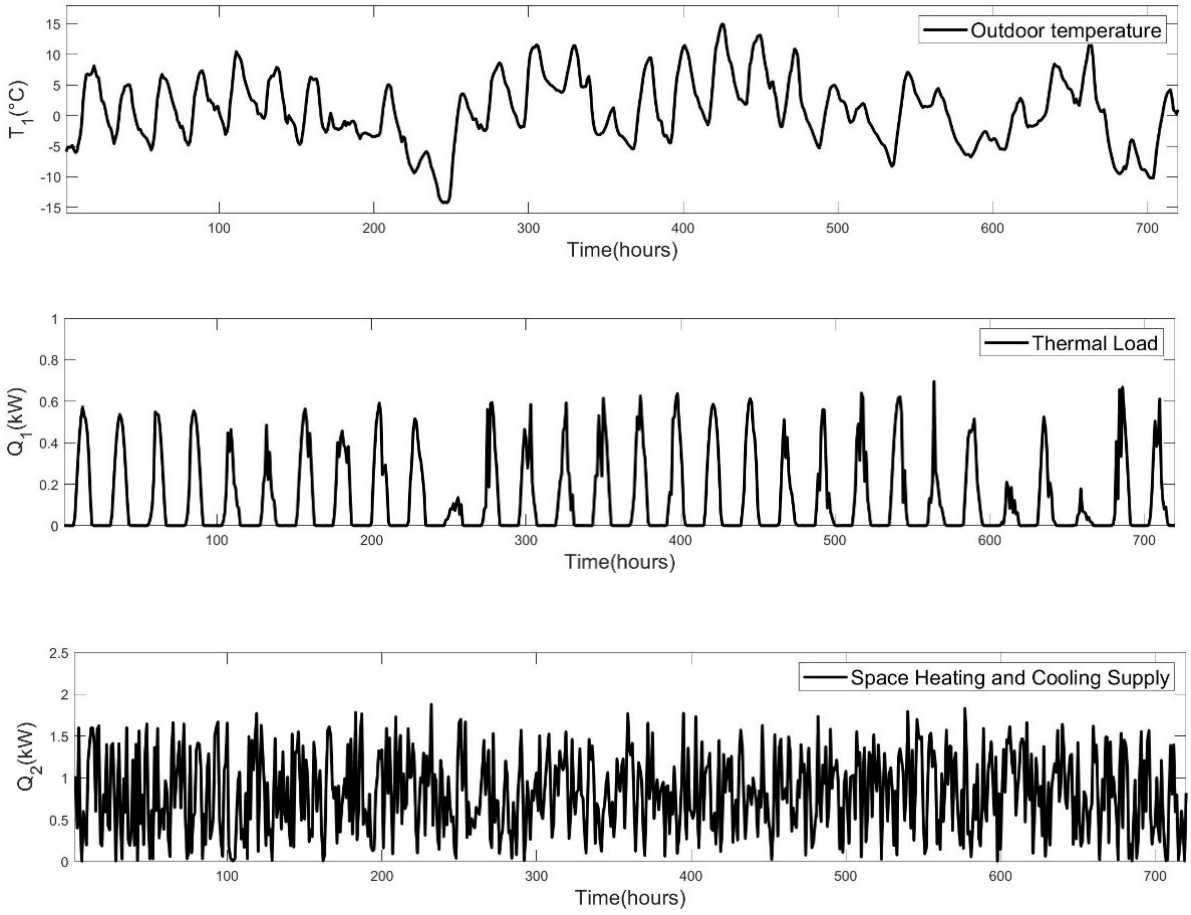

Figure A.1 2R2C model inputs

Regarding the results for 2R2C-2 and 2R2C-3 scenarios, the last estimated model parameters are shown in Table A.1

Table A.1 Last estimated model parameters for Scenarios for 2R2C-2 and 2R2C-3

Model parameters	True values	2R2C-2	2R2C-3
R_2	4.45	2.85	3.45
R_3	26.35	25.1	25.23
C_2	2.64	2.3	2.63
C_3	1.2	1.2	1.14

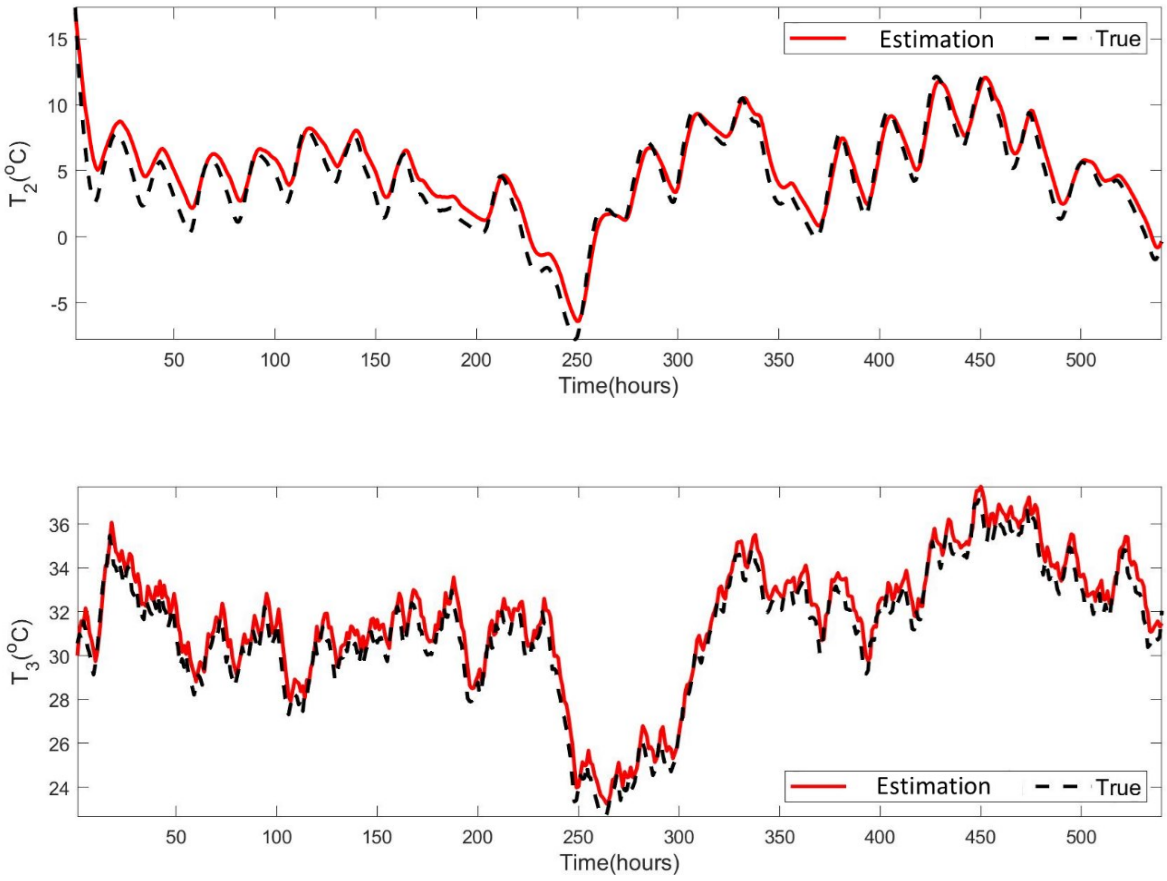

Figure A. 2Comparison between true and estimated temperature responses for Scenario 2R2C-2

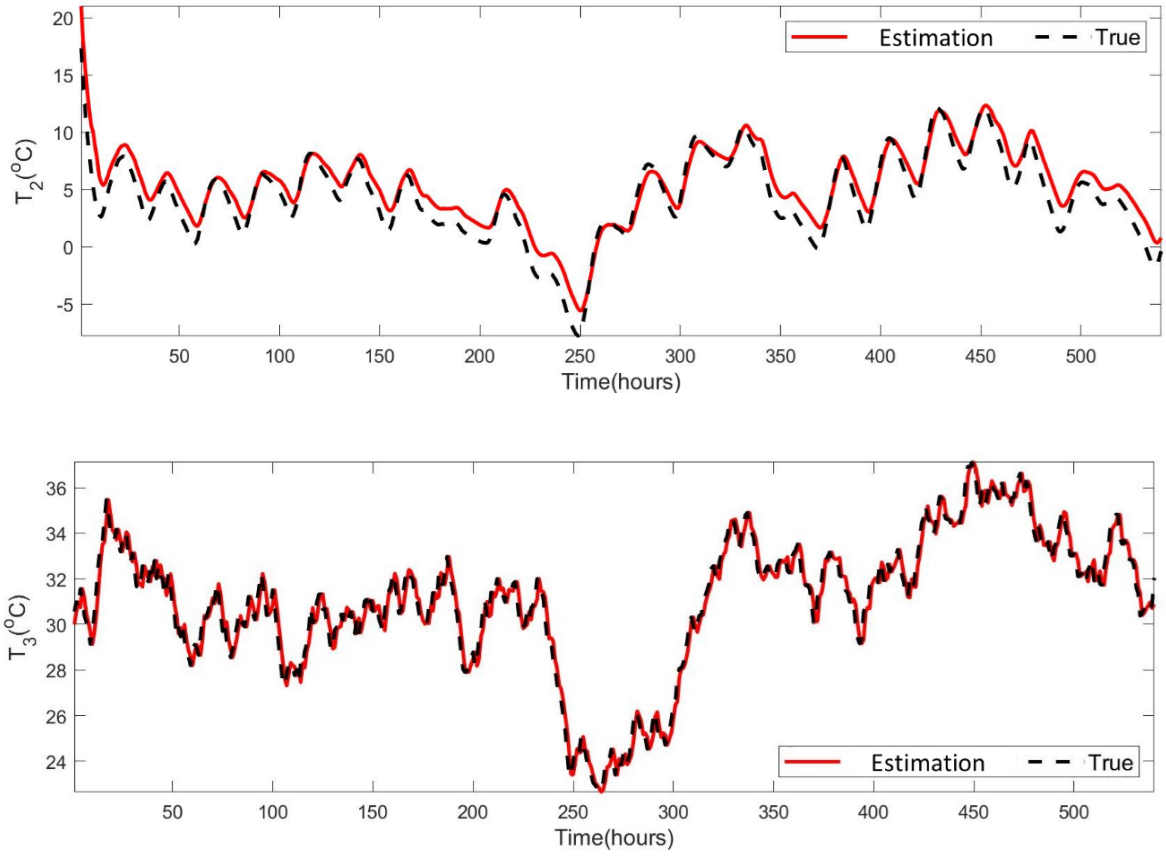

Figure A. 3Comparison between true and estimated temperature responses for Scenario 2R2C-3

Comparison between true and estimated model input for Scenario 2R2C-1:

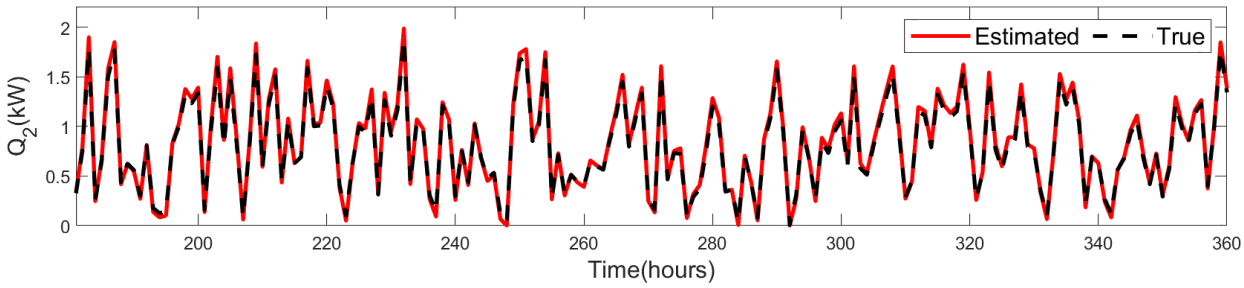

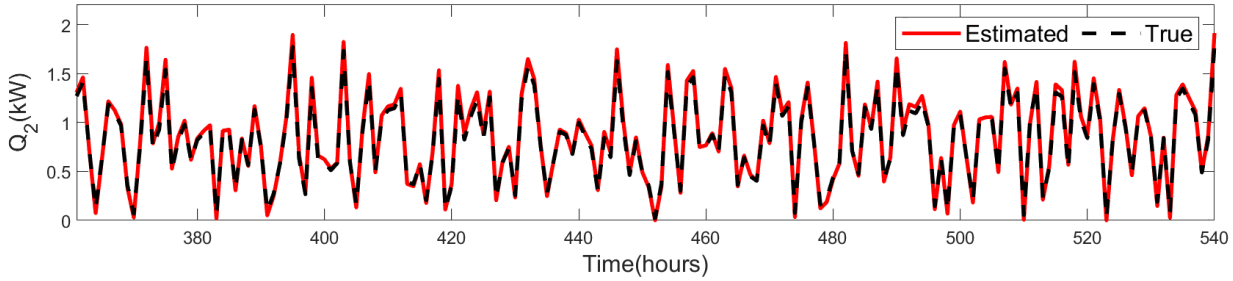

Figure A. 4 Comparison between true and estimated model input for Scenario 2R2C-1

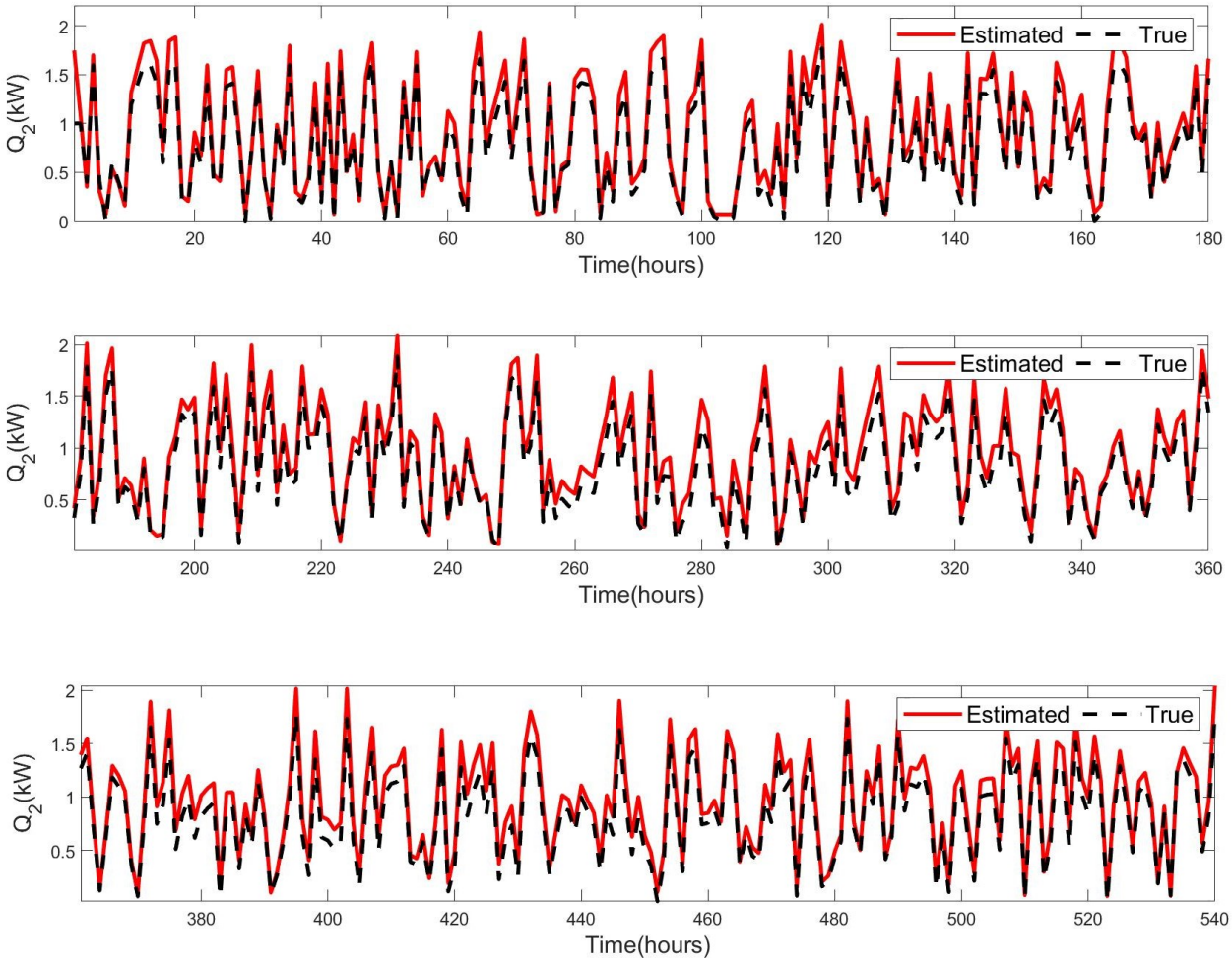

Figure A. 5 Comparison between true and estimated model input for Scenario 2R2C-2

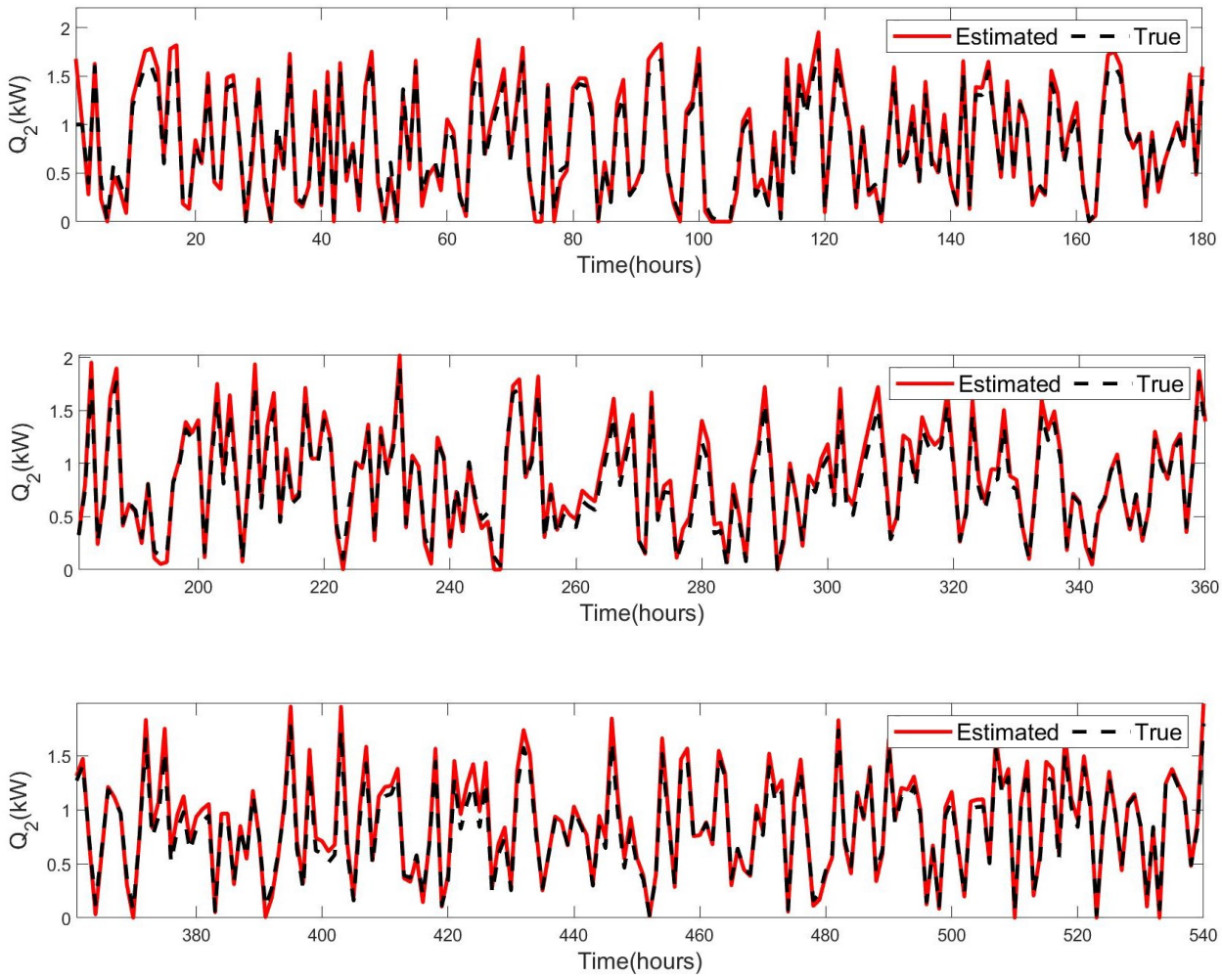

Figure A. 6 Comparison between true and estimated model input for Scenario 2R2C-3

Appendix B – Real-world case study information and results for parameter-input estimations

The ODEs shown below are derived for the 10R6C model:

$$C_{ui}\frac{dT_u}{dt} = \frac{T_0 - T_u}{R_3} + \frac{T_{um} - T_u}{R_1} + \frac{T_{um} - T_u}{R_2} + \alpha_{hpu}Q_{hp} + \alpha_{su}Q_s$$

$$C_{um}\frac{dT_{um}}{dt} = \frac{T_u - T_{um}}{R_1}$$

$$C_{mi}\frac{dT_m}{dt} = \frac{T_0 - T_m}{R_6} + \frac{T_{mm} - T_m}{R_4} + \frac{T_b - T_m}{R_5} + \frac{T_u - T_m}{R_2} + \alpha_{hpm}Q_{hp} + \alpha_{sm}Q_s + \alpha_{em}Q_{elec} \quad \text{(B.1)}$$

$$C_{mm}\frac{dT_{mm}}{dt} = \frac{T_m - T_{mm}}{R_4} + \frac{T_b - T_{mm}}{R_7}$$

$$C_{bi}\frac{dT_b}{dt} = \frac{T_0 - T_b}{R_9} + \frac{T_{bm} - T_b}{R_8} + \frac{T_{mm} - T_b}{R_7} + \frac{T_m - T_b}{R_5} + \alpha_{hpb}Q_{hp} + \alpha_{sb}Q_s + \alpha_{eb}Q_{elec}$$

$$C_{bm}\frac{dT_{bm}}{dt} = \frac{T_b - T_{bm}}{R_8} + \frac{T_g - T_{bm}}{R_{10}} + Q_{vcs}$$

Therefore, the state space form of the 10R6C model can be written as follows:

$$\frac{d}{dt}\begin{bmatrix} T_u \\ T_{um} \\ T_m \\ T_{mm} \\ T_b \\ T_{bm} \end{bmatrix} = A_c \begin{bmatrix} T_u \\ T_{um} \\ T_m \\ T_{mm} \\ T_b \\ T_{bm} \end{bmatrix} + B_c \begin{bmatrix} T_0 \\ T_{\mathrm{g}} \\ Q_{\mathrm{s}} \\ Q_{\mathrm{hp}} \\ Q_{\mathrm{elec}} \\ Q_{\mathrm{vcs}} \end{bmatrix}$$

where

$$A_c = \begin{bmatrix} \frac{-1}{C_{ui}}\left(\frac{1}{R_1}+\frac{1}{R_2}+\frac{1}{R_3}\right) & \frac{1}{R_1 * C_{ui}} & \frac{1}{R_2 * C_{ui}} & 0 & 0 & 0 \\ \frac{1}{R_1 * C_{um}} & \frac{-1}{R_1 * C_{um}} & 0 & 0 & 0 & 0 \\ \frac{1}{R_2 * C_{mi}} & 0 & \frac{-1}{C_{mi}}\left(\frac{1}{R_2}+\frac{1}{R_4}+\frac{1}{R_5}+\frac{1}{R_6}\right) & \frac{1}{R_4 * C_{mi}} & \frac{1}{R_5 * C_{mi}} & 0 \\ 0 & 0 & \frac{1}{R_4 * C_{mm}} & \frac{-1}{C_{mm}}\left(\frac{1}{R_4}+\frac{1}{R_7}\right) & \frac{1}{R_7 * C_{mm}} & 0 \\ 0 & 0 & \frac{1}{R_5 * C_{bi}} & \frac{1}{R_7 * C_{bi}} & \frac{-1}{C_{bi}}\left(\frac{1}{R_5}+\frac{1}{R_7}+\frac{1}{R_8}+\frac{1}{R_9}\right) & \frac{1}{R_8 * C_{bi}} \\ 0 & 0 & 0 & 0 & \frac{1}{R_8 * C_{bm}} & \frac{-1}{C_{bm}}\left(\frac{1}{R_8}+\frac{1}{R_{10}}\right) \end{bmatrix}$$

$$\mathrm{B}_c = \begin{bmatrix} \frac{1}{R_3 * C_{\mathrm{ui}}} & 0 & \frac{\alpha_{\mathrm{su}}}{C_{\mathrm{ui}}} & \frac{\alpha_{\mathrm{hpu}}}{C_{\mathrm{ui}}} & 0 & 0 \\ 0 & 0 & 0 & 0 & 0 & 0 \\ \frac{1}{R_6 * C_{\mathrm{mi}}} & 0 & \frac{\alpha_{\mathrm{sm}}}{C_{\mathrm{mi}}} & \frac{\alpha_{\mathrm{hpm}}}{C_{\mathrm{mi}}} & \frac{\alpha_{\mathrm{em}}}{C_{\mathrm{mi}}} & 0 \\ 0 & 0 & 0 & 0 & 0 & 0 \\ \frac{1}{R_9 * C_{\mathrm{bi}}} & 0 & \frac{\alpha_{\mathrm{sb}}}{C_{\mathrm{bi}}} & \frac{\alpha_{\mathrm{hpb}}}{C_{\mathrm{bi}}} & \frac{\alpha_{\mathrm{eb}}}{C_{\mathrm{bi}}} & 0 \\ 0 & \frac{1}{R_{10} * C_{\mathrm{bm}}} & 0 & 0 & 0 & \frac{1}{C_{bm}} \end{bmatrix} \quad \text{(B.2)}$$

$$\boldsymbol{A}^{dx} = \begin{bmatrix} \boldsymbol{A}^{d}{}_{6\times6} & 0_{6\times24} \\ 0_{24\times6} & diag(1)_{24\times24} \end{bmatrix}_{30\times30} \qquad \boldsymbol{B}^{dx} = \begin{bmatrix} \boldsymbol{B}^{d}{}_{6\times6} \\ 0_{24\times6} \end{bmatrix}_{30\times6} \tag{B.3}$$

Single detached house (10R6C) model inputs:

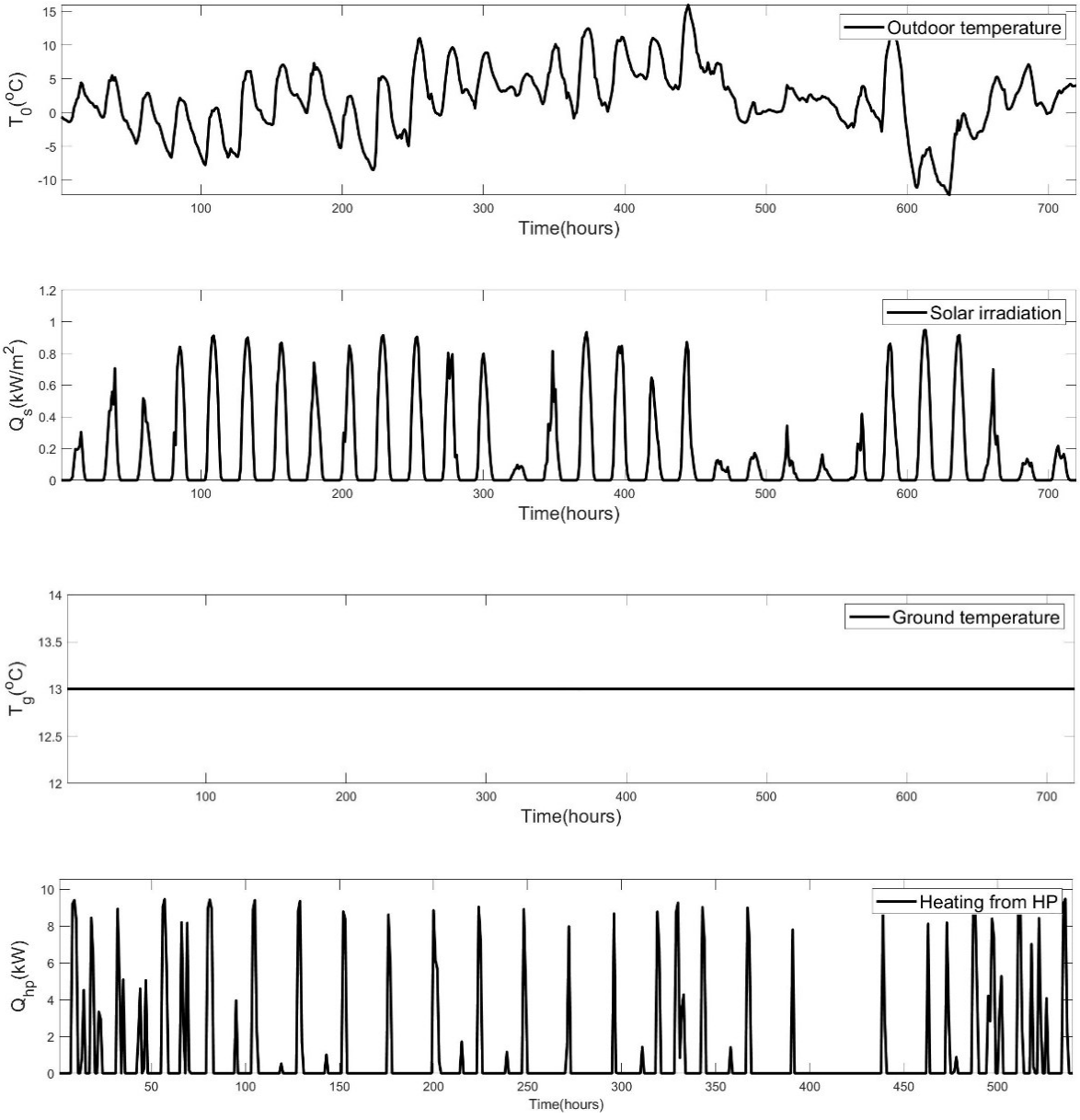

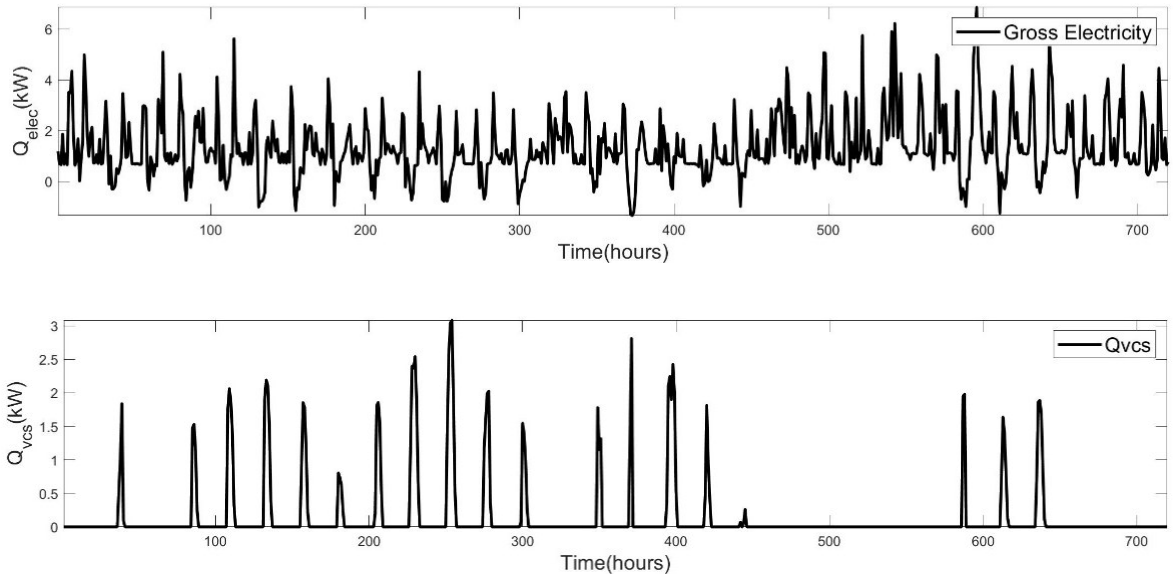

Figure B.1 10R6C model inputs

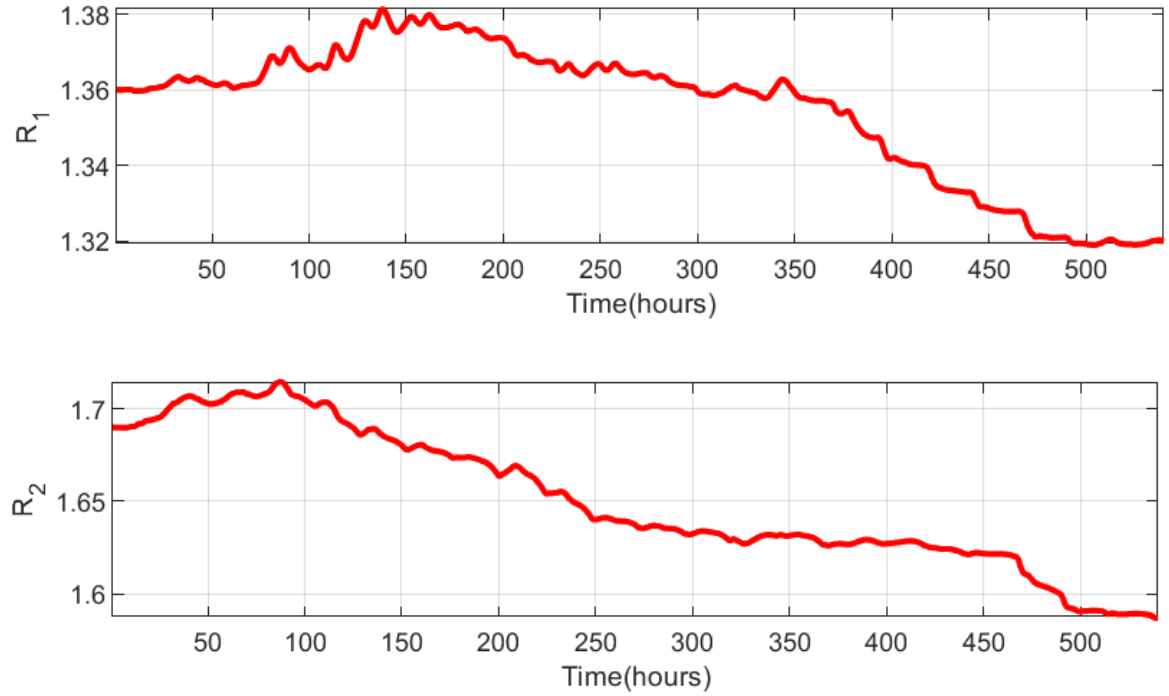

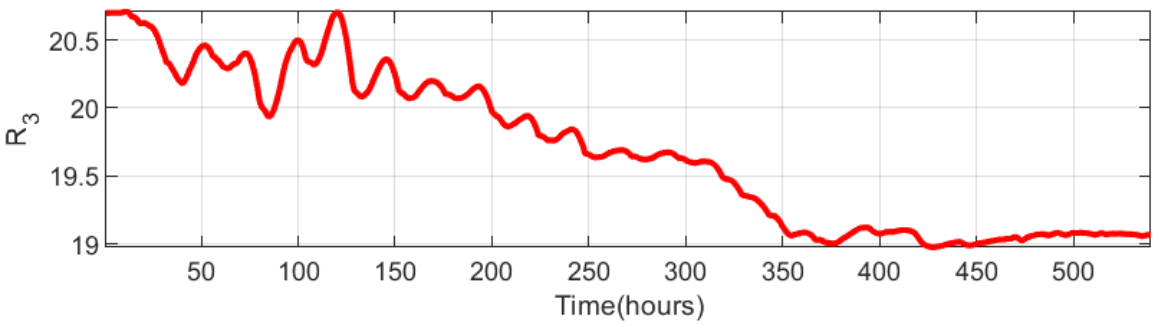
20.5
20
19.5
19
R_3
50
100
150
200
250
300
350
400
450
500
Time(hours)

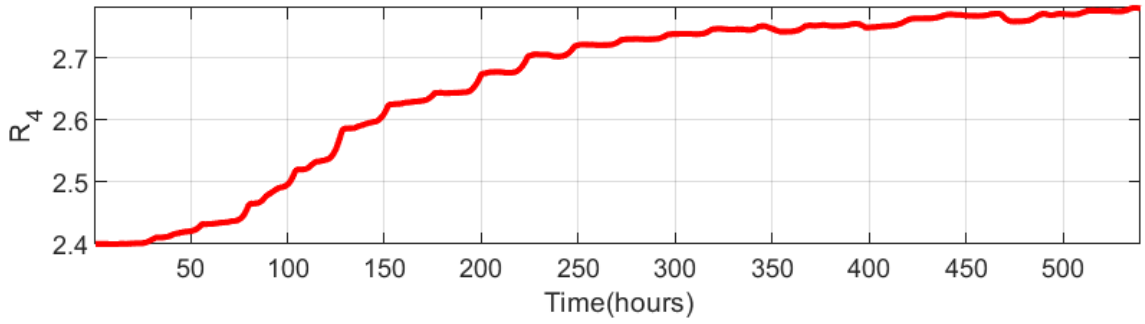
2.7
2.6
2.5
2.4
R_4
50
100
150
200
250
300
350
400
450
500
Time(hours)

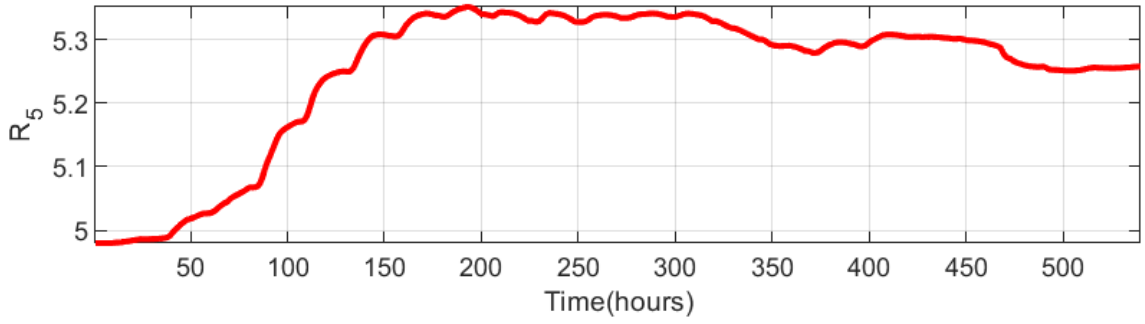
5.3
5.2
5.1
5
R_5
50
100
150
200
250
300
350
400
450
500
Time(hours)

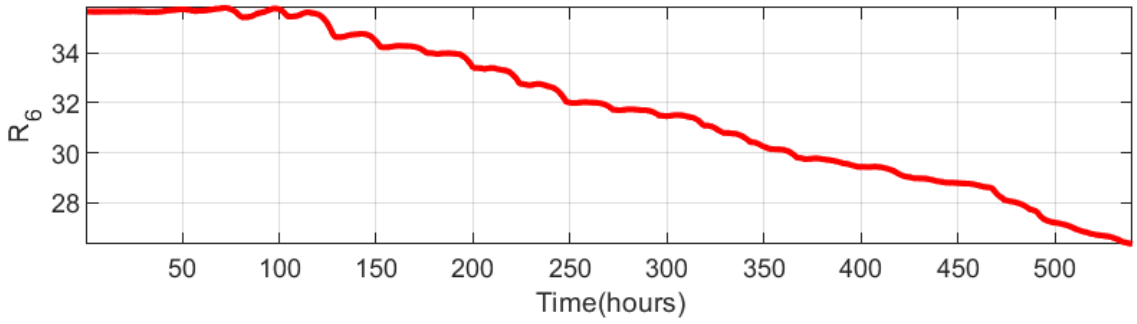
34
32
30
28
R_6
50
100
150
200
250
300
350
400
450
500
Time(hours)

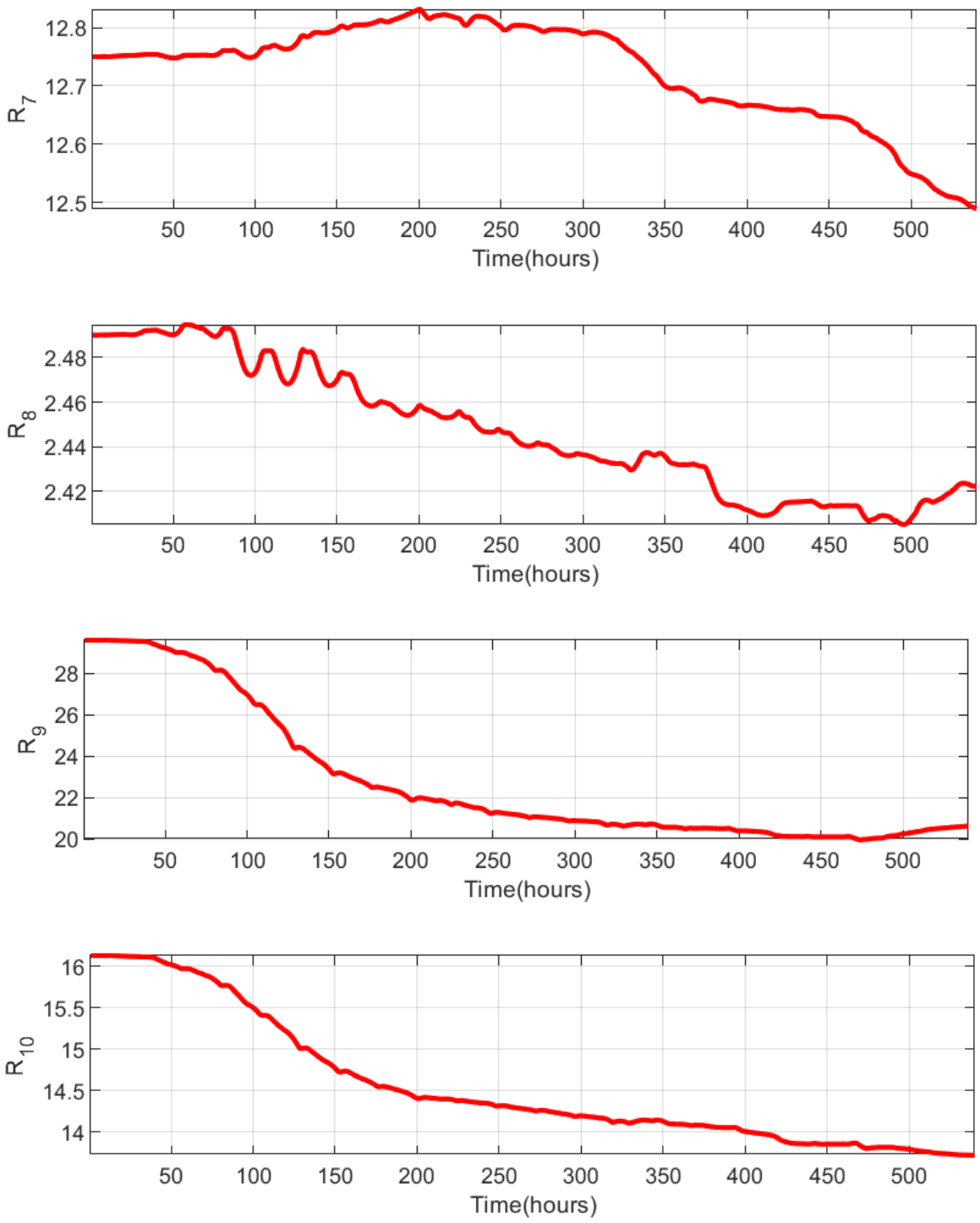

Figure B. 2 10R6C model parameters estimation: thermal resistances for Scenario 10R6C-1

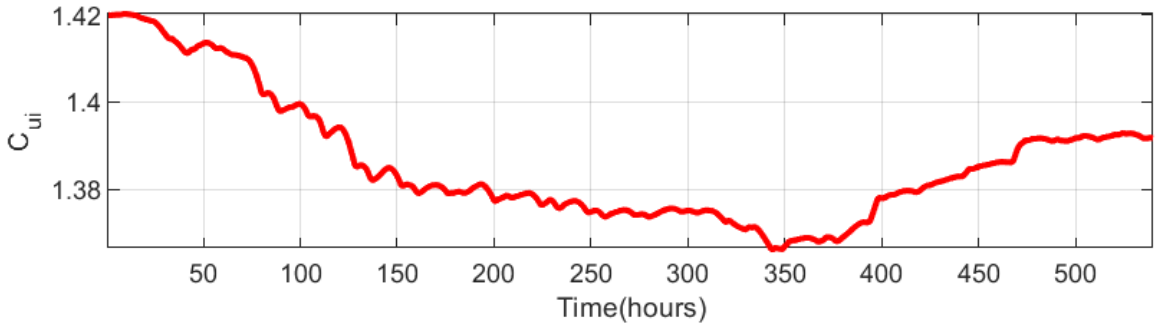
1.42
1.4
1.38
C_{ui}
50
100
150
200
250
300
350
400
450
500
Time(hours)

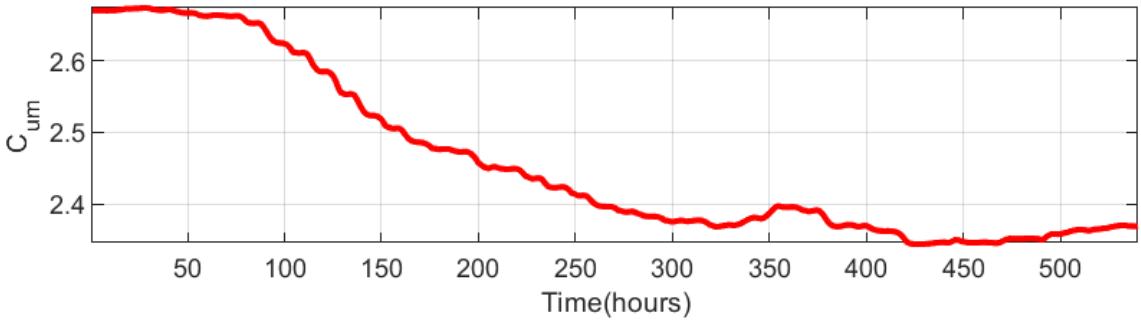
2.6
2.5
2.4
C_{um}
50
100
150
200
250
300
350
400
450
500
Time(hours)

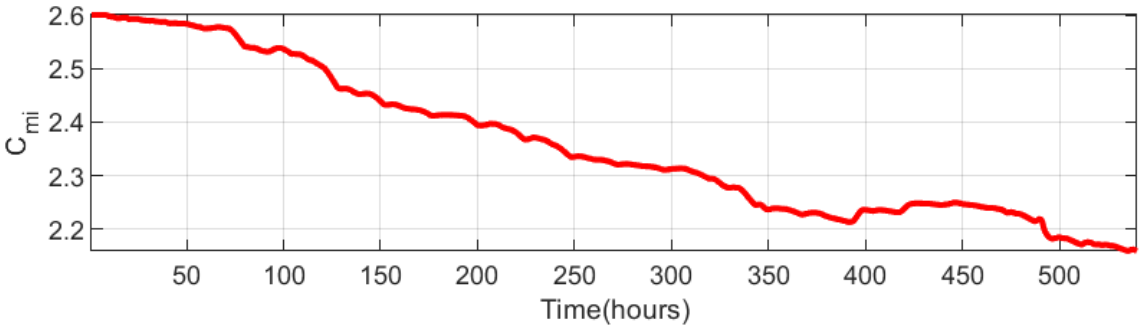
2.6
2.5
2.4
2.3
2.2
C_{mi}
50
100
150
200
250
300
350
400
450
500
Time(hours)

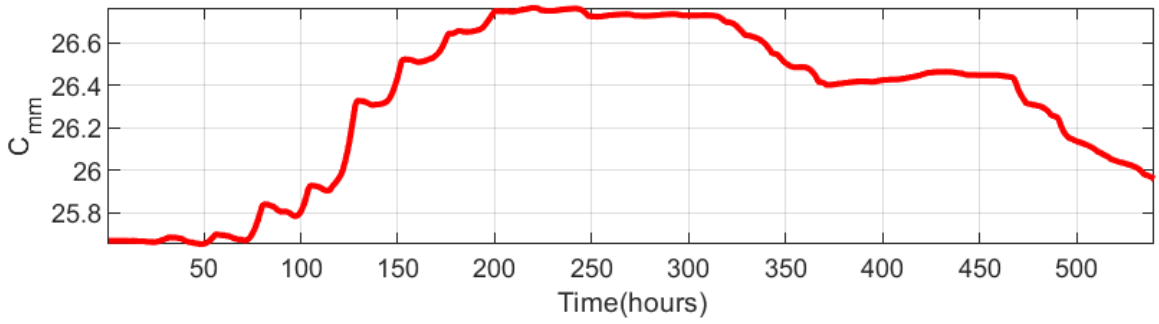
26.6
26.4
26.2
26
25.8
C_{mm}
50
100
150
200
250
300
350
400
450
500
Time(hours)

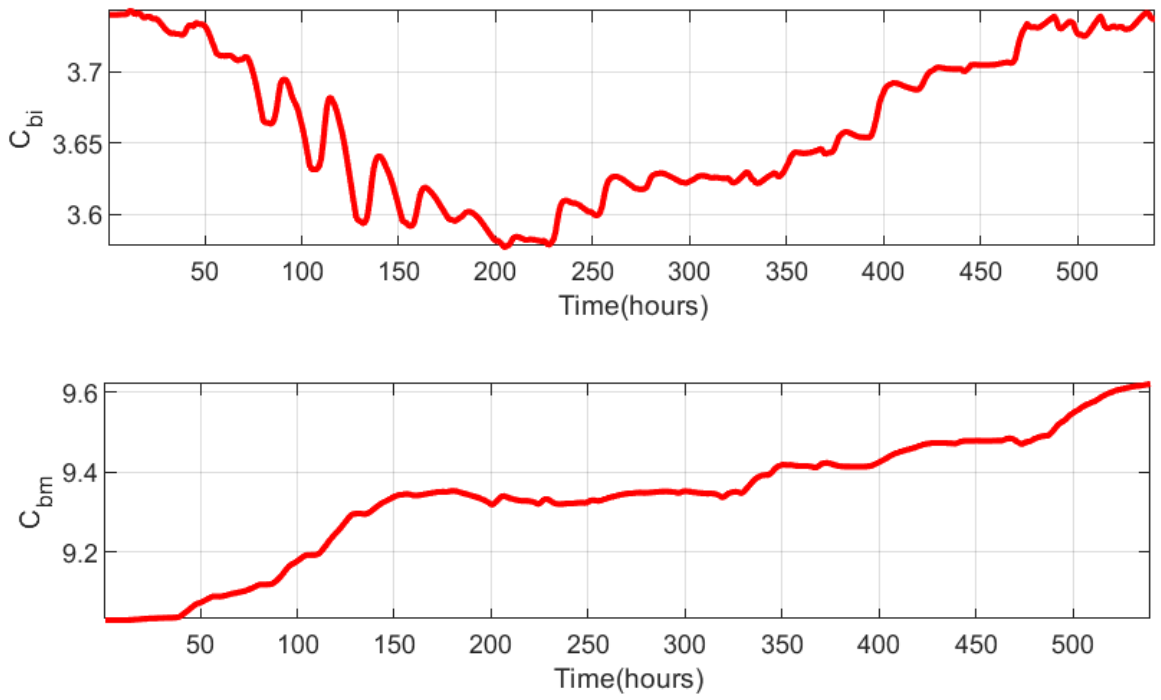

Figure B.3 10R6C model parameters estimation: thermal capacitances for Scenario 10R6C-1

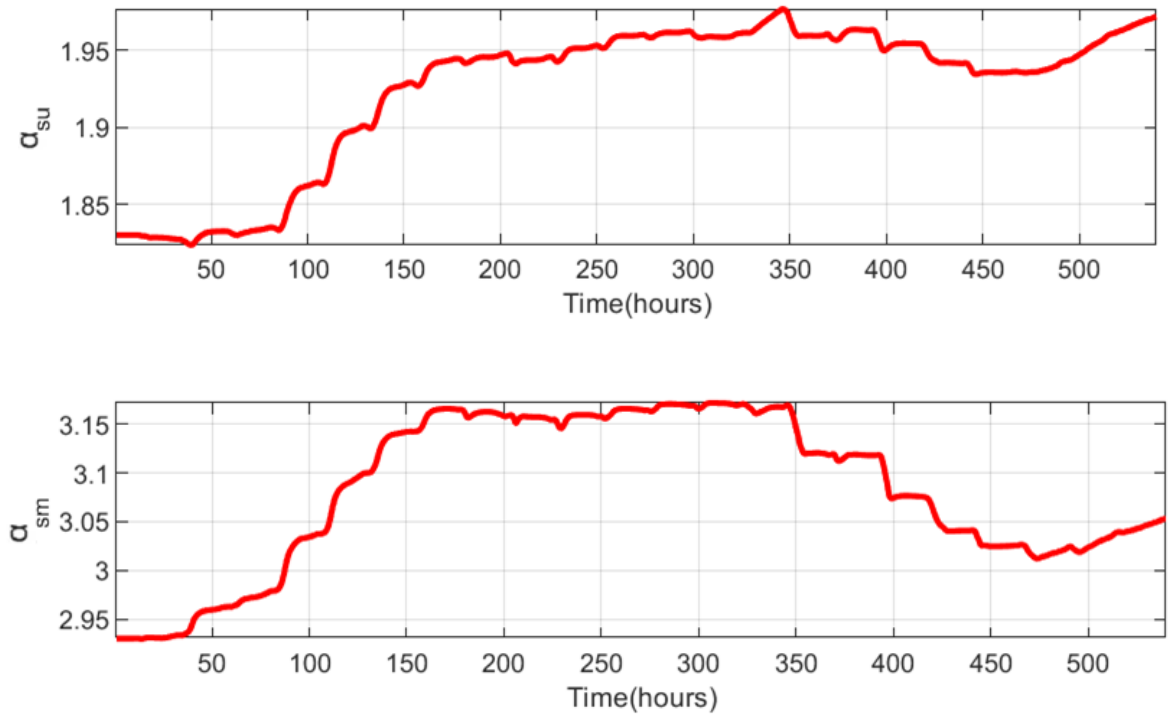

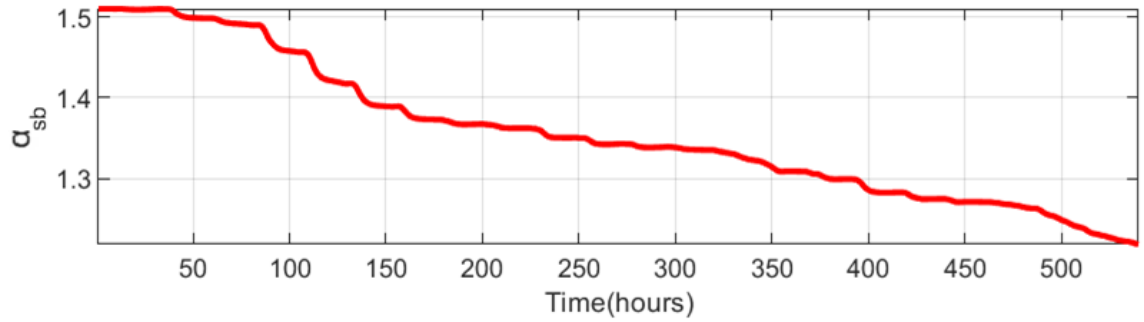
1.5
1.4
1.3
α_{sb}
50
100
150
200
250
300
350
400
450
500
Time(hours)

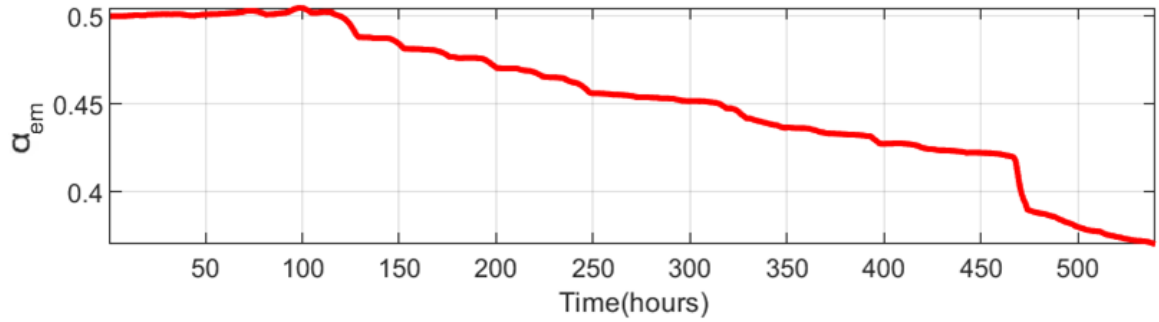
0.5
0.45
0.4
α_{em}
50
100
150
200
250
300
350
400
450
500
Time(hours)

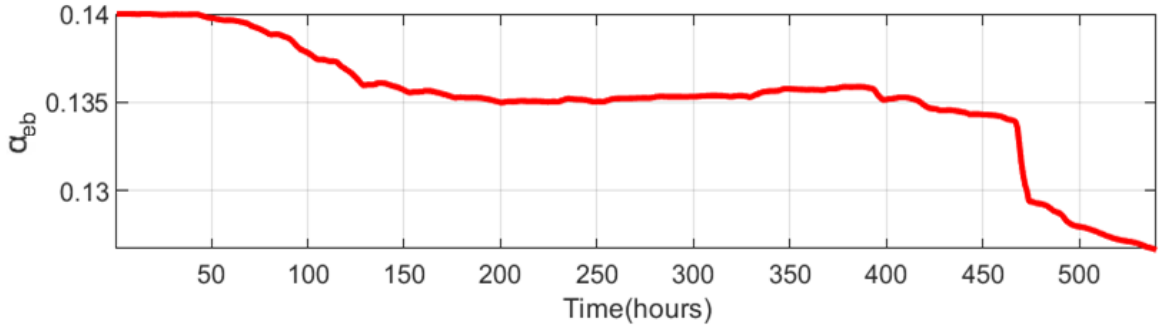
0.14
0.135
0.13
α_{eb}
50
100
150
200
250
300
350
400
450
500
Time(hours)

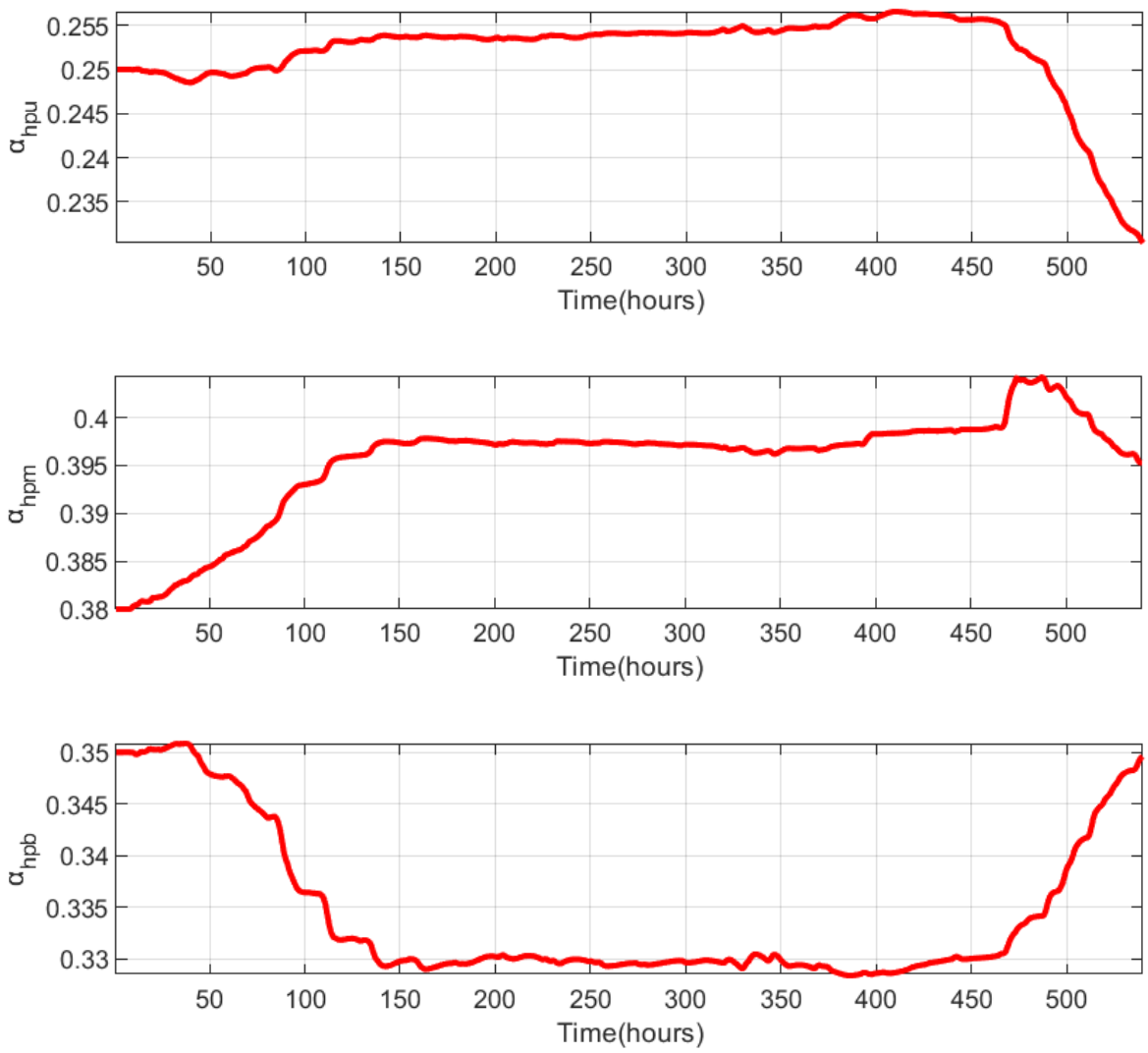

Figure B. 410R6C model parameters estimation: solar and internal gain factors for Scenario 10R6C-1

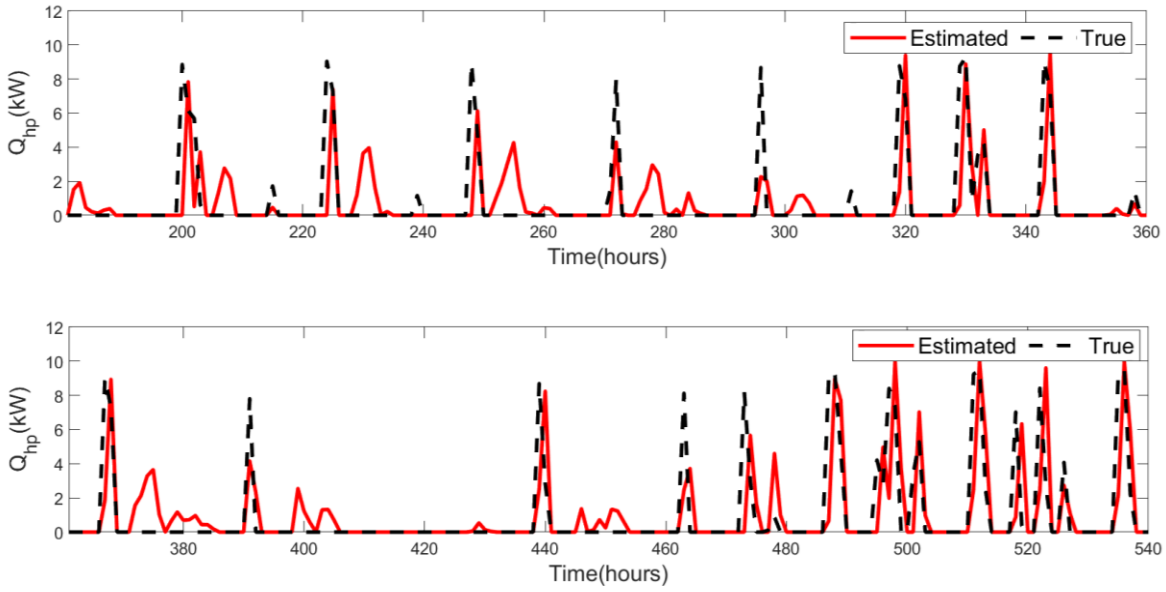

Figure B. 5 Comparison between true and estimated model input for Scenario 10R6C-1

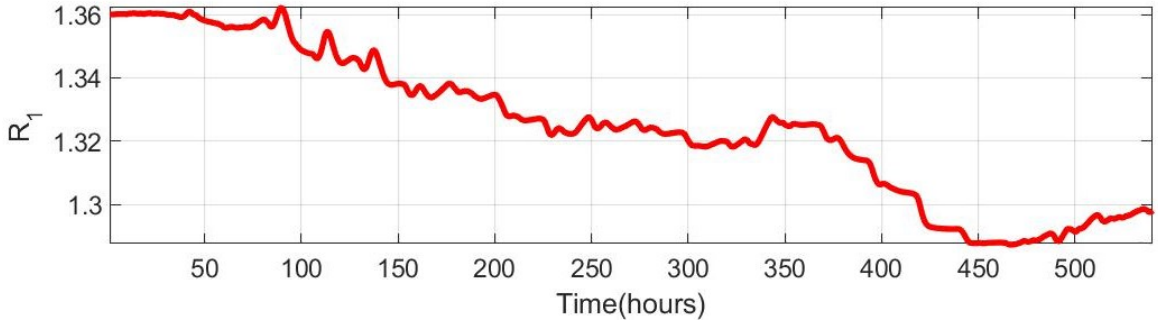

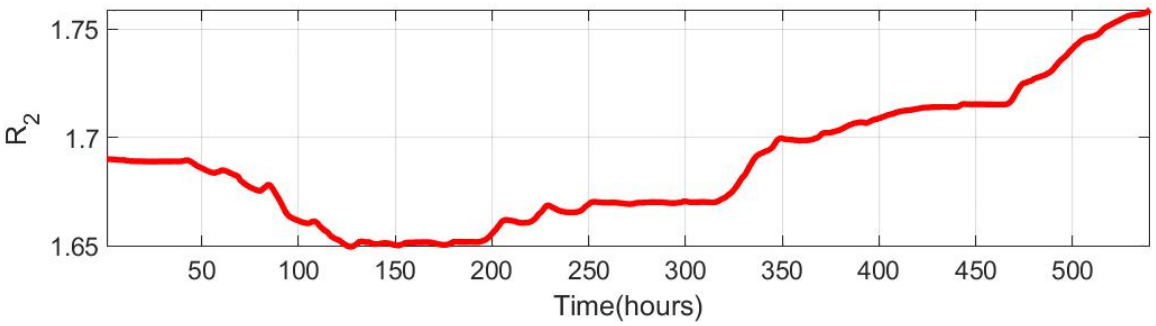
1.75
1.7
1.65
R_2
50
100
150
200
250
300
350
400
450
500
Time(hours)

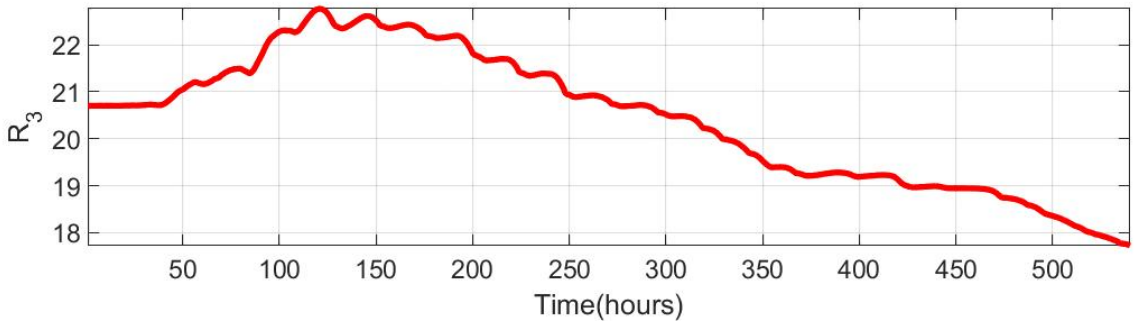
22
21
20
19
18
R_3
50
100
150
200
250
300
350
400
450
500
Time(hours)

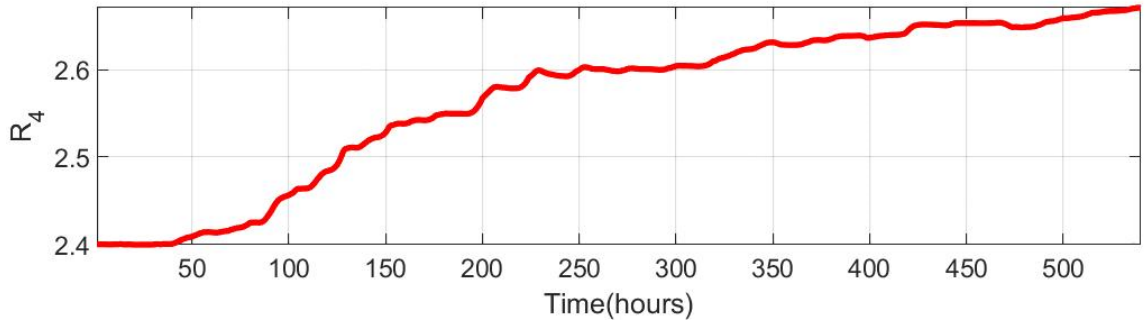
2.6
2.5
2.4
R_4
50
100
150
200
250
300
350
400
450
500
Time(hours)

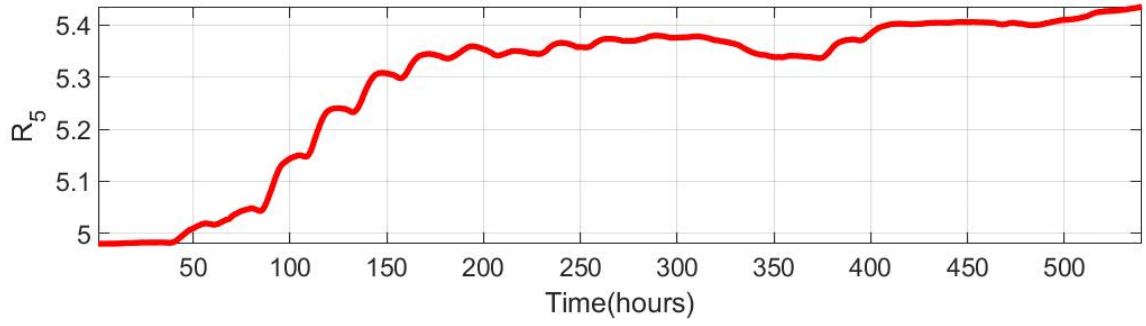
5.4
5.3
5.2
5.1
5
R_5
50
100
150
200
250
300
350
400
450
500
Time(hours)

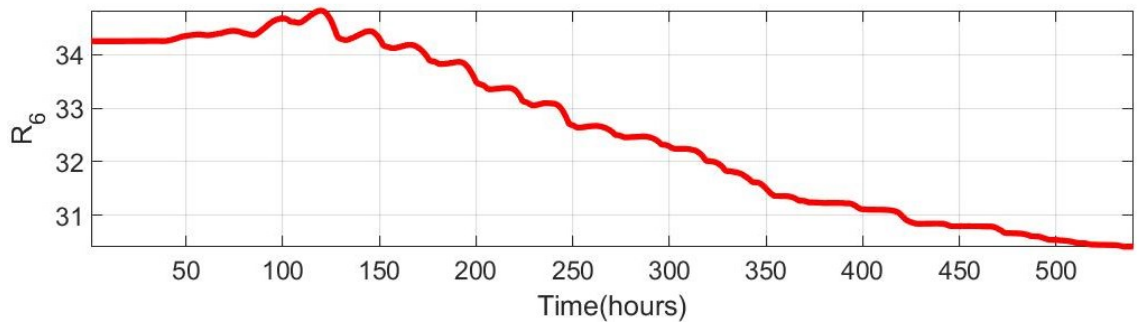
34
33
32
31
R_6
50
100
150
200
250
300
350
400
450
500
Time(hours)

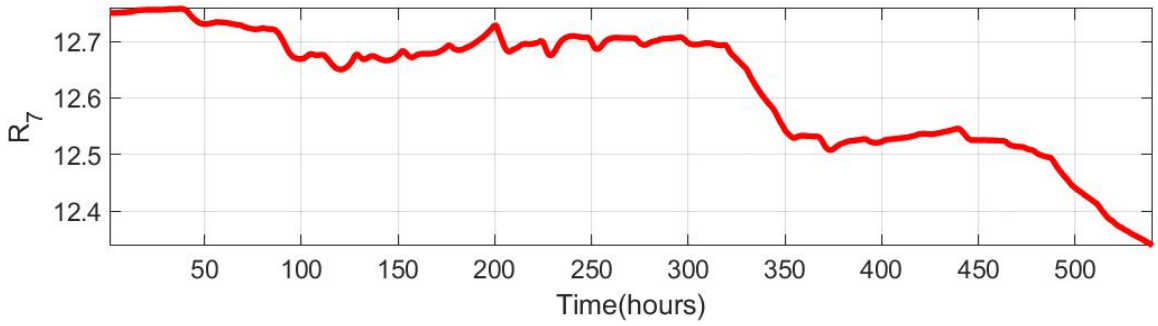
12.7
12.6
12.5
12.4
R_7
50
100
150
200
250
300
350
400
450
500
Time(hours)

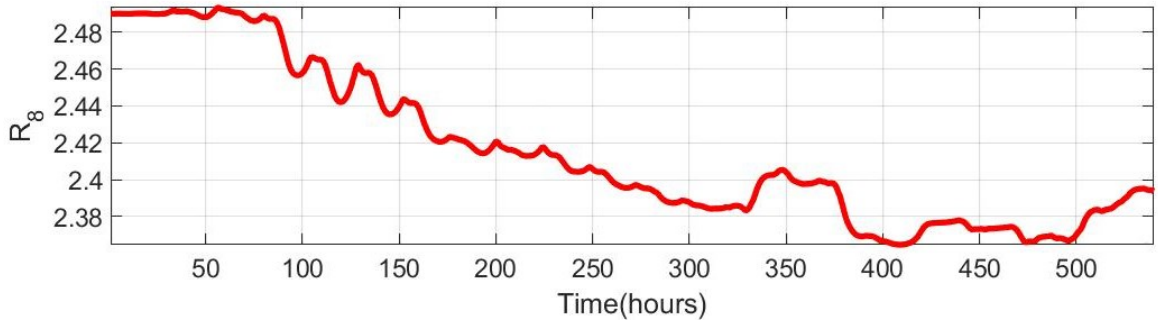
2.48
2.46
2.44
2.42
2.4
2.38
R_8
50
100
150
200
250
300
350
400
450
500
Time(hours)

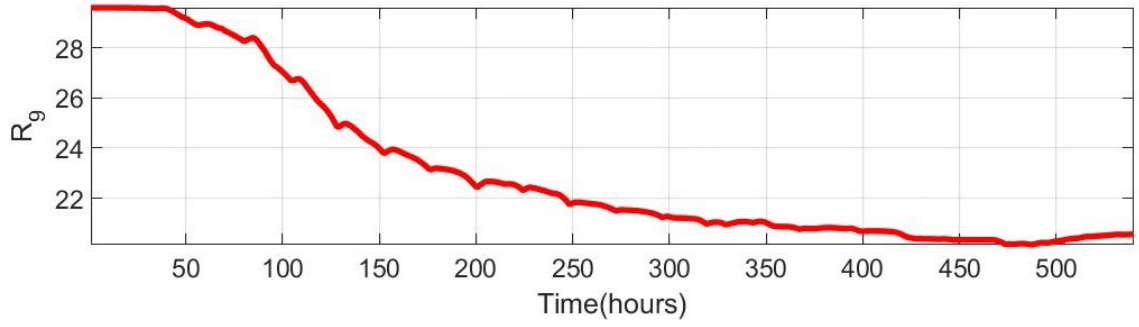
28
26
24
22
R_9
50
100
150
200
250
300
350
400
450
500
Time(hours)

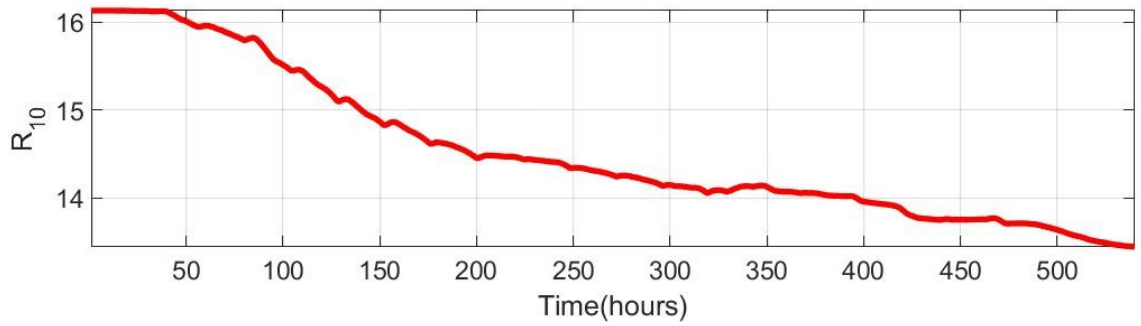

Figure B. 6 10R6C model parameters estimation: thermal resistances for scenario 10R6C-3

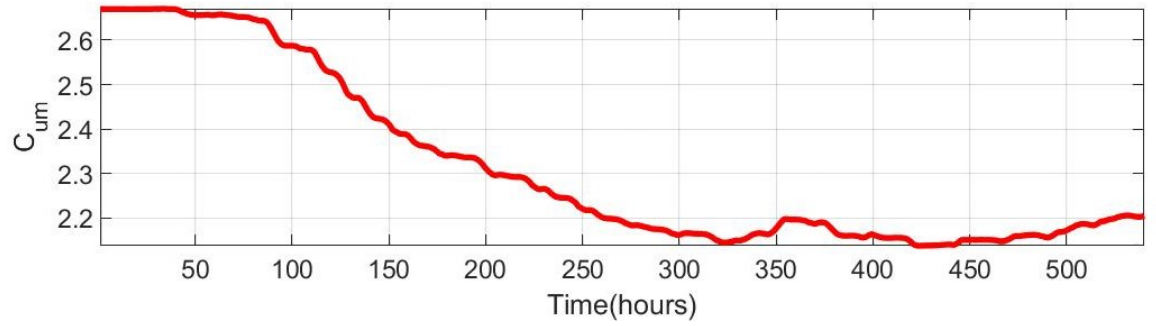

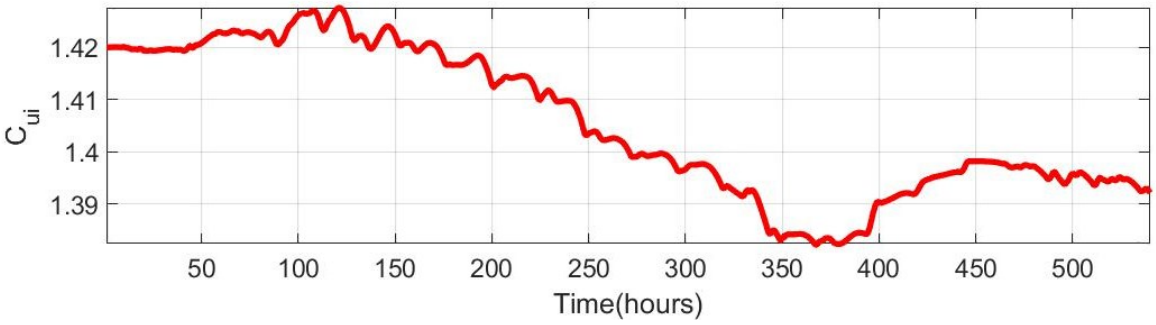

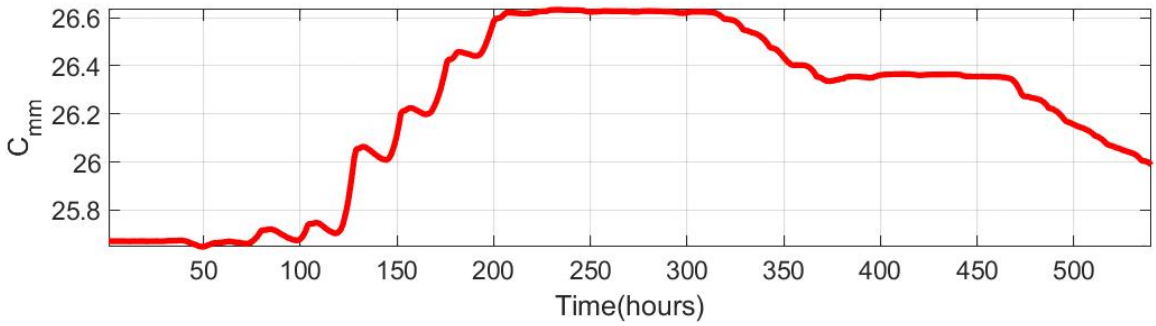

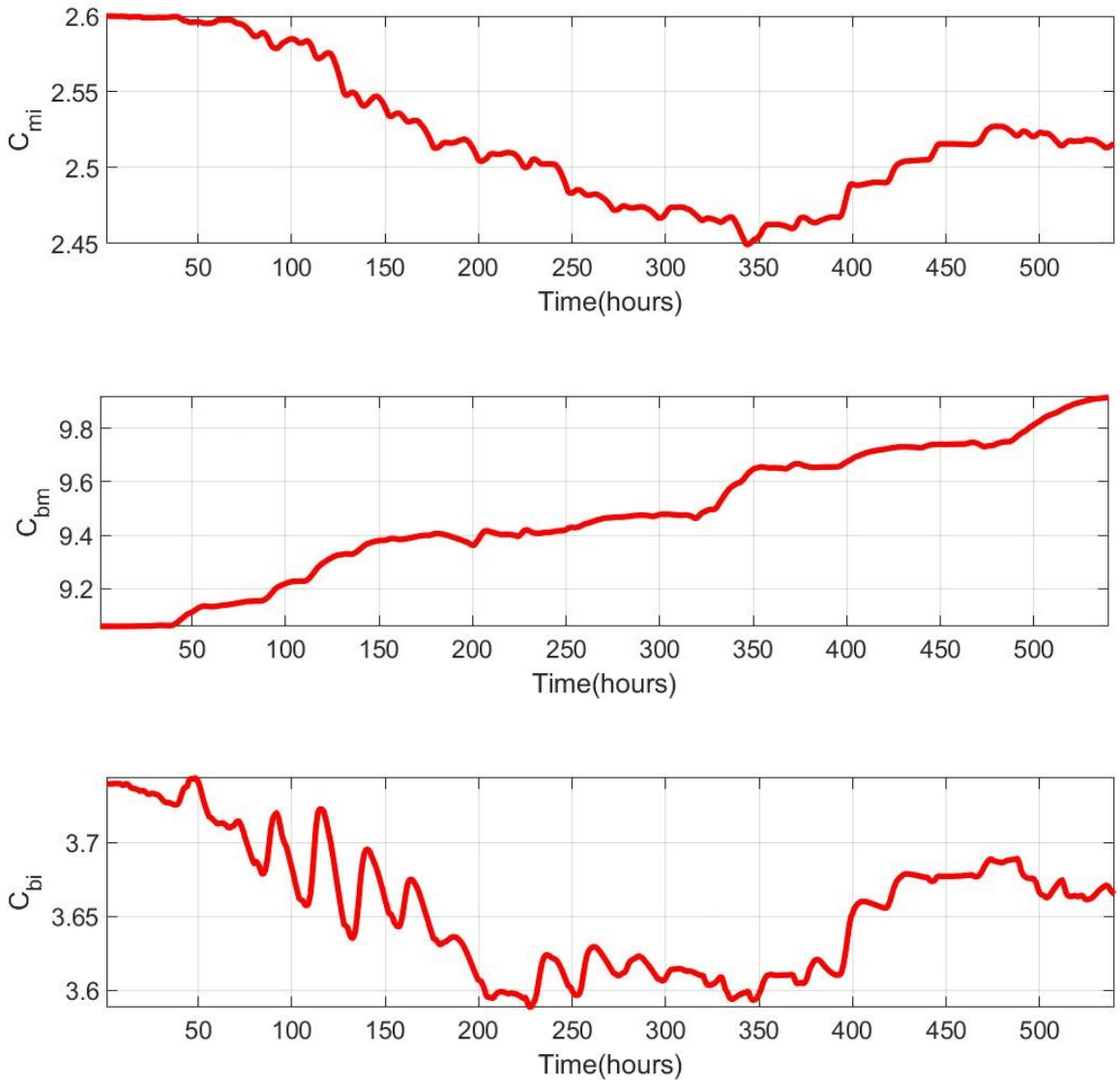

Figure B. 710R6C model parameters estimation: thermal capacitances for scenario 10R6C-3

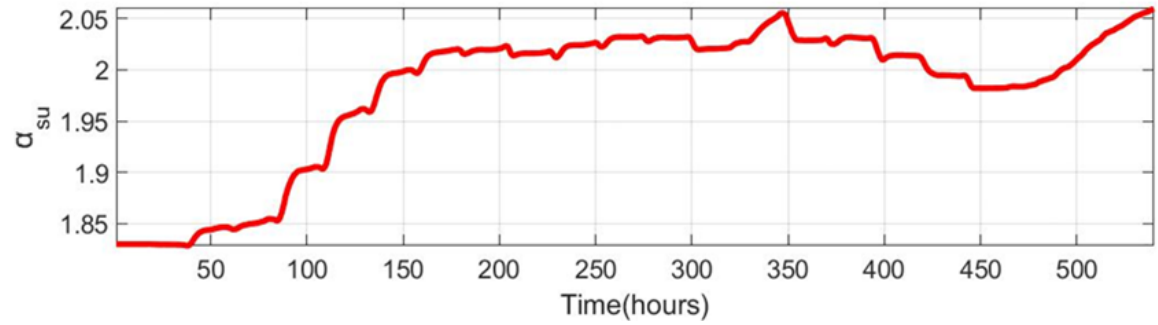

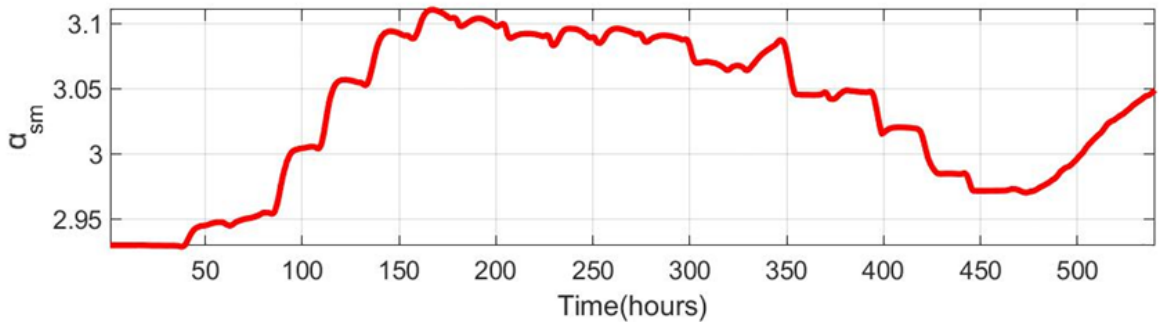
3.1
3.05
3
2.95
α_{sm}
50 100 150 200 250 300 350 400 450 500
Time(hours)

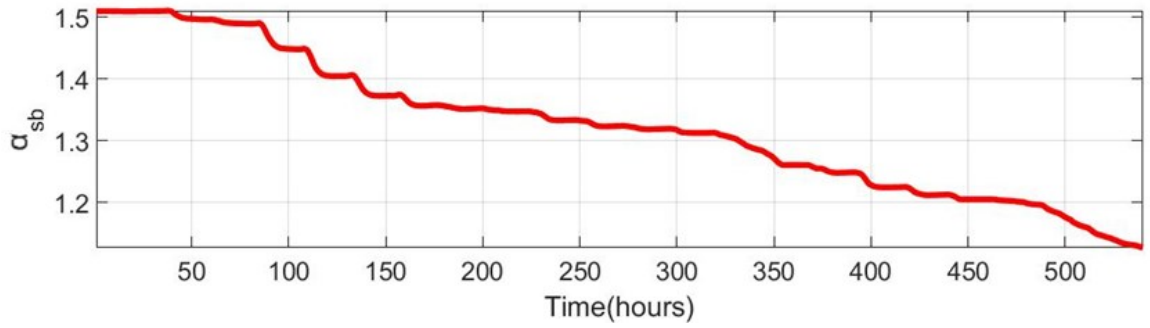
1.5
1.4
1.3
1.2
α_{sb}
50 100 150 200 250 300 350 400 450 500
Time(hours)

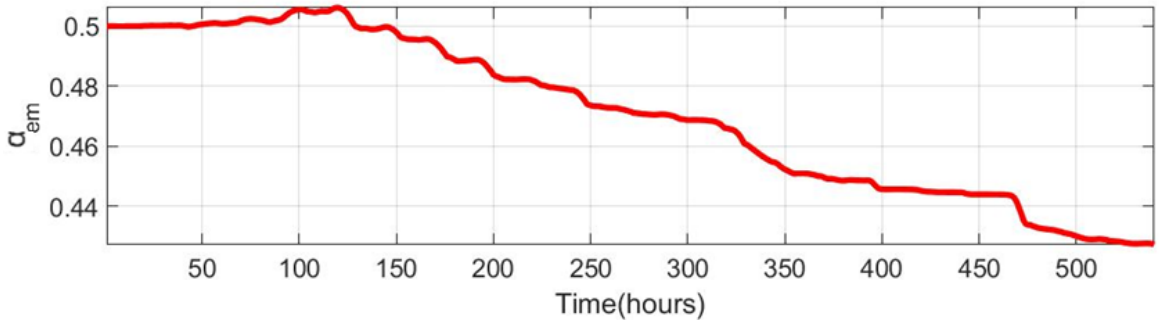
0.5
0.48
0.46
0.44
α_{em}
50 100 150 200 250 300 350 400 450 500
Time(hours)

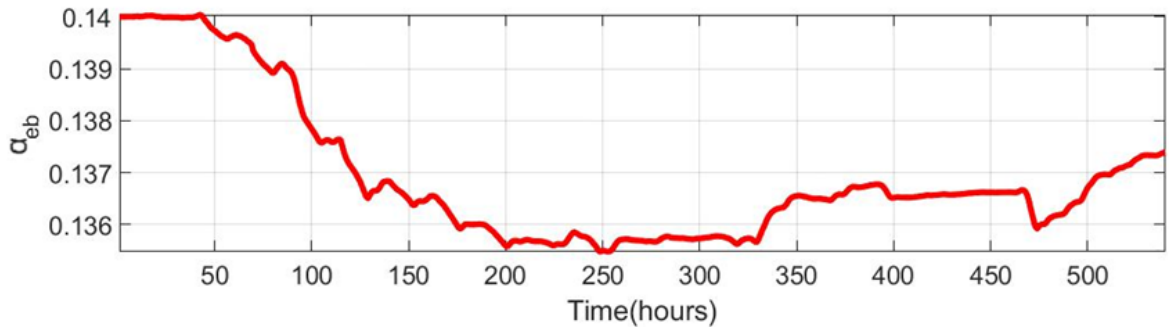
0.14
0.139
0.138
0.137
0.136
α_{eb}
50 100 150 200 250 300 350 400 450 500
Time(hours)

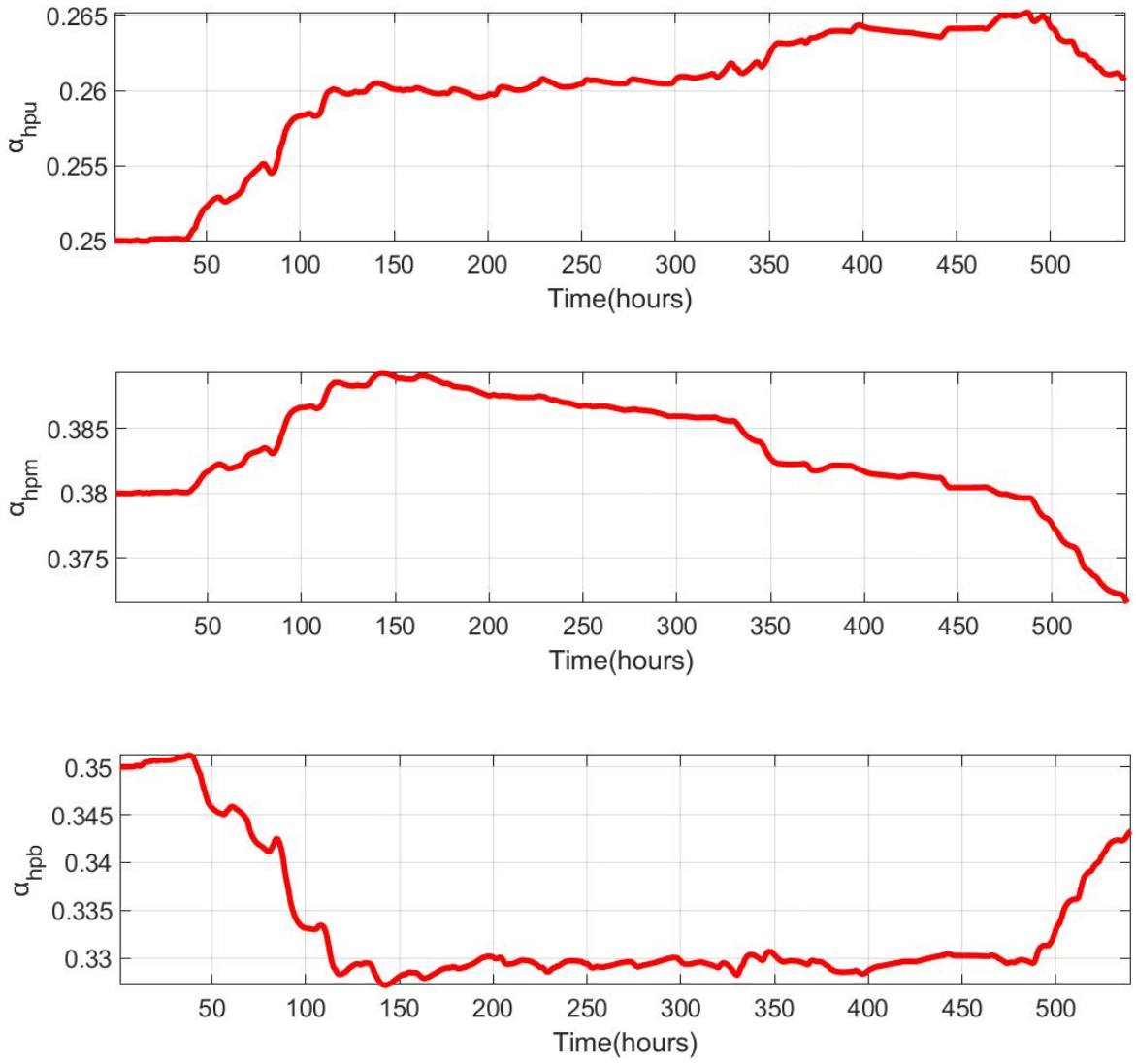

Figure B. 810R6C model parameters estimation: solar and internal gain factors for scenario 10R6C-3

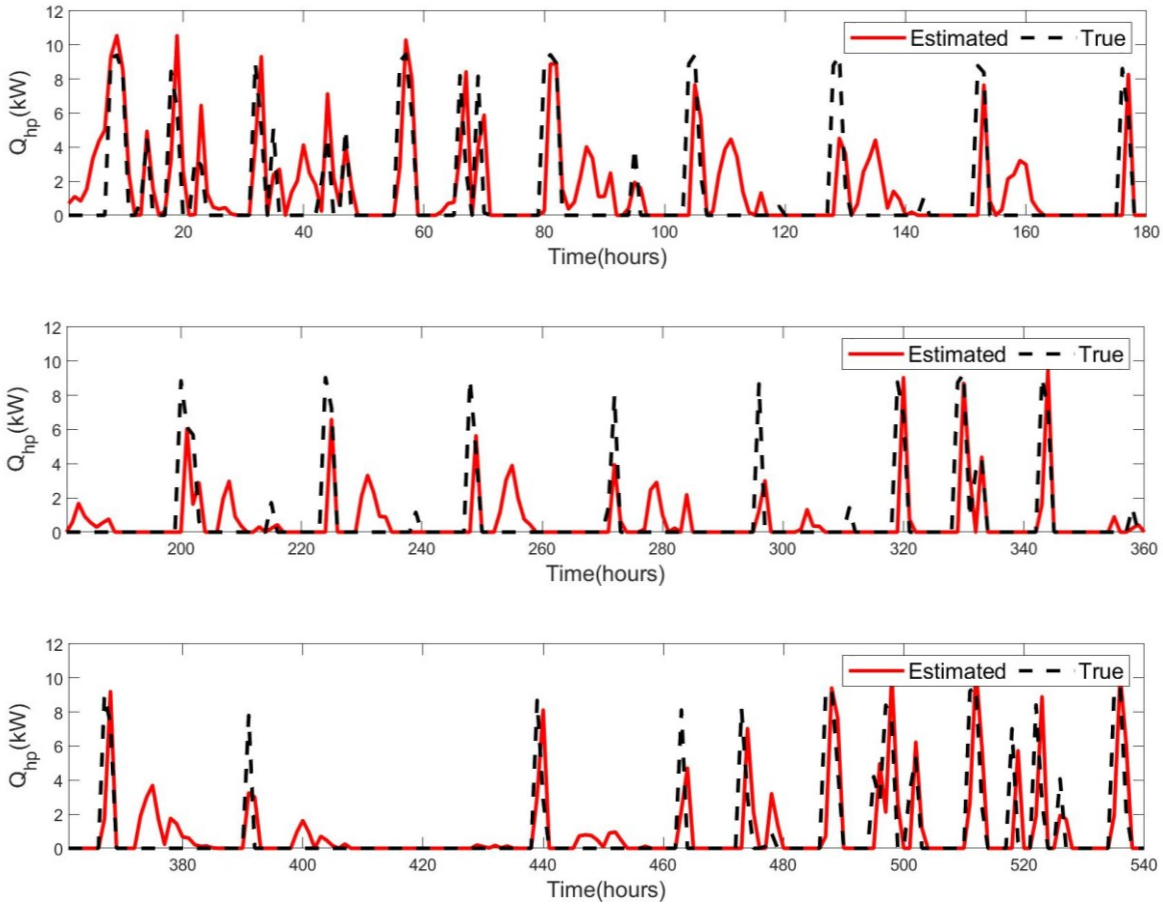

Figure B. 9 Comparison between true and estimated model input for scenario 10R6C-3

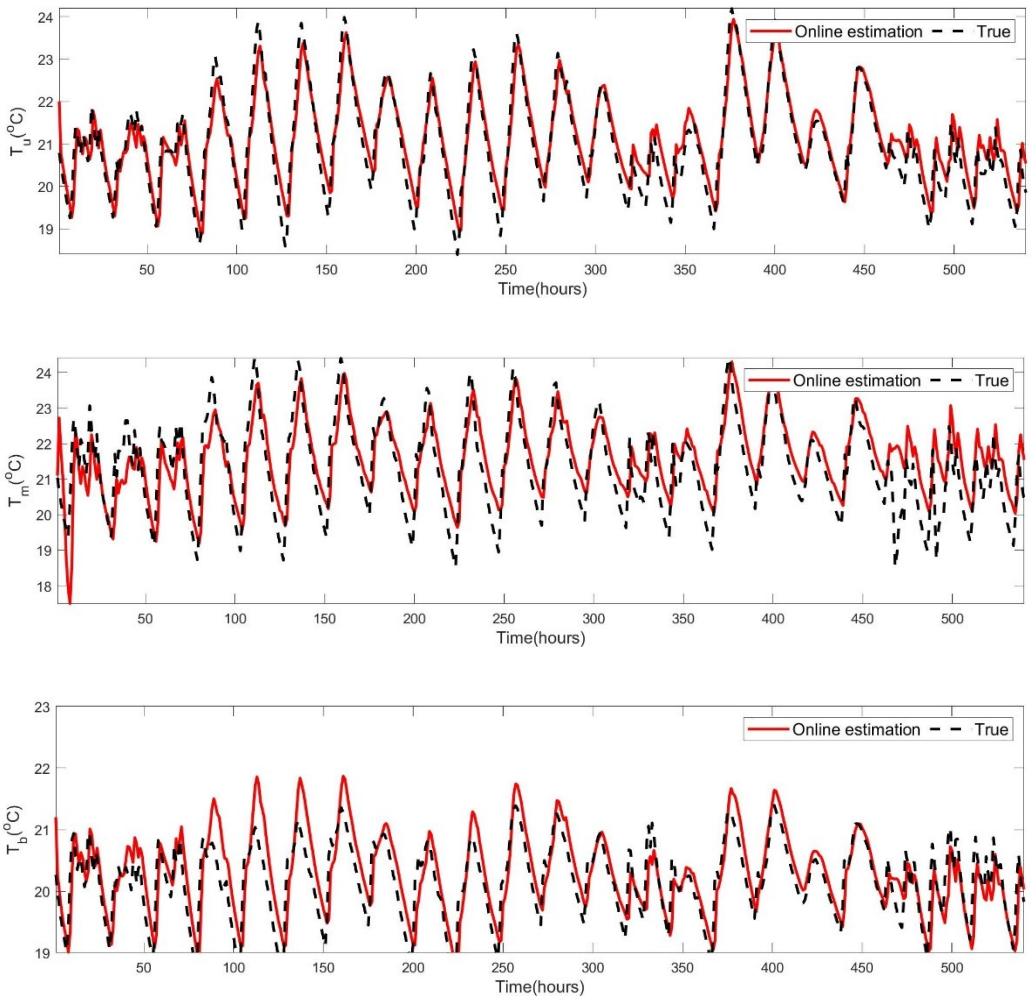

Figure B. 10Comparison between true and estimated temperature responses for scenario 10R6C-3

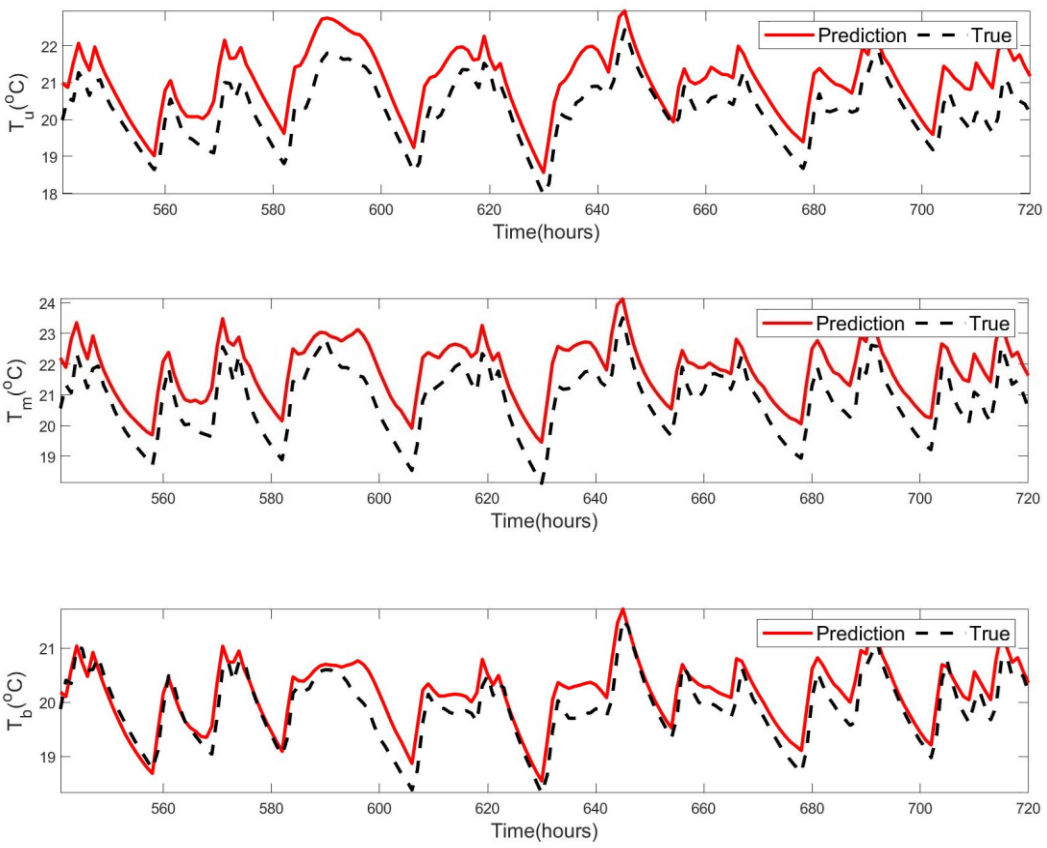

Figure B. 11Comparison between true and predicted temperature responses for scenario 10R6C-3

Appendix C – A simple case study information for temperature control

For the case study with made-up data, i.e., the 2R2C model, the ordinary differential equation can be shown below:

$$C_2 \frac{dT_2}{dt} = \frac{T_1 - T_2}{R_2} + \frac{T_3 - T_2}{R_3} \tag{C.1}$$

$$C_3 \frac{dT_3}{dt} = \frac{T_2 - T_3}{R_3} + Q_1 + Q_3 \tag{C.2}$$

Accordingly, the state-space equation of the 2R2C model, when Q_2 needs to be estimated.

$$\frac{d}{dt}\begin{bmatrix}T_2\\T_3\end{bmatrix}=\begin{bmatrix}\frac{-1}{R_2C_2}-\frac{1}{R_3C_2} & \frac{1}{R_3C_2}\\ \frac{1}{R_3C_3} & -\frac{1}{R_3C_3}\end{bmatrix}\begin{bmatrix}T_2\\T_3\end{bmatrix}+\begin{bmatrix}\frac{1}{R_2C_2} & 0 & \frac{1}{C_2} & 0\\ 0 & \frac{1}{C_3} & 0 & \frac{1}{C_3}\end{bmatrix}\begin{bmatrix}T_1\\Q_1\\Q_2\\Q_3\end{bmatrix} \tag{C.3}$$

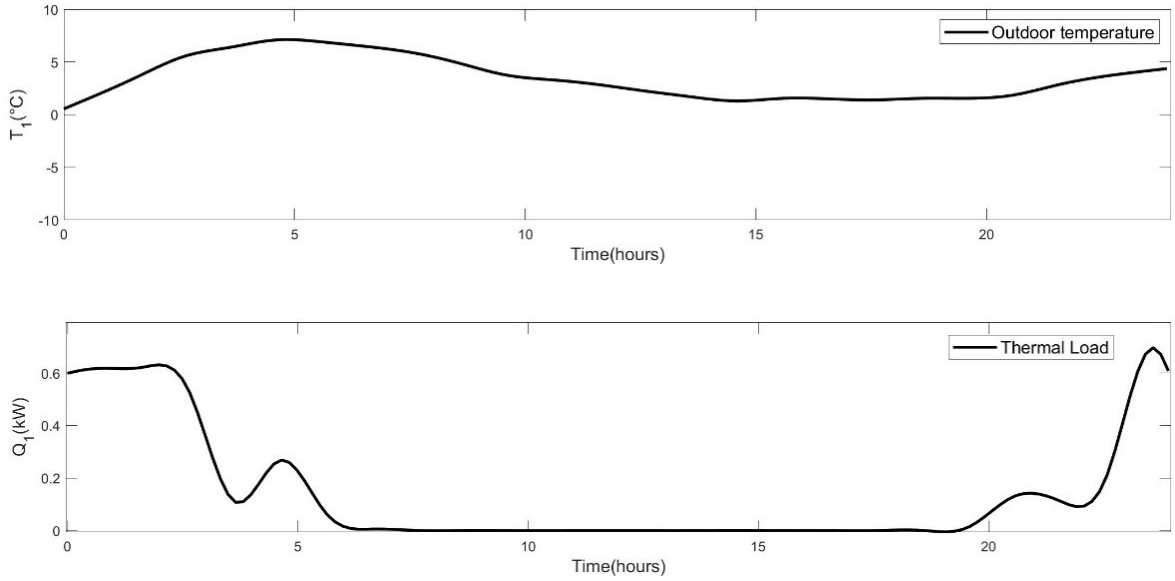

Figure C.1 2R2C model inputs

Appendix D – Real-world case study information for temperature control

The ODEs shown below are derived for the 10R6C model:

$$C_{ui}\frac{dT_u}{dt}=\frac{T_0-T_u}{R_3}+\frac{T_{um}-T_u}{R_1}+\frac{T_{um}-T_u}{R_2}+\alpha_{hpu}Q_{hp}+F_{su}Q_s$$

$$C_{um}\frac{dT_{um}}{dt}=\frac{T_u-T_{um}}{R_1}$$

$$C_{mi}\frac{dT_m}{dt}=\frac{T_0-T_m}{R_6}+\frac{T_{mm}-T_m}{R_4}+\frac{T_b-T_m}{R_5}+\frac{T_u-T_m}{R_2}+\alpha_{hpm}Q_{hp}+\alpha_{sm}Q_s+\alpha_{em}Q_{elec}$$

$$C_{mm}\frac{dT_{mm}}{dt}=\frac{T_m-T_{mm}}{R_4}+\frac{T_b-T_{mm}}{R_7} \tag{D1}$$

$$C_{bi}\frac{dT_b}{dt}=\frac{T_0-T_b}{R_9}+\frac{T_{bm}-T_b}{R_8}+\frac{T_{mm}-T_b}{R_7}+\frac{T_m-T_b}{R_5}+\alpha_{hpb}Q_{hp}+\alpha_{sb}Q_s+\alpha_{eb}Q_{elec}$$

$$C_{bm}\frac{dT_{bm}}{dt}=\frac{T_b-T_{bm}}{R_8}+\frac{T_g-T_{bm}}{R_{10}}$$

Therefore, the state space form of the 10R6C model can be written as follows:

$$\frac{d}{dt}\begin{bmatrix} T_u \\ T_{um} \\ T_m \\ T_{mm} \\ T_b \\ T_{bm} \end{bmatrix} = A_c \begin{bmatrix} T_u \\ T_{um} \\ T_m \\ T_{mm} \\ T_b \\ T_{bm} \end{bmatrix} + B_c \begin{bmatrix} T_0 \\ T_{\mathrm{g}} \\ Q_{\mathrm{s}} \\ Q_{\mathrm{elec}} \\ Q_{\mathrm{hp}} \end{bmatrix} \tag{D.2}$$

where

$$A_c = \begin{bmatrix} \frac{-1}{C_{ui}}\left(\frac{1}{R_1}+\frac{1}{R_2}+\frac{1}{R_3}\right) & \frac{1}{R_1 * C_{ui}} & \frac{1}{R_2 * C_{ui}} & 0 & 0 & 0 \\ \frac{1}{R_1 * C_{um}} & \frac{-1}{R_1 * C_{um}} & 0 & 0 & 0 & 0 \\ \frac{1}{R_2 * C_{mi}} & 0 & \frac{-1}{C_{mi}}\left(\frac{1}{R_2}+\frac{1}{R_4}+\frac{1}{R_5}+\frac{1}{R_6}\right) & \frac{1}{R_4 * C_{mi}} & \frac{1}{R_5 * C_{mi}} & 0 \\ 0 & 0 & \frac{1}{R_4 * C_{mm}} & \frac{-1}{C_{mm}}\left(\frac{1}{R_4}+\frac{1}{R_7}\right) & \frac{1}{R_7 * C_{mm}} & 0 \\ 0 & 0 & \frac{1}{R_5 * C_{bi}} & \frac{1}{R_7 * C_{bi}} & \frac{-1}{C_{bi}}\left(\frac{1}{R_5}+\frac{1}{R_7}+\frac{1}{R_8}+\frac{1}{R_9}\right) & \frac{1}{R_8 * C_{bi}} \\ 0 & 0 & 0 & 0 & \frac{1}{R_8 * C_{bm}} & \frac{-1}{C_{bm}}\left(\frac{1}{R_8}+\frac{1}{R_{10}}\right) \end{bmatrix}$$

$$\mathrm{B}_c = \begin{bmatrix} \frac{1}{R_3 * C_{\mathrm{ui}}} & 0 & \frac{\alpha_{\mathrm{su}}}{C_{\mathrm{ui}}} & 0 & \frac{\alpha_{\mathrm{hpu}}}{C_{\mathrm{ui}}} \\ 0 & 0 & 0 & 0 & 0 \\ \frac{1}{R_6 * C_{\mathrm{mi}}} & 0 & \frac{\alpha_{\mathrm{sm}}}{C_{\mathrm{mi}}} & \frac{\alpha_{\mathrm{em}}}{C_{\mathrm{mi}}} & \frac{\alpha_{\mathrm{hpm}}}{C_{\mathrm{mi}}} \\ 0 & 0 & 0 & 0 & 0 \\ \frac{1}{R_9 * C_{\mathrm{bi}}} & 0 & \frac{\alpha_{\mathrm{sb}}}{C_{\mathrm{bi}}} & \frac{\alpha_{\mathrm{eb}}}{C_{\mathrm{bi}}} & \frac{\alpha_{\mathrm{hpb}}}{C_{\mathrm{bi}}} \\ 0 & \frac{1}{R_{10} * C_{\mathrm{bm}}} & 0 & 0 & 0 \end{bmatrix}$$

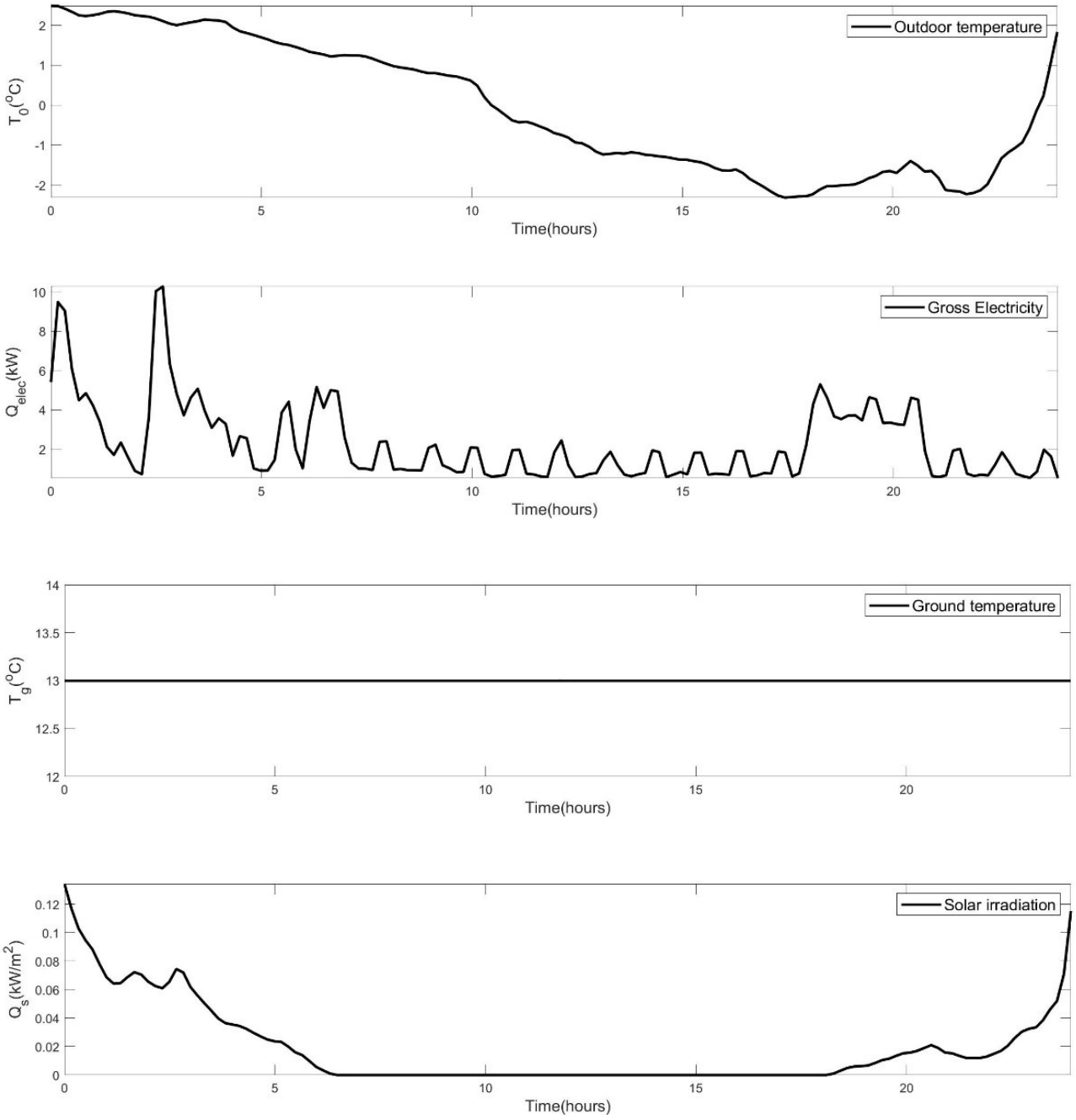

Figure D. 1. 10R6C Model inputs

The ordinary differential equations for the RC thermal model for controlling two zones' temperatures is depicted below:

$$C_{ui}\frac{dT_u}{dt} = \frac{T_0 - T_u}{R_3} + \frac{T_{um} - T_u}{R_1} + \frac{T_{um} - T_u}{R_2} + Q_u + \alpha_{su}Q_s$$

$$C_{um}\frac{dT_{um}}{dt} = \frac{T_u - T_{um}}{R_1}$$

$$C_{mi}\frac{dT_m}{dt} = \frac{T_0 - T_m}{R_6} + \frac{T_{mm} - T_m}{R_4} + \frac{T_b - T_m}{R_5} + \frac{T_u - T_m}{R_2} + Q_m + \alpha_{sm}Q_s + \alpha_{em}Q_{elec}$$

$$C_{mm}\frac{dT_{mm}}{dt} = \frac{T_m - T_{mm}}{R_4} + \frac{T_b - T_{mm}}{R_7} \tag{B3}$$

$$C_{bi}\frac{dT_b}{dt} = \frac{T_0 - T_b}{R_9} + \frac{T_{bm} - T_b}{R_8} + \frac{T_{mm} - T_b}{R_7} + \frac{T_m - T_b}{R_5} + \alpha_{sb}Q_s + \alpha_{eb}Q_{elec}$$

$$C_{bm}\frac{dT_{bm}}{dt} = \frac{T_b - T_{bm}}{R_8} + \frac{T_g - T_{bm}}{R_{10}}$$

The state space model of the new RC thermal model can be written as follow.

$$\frac{d}{dt}\begin{bmatrix} T_u \\ T_{um} \\ T_m \\ T_{mm} \\ T_b \\ T_{bm} \end{bmatrix} = A_c \begin{bmatrix} T_u \\ T_{um} \\ T_m \\ T_{mm} \\ T_b \\ T_{bm} \end{bmatrix} + B_c \begin{bmatrix} T_0 \\ T_{\mathrm{g}} \\ Q_{\mathrm{s}} \\ Q_{\mathrm{elec}} \\ Q_u \\ Q_m \end{bmatrix} \tag{E.4}$$

which

$$A_c = \begin{bmatrix} \frac{-1}{C_{ui}}\left(\frac{1}{R_1}+\frac{1}{R_2}+\frac{1}{R_3}\right) & \frac{1}{R_1 * C_{ui}} & \frac{1}{R_2 * C_{ui}} & 0 & 0 & 0 \\ \frac{1}{R_1 * C_{um}} & \frac{-1}{R_1 * C_{um}} & 0 & 0 & 0 & 0 \\ \frac{1}{R_2 * C_{mi}} & 0 & \frac{-1}{C_{mi}}\left(\frac{1}{R_2}+\frac{1}{R_4}+\frac{1}{R_5}+\frac{1}{R_6}\right) & \frac{1}{R_4 * C_{mi}} & \frac{1}{R_5 * C_{mi}} & 0 \\ 0 & 0 & \frac{1}{R_4 * C_{mm}} & \frac{-1}{C_{mm}}\left(\frac{1}{R_4}+\frac{1}{R_7}\right) & \frac{1}{R_7 * C_{mm}} & 0 \\ 0 & 0 & \frac{1}{R_5 * C_{bi}} & \frac{1}{R_7 * C_{bi}} & \frac{-1}{C_{bi}}\left(\frac{1}{R_5}+\frac{1}{R_7}+\frac{1}{R_8}+\frac{1}{R_9}\right) & \frac{1}{R_8 * C_{bi}} \\ 0 & 0 & 0 & 0 & \frac{1}{R_8 * C_{bm}} & \frac{-1}{C_{bm}}\left(\frac{1}{R_8}+\frac{1}{R_{10}}\right) \end{bmatrix}$$

$$\mathrm{B}_c = \begin{bmatrix} \frac{1}{R_3 * C_{\mathrm{ui}}} & 0 & \frac{\alpha_{\mathrm{su}}}{C_{\mathrm{ui}}} & 0 & \frac{1}{C_{\mathrm{ui}}} & 0 \\ 0 & 0 & 0 & 0 & 0 & 0 \\ \frac{1}{R_6 * C_{\mathrm{mi}}} & 0 & \frac{\alpha_{\mathrm{sm}}}{C_{\mathrm{mi}}} & \frac{\alpha_{\mathrm{em}}}{C_{\mathrm{mi}}} & 0 & \frac{1}{C_{\mathrm{mi}}} \\ 0 & 0 & 0 & 0 & 0 & 0 \\ \frac{1}{R_9 * C_{\mathrm{bi}}} & 0 & \frac{\alpha_{\mathrm{sb}}}{C_{\mathrm{bi}}} & \frac{\alpha_{\mathrm{eb}}}{C_{\mathrm{bi}}} & 0 & 0 \\ 0 & \frac{1}{R_{10} * C_{\mathrm{bm}}} & 0 & 0 & 0 & 0 \end{bmatrix}$$